UNIVERSITY OF OKLAHOMA

GRADUATE COLLEGE

# QUANTITATIVE ANALYSIS OF MATERIAL CONTRASTS AND WAVE PROPAGATION IN PERIODIC LAYERED MEDIA

A DISSERTATION

SUBMITTED TO THE GRADUATE FACULTY

in partial fulfillment of the requirements for the

degree of

Doctor of Philosophy

By

JAMIE RICH
Norman, Oklahoma
2006

UMI Number: 3242284

UMI Microform 3242284


ProQuest Information and Learning Company
300 North Zeeb Road
P.O. Box 1346
Ann Arbor, MI 48106-1346

QUANTITATIVE ANALYSIS OF MATERIAL CONTRASTS AND WAVE PROPAGATION IN PERIODIC LAYERED MEDIA

A DISSERTATION APPROVED FOR THE
SCHOOL OF GEOLOGY AND GEOPHYSICS

**By**

Evgeni M. Chesnokov

Roger A. Young

John D. Pigott

Jean-Claude Roegiers

Raymon L. Brown

Jerry M. Harris **(Stanford University)**

# Acknowledgements

I must start by thanking my first graduate advisor, Alan Witten. The opportunities provided to me by Alan helped give me the background I needed to be able to complete my dissertation research. I must also thank Sean Lehman for getting me started on what would have been my dissertation topic if everything had gone as originally planned.

Thanks to my advisor Evgeni Chesnokov for taking me on as a student after the loss of Alan. Thanks to all the other people involved with the 'Quake group' and their insightful suggestions on my research. Thanks to my committee members for their guidance and willingness to serve. Thanks to Devon Energy for the continuing support they provide for the OU Institute for Theoretical Geophysics.

Lastly, thank you to my wife and son for their continuing love and support and giving me something to look forward to when I would get frustrated or burned out from working on a problem.

# Contents

# List Of Tables

# List Of Figures

# Abstract

Effective wave behavior in periodic media can be both anisotropic and dispersive. These behaviors depend on two factors, the wavelength of the insonifying field and the relative material properties of the individual layers. This research takes a quantitative look at those two factors and asks how they control the anisotropic and dispersive behavior. The fields of research that this work draws from are diverse in scale, from the quantum with respect to solid state physics to solid earth scales in the case of earthquake seismology; however, the problem is very similar.

The sensitivity of long-wave effective anisotropy with respect to the individual material properties is examined in detail, reinforcing previous research in this area. Long-wave anisotropy is also examined with respect to anisotropic layers, and fractured layered media. The dependence of the dispersive limit on material contrast is demonstrated and a new approach is used to quantify what is meant by long-wave approximation.

Dispersive behavior is studied in detail. It is shown that there are critical contrasts at which different stop-bands disappear, as well as a critical angle at which all stop-bands disappear. This characterization of the higher order stop-bands at

various contrasts is vital for a complete understanding of the effective behavior of layered media across the entire frequency spectrum.

# Chapter 1

# Introduction

Layered media are of fundamental importance to exploration geophysics. Sedimentary basins exhibit layering at multiple scales, from microscopic to macroscopic. Since seismic exploration is the most commonly used geophysical method in hydrocarbon exploration, wave propagation in layered media is obviously an area that has been extensively studied, and continues to be so. This dissertation will extend the current knowledge base by focusing on periodic layering and how material contrasts between layers control the effective wave behavior in periodic media at different scales. Emphasis will be placed not only on elastic waves, but also on comparison with electromagnetic waves which in some cases have a richer research base due to applications of periodic media in solid state physics.

On the small scale, shales are the most commonly encountered periodic media in sedimentary basins. The laminar structure of shales is easily treated as a periodic layered medium. Vernik and Nur (1992) successfully model a shale by considering

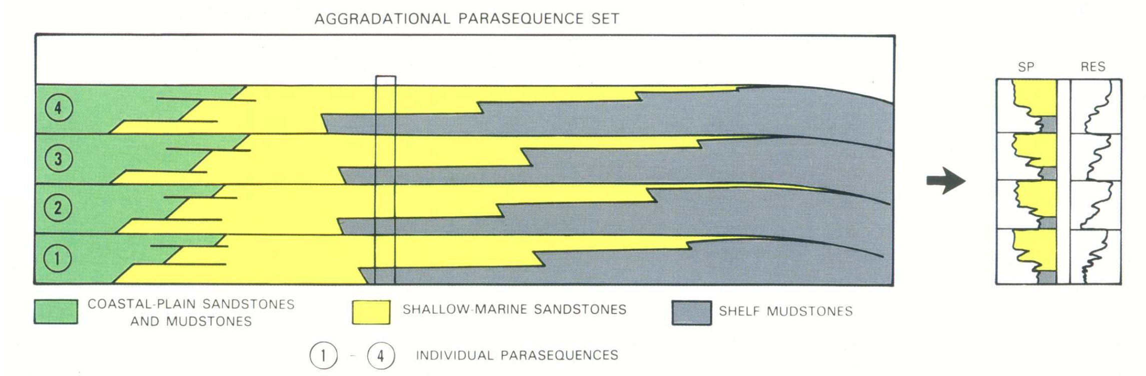


Figure 1.1: Aggradational parasequence set modified from Van Wagoner et al. (1990)

it to consist of alternating layers of illite and kerogen. The small scale of layering in shales leads to an effective anisotropy that is discussed in detail in chapter 2.

On a larger scale cyclical geological processes can lead to periodic sections. For example figure 1.1 shows an aggradational parasequence set created by the rise and fall of local sea level, which is approximately periodic. Another example is shown in figure 1.2 which consists of alternating limestones and mudstones caused by cyclical climatic changes.

An understanding of wave behavior in periodic media can also be extended to random layering. The scattering in a periodic media can give direct insight into random scattering. For instance a random media can be considered to be a superposition of periodic layers (Marion et al., 1994). Hence, an examination of periodic behavior is not completely restricted in applicability to only periodic media.

The general model of a two constituent periodic medium is shown in figure 1.3. The properties of concern for a given layer are the elastic constants, $C_{ijkl}$; density,

Figure 1.2: Interbedded limestones and mudstones from Coe et al. (2003) illustrate a naturally occurring example of periodic media

$\rho$; electrical permittivity, $\epsilon$; magnetic permeability, $\nu$; and layer thickness, $d$. For simplicity in this dissertation the coordinate system is always taken with the z-axis normal to the layering. The layers are always assumed to be infinite in the x-y plane.

An underlying concern in this dissertation is that of scale with reference to wavelength. Chapter 2 considers the simplest case when the wavelength of insonification is much larger than the period of the media. The subsequent chapters then consider the more complex case when the wavelength may be of the same order as the period of the media.

In the long wave case, effective anisotropy is explored with particular attention to how different material contrasts control the degree and behavior of the anisotropy. Of particular interest is the modeling of general anisotropic behavior when the individual layers themselves are anisotropic. Both elastic waves and electromagnetic waves are considered and the effective anisotropy compared.

When the wavelength is not much longer then the period of the medium, periodic scattering of waves leads to behavior that is both dispersive and anisotropic. The most interesting effect of this scattering in periodic media is the appearance of stop-bands, frequencies at which only complex (attenuating) wavenumbers are allowed. There are a number of papers which attempt to characterize the onset of this dispersive behavior, but without a complete analysis of the effect of the material contrasts. Chapter 4 fills this gap. The analysis is also expanded beyond the first stop-zone, examining stop-bandwidth as a function of both contrast and angle of propagation. While there has been some recent work on stop-bands as a function of angle (Manzanares-Martinez and Ramos-Mendieta, 2000; Dukin et al., 2006), it has been restricted to the study of superlattices and photonic crystals. Chapter 4 expands these observations to geologic materials and contrasts.

Chapter 5 considers the case of long wave propagation, but includes the effect of fractures. Geophysical studies often reveal anisotropy of orthorhombic symmetry. Vertical fractures in a layered background are believed to be one of the most prominent sources for this type of behavior. Through sequential averaging, this behavior is approximated and explored and the role of layering contrast in this effective anisotropy is explored.

It is assumed that the reader possesses a basic knowledge of the elastic wave equation in anisotropic media, along with an understanding of the terms anisotropy and dispersion as they relate to wave propagation in homogeneous media. Appendix A provides a brief review of the origin of these effects from a continuum mechanics point of view. For a more complete review Helbig (1994) and Mavko et al. (1998) are excellent sources.

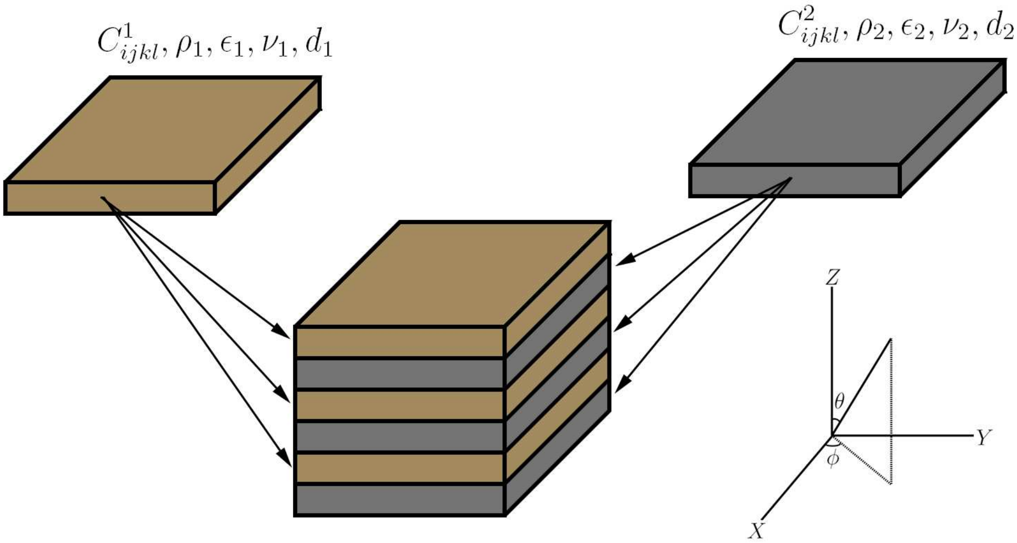


Figure 1.3: Two constituent periodically layered media

# Chapter 2

# Layered Periodic Media: Long Wave Limit

## 2.1 Background Model

The simplest and most studied case of wave propagation in layered media is the thin layered periodic media. This problem has a long history and has been explored by many authors in various fields, ranging from materials science and engineering to geophysics (Postma, 1955; Backus, 1962; Delph et al., 1978; Berryman, 1979). Because of its simplicity it still remains a very interesting area of study. This chapter provides a description of the problem, an overview of the most important work which has been done in the long wave case, and extends the body of knowledge by modeling variations in material contrasts and comparing this case for both electromagnetic and elastic wave insonification.

The thin layered periodic media considered is composed of two alternating layers of isotropic or anisotropic materials. Each layer is characterized by its elastic constants $C_{ijkl}$, density $\rho$, magnetic permeability $\nu$, electrical permittivity $\epsilon$, and

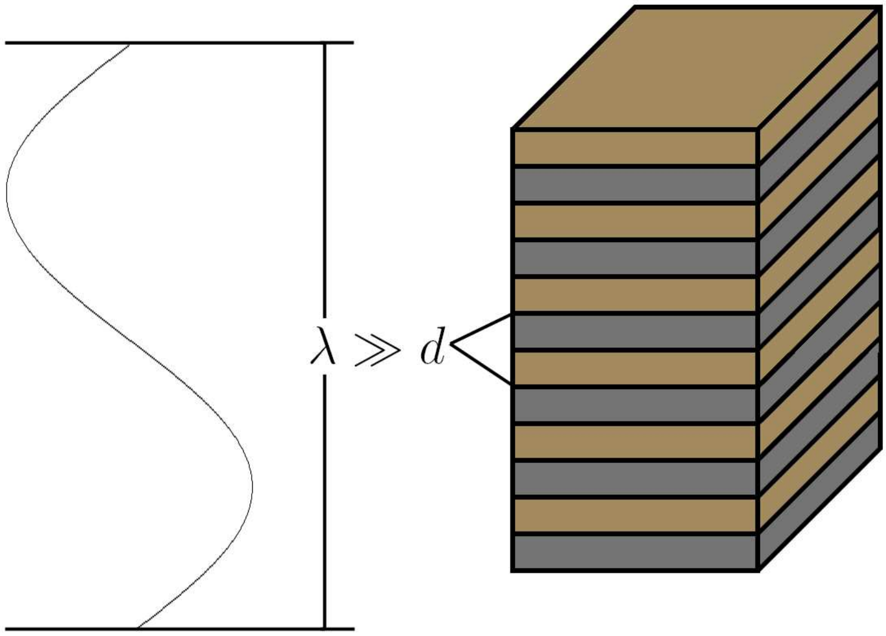


Figure 2.1: Wavelength much greater than the period of the media

thickness. None of these approaches include intrinsic attenuation, so electrical conductivity is assumed to be negligible. The 'thin' qualifier refers to the limiting case in which the insonifying wavelength is much greater then the period of the media. What is meant by 'much greater' will be explored in detail in Chapter 4. The thin layering condition is illustrated in Figure 2.1.

For the case of individual isotropic layers, the effective behavior of the thin layered periodic media is that of a transversely isotropic medium. Individual anisotropic layers can result in more complex anisotropic symmetries. This effective anisotropy is well documented in the existing literature (Rytov, 1956a; Backus, 1962; Berryman, 1979; Schoenberg and Muir, 1989; Carcione et al., 1991). While there are a multitude of papers on this topic there are two basic approaches that have been taken in order to characterize the elastic constants of the effective media and the corresponding wave propagation in the thin layered media.

While this case of anisotropy due to thin layers is well understood, a direct comparison of the sensitivities under both elastic and electromagnetic waves has never been undertaken. This chapter proceeds with a sensitivity comparison in order to fill this gap. This is very important to understand, particulary with the use of electromagnetic imaging becoming more common in applied geophysics. Techniques such as crosswell EM tomography are particularly useful because of the increased sensitivity of EM wave propagation to fluid content as opposed to elastic wave propagation.

One of the earliest characterizations of long wave effective behavior was done by Rytov (1956a,b). He investigated both the elastic and electromagnetic cases for isotropic constituents in two papers. In his solution he used the so-called Floquet theorem (Floquet, 1883) to write the solution to the wave equation in the periodic media. The resulting dispersion equations were then solved in the long wavelength limit giving results for the effective elastic constants in the elastic case, and the effective permittivities and magnetic permeabilities in the EM case. It is of interest to point out that the most laborious calculation for Rytov, that of $c_{13}$, which requires solution of an order-8 determinant appears to be incorrect. This is suggested by Helbig (1984), and is apparent in simulations completed in this research comparing Rytov's solution with other techniques.

The use of Floquet's theorem is very common to the solution of periodic media. Floquet's theory, also commonly called Bloch theory in the three-dimensional, case gives solutions for differential equations with periodic coefficients. It will be examined in detail in the next chapter, due to it's importance in understanding the dispersion effects caused by periodic layering.

The most commonly cited work for elastic waves in thin layered media is Backus (1962). The Backus averaging approach is advantageous for two reasons. First it gives simple expressions for the elastic constants as averages of algebraic quantities. Secondly, it can be applied to non-periodic layered media with more than two constituents, which may be transversely isotropic themselves. Also, it has been extended to the case where the constituents themselves are anisotropic (Schoenberg and Muir, 1989). However, one important difference from Floquet's theory is that the Backus method is only applicable to the long wavelength case, i.e. no dispersion relation.

Backus is actually a generalization of the approach given by Postma (1955), who gave the averaging solution for only two periodic constituents. He then explored relations between the constants, and the three unique velocities that arise in this case. For a simple explanation of Postma's method see Carcione (2001).

Most of the work on the electromagnetic problem only gives passing notice of the long wave case, while focusing on dispersion and stop bands. However, Lekner (1994) does give the expression for the long wave equivalent permittivity which is in agreement with Rytov (1956b). An overview of these papers will be given in the next chapter when discussing dispersion relations.

## 2.2 Elastic Waves: Isotropic Constituents

Elastic wave propagation in homogenous and isotropic media is controlled by Lamé's parameters $\lambda$ and $\mu$, and by density $\rho$. For this consideration of the layered periodic media of two isotropic constituents it is also necessary to include the layer thicknesses $d_1$ and $d_2$. In most of the discussions, the bulk modulus, $K$, will be used instead of $\lambda$ due to its physical significance. The solution of the elastic wave equation in isotropic and homogeneous media has two solutions, the compressional wave characterized by a velocity:

$$V_p = \sqrt{\frac{\lambda + 2\mu}{\rho}} = \sqrt{\frac{K + \frac{4}{3}\mu}{\rho}} \tag{2.1}$$

and the shear wave, which has a velocity:

$$V_s = \sqrt{\frac{\mu}{\rho}} \tag{2.2}$$

In order to study the effective medium formed by two periodic isotropic constituents, the relations given by Postma (1955) were used. It should be noted that these relations are equivalent to those given by Backus (1962), and Rytov (1956a)(with the exception of $C_{13}$). The equivalence with Backus can be easily shown mathematically, and both where confirmed with numerical simulations. All of the following simulations where done using MATLAB software.

The effective elastic constants are given in terms of the isotropic layer parameters. The subscript $l$ refers to layer 1 or 2.

$$c_{11} = [d^2 E_1 E_2 + 4 d_1 d_2 (\mu_1 - \mu_2)(\lambda_1 + \mu_1 - \lambda_2 - \mu_2)] D^{-1} \tag{2.3}$$

$$c_{12} = [d^2 \lambda_1 \lambda_2 + 2(\lambda_1 d_1 + \lambda_2 d_2)(\mu_2 d_1 + \mu_1 d_2)] D^{-1} \tag{2.4}$$

$$c_{13} = d(\lambda_1 d_1 E_2 + \lambda_2 d_2 E_1) D^{-1} \tag{2.5}$$

$$c_{33} = d^2 E_1 E_2 D^{-1} \tag{2.6}$$

$$c_{44} = \frac{d \mu_1 \mu_2}{d_1 \mu_2 + d_2 \mu_1} \tag{2.7}$$

$$c_{66} = \frac{(d_1 \mu_1 + d_2 \mu_2)}{d} = \frac{c_{11} - c_{12}}{2} \tag{2.8}$$

where,

$$E_l = \lambda_l + 2\mu_l$$

$$d = d_1 + d_2$$

$$D = d(d_1 E_2 + d_2 E_1)$$

The Backus relations which extend to higher numbers of layers, and reduce the requirement of periodicity to that of stationarity are:

$$c_{11} = \langle c_{11} - c_{13}^2 c_{33}^{-1} \rangle + \langle c_{33}^{-1} \rangle^{-1} \langle c_{33}^{-1} c_{13} \rangle^2$$

$$c_{33} = \langle c_{33}^{-1} \rangle^{-1}$$

$$c_{13} = \langle c_{33}^{-1} \rangle^{-1} \langle c_{33}^{-1} c_{13} \rangle$$

$$c_{55} = \langle c_{55}^{-1} \rangle^{-1}$$

$$c_{66} = \langle c_{66} \rangle$$

$$\langle c \rangle = \sum_{n=1}^{N} f_n c_n$$

Three velocities can be found corresponding to the VTI medium described by these six (five independent) elastic constants. Postma (1955) first gave a graphical method for determining the velocities as a function of propagation angle. The values for the velocities in any anisotropic media are given by solving the Green Christoffell equation.

$$(\Gamma_{ik} - \rho V^2 \delta_{ik}) u_k = 0 \tag{2.9}$$

where $\Gamma$ is the Green-Christoffell tensor and the eigenvectors $u_k$ are the direction cosines of the displacement vector. The Green-Christoffel equation is easily obtained by substituting plane wave solutions into the elastodynamic wave equation (see appendix A). It is apparent then that the Green-Christoffel equation is the condition that must be satisfied for plane waves to exist in a given anisotropic homogeneous media (Helbig, 1994).

The solution for the eigenvalues in the case of VTI media is simple and can be seen in Daley and Hron (1977). The following is that solution, expressed in the form given by Thomsen (1986):

$$V_p^2(\theta) = \frac{1}{2\rho}[c_{33} + c_{44} + (c_{11} - c_{33})\sin^2\theta + D] \tag{2.10}$$

$$V_{sv}^2(\theta) = \frac{1}{2\rho}[c_{33} + c_{44} + (c_{11} - c_{33})\sin^2\theta - D] \tag{2.11}$$

$$V_{sh}^2(\theta) = \frac{1}{\rho}[c_{44}\cos^2\theta + c_{66}\sin^2\theta] \tag{2.12}$$

where

$$\begin{aligned} D^2 \equiv &(c_{33} - c_{44})^2 + 2[2(c_{13} + c_44)^2 - (c_{33} - c_{44})(c_{11} + c_{33} - 2c_{44})]\sin^2\theta + \\ &[(c_{11} + c_{33} - 2c_{44})^2 - 4(c_{13} + c_{44})^2]\sin^4\theta \end{aligned} \tag{2.13}$$

One interesting thing that comes out of the preceding expressions is the importance of the shear modulus $\mu$ in controlling the anisotropy. It can be shown that without a difference in shear modulus, there is no effective anisotropy regardless of how different the other parameters are (Mavko et al., 1998; Berryman, 2005). This can be shown by substituting $\mu_1 = \mu_2$ into equations 2.3-2.8. First, it is obvious that for this condition the second part in the parentheses of Equation 2.3 disappears, leaving $c_{11} = c_{33}$. The elastic constants $c_{12}$ and $c_{13}$ also reduce to equivalent forms as shown below:

$$c_{12} = \frac{d^2\lambda_1\lambda_2 + 2\mu d(\lambda_1 d_1 + \lambda_2 d_2)}{d(d_1 E_2 + d_2 E_1)}$$

$$= \frac{d\lambda_1\lambda_2 + 2\mu(\lambda_1 d_1 + \lambda_2 d_2)}{d_1 E_2 + d_2 E_1}$$

$$c_{13} = \frac{d[\lambda_1 d_1(\lambda_2 + 2\mu) + \lambda_2 d_2(\lambda_1 + 2\mu)]}{d(d_1 E_2 + d_2 E_1)}$$

$$= \frac{\lambda_1\lambda_2 d_1 + 2\lambda_1 d_1 \mu + \lambda_2\lambda_1 d_2 + 2\lambda_2 d_2 \mu}{d(d_1 E_2 + d_2 E_1)} = c_{12}$$

It is also simple to see that both Equations 2.7 and 2.8 reduce to $c_{44} = c_{66} = \mu$. This results in having only three elastic constants. To show that this effective medium will exhibit isotropic behavior it is necessary to show that $c_{11} = c_{12} + 2c_{44}$ or $c_{11} - c_{12} = 2\mu$.

$$c_{11} - c_{12} = \frac{d(\lambda_1\lambda_2 + 2\lambda_1\mu + 2\lambda_2\mu + 4\mu^2)}{2\mu d + d_1\lambda_2 + d_2\lambda_1} - \frac{d\lambda_1\lambda_2 + 2d_1\lambda_1\mu + 2d_2\lambda_2\mu}{2d\mu + d_1\lambda_2 + d_2\lambda_1}$$

$$= \frac{2\mu(d\lambda_1 + d\lambda_2 + 2d\mu - d_1\lambda_1 - d_2\lambda_2)}{2d\mu + d_1\lambda_2 + d_2\lambda_1}$$

$$= \frac{2\mu(2d\mu + d_1\lambda_2 + d_2\lambda_1)}{2d\mu + d_1\lambda_2 + d_2\lambda_1} = 2\mu$$

This leads to the following expressions for the elastic constants when $\mu_1 = \mu_2$.

$$c_{12} = c_{13} = \frac{\lambda_1\lambda_2 d + 2\mu(d_1\lambda_1 + d_2\lambda_2)}{2d\mu + d_1\lambda_2 + d_2\lambda_1}$$

$$c_{44} = c_{66} = \mu$$

$$c_{11} = c_{33} = 2c_{44} + c_{12}$$

It is immediately evident that this describes an isotropic system where the effective $\lambda$ is given by $\lambda_{eff} = c_{12}$. Accordingly if one uses these values in Equations 2.10-2.12 one finds that $D = \lambda_{eff} + \mu$; and

$$V_p^2 = \frac{\lambda_{eff} + 2\mu}{\rho}$$

$$V_{sv}^2 = V_{sh}^2 = \frac{\mu}{\rho}$$

as would be expected for an isotropic medium. An important consequence of this is that the essential requirement for layer induced effective anisotropy is that $\mu$ must vary between the layers. If our two layers were identical isotropic rock materials with different fluid saturations, there would be no shear modulus contrast and, hence, no anisotropy. So a difference in Poisson's (Equation 2.14) ratio between layers does not necessarily lead to long-wave layer anisotropy.

$$\sigma = \frac{(V_p/V_s)^2 - 2}{2((V_p/V_s)^2 - 1)} \tag{2.14}$$

Another observation can be made by examining the limit of Equation 2.7.

$$\lim_{\mu_2 \to \infty} c_{44} = \frac{d\mu_1}{d_1}$$

This, along with the equation for the velocities, shows that the velocity of shear waves normal to the layering are restricted by the smaller shear modulus as the other gets very large.

Before continuing with a closer examination of sensitivities, it is first necessary to provide a quantitative definition of anisotropy. For all purposes in this dissertation fractional anisotropy will be defined as:

$$Anisotropy = \frac{Velocity(\theta) - Velocity(\theta = 0)}{Velocity(\theta = 0)}$$

where $\theta = 0$ is normal to the layers and the velocity considered is the phase velocity. Maximum anisotropy is simply the anisotropy at the angle for which the preceding expression is a maximum.

The first approach in exploring sensitivities will be to examine the effect of each parameter separately, starting with the shear modulus. While this is not a geologically realistic approach it will assist in understanding what physical rock properties are more important in controlling layer induced anisotropy. Figure 2.2 shows the effect of varying shear modulus contrast between the two layers, with no other contrast. The $S_h$ and $P$ waves both show a strong increase in anisotropy as the contrast increases. Figure 2.3 examines this same question but looks at the anisotropy as a function of angle. This shows that the maximum $S_v$ wave velocity shifts to shallower angles with increasing contrast.

There is no need to examine the effect of varying the other parameters independently of $\mu$, as it has already been shown that there is no anisotropy unless there is a contrast in shear modulus. Instead the other parameters will be considered while maintaining a constant shear modulus contrast of $\mu_1 = 5\mu_2$.

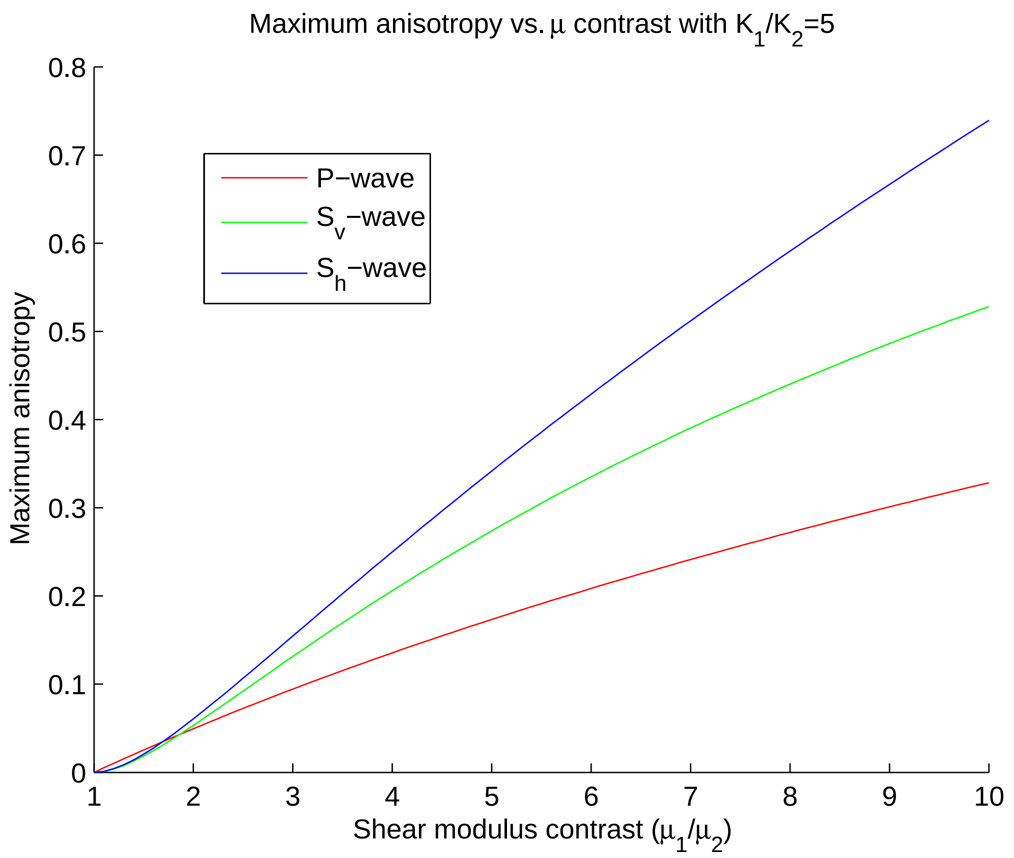


Figure 2.2: Effect of varying shear modulus contrast on maximum anisotropy, with a constant bulk modulus contrast of $K_1 = 5K_2$

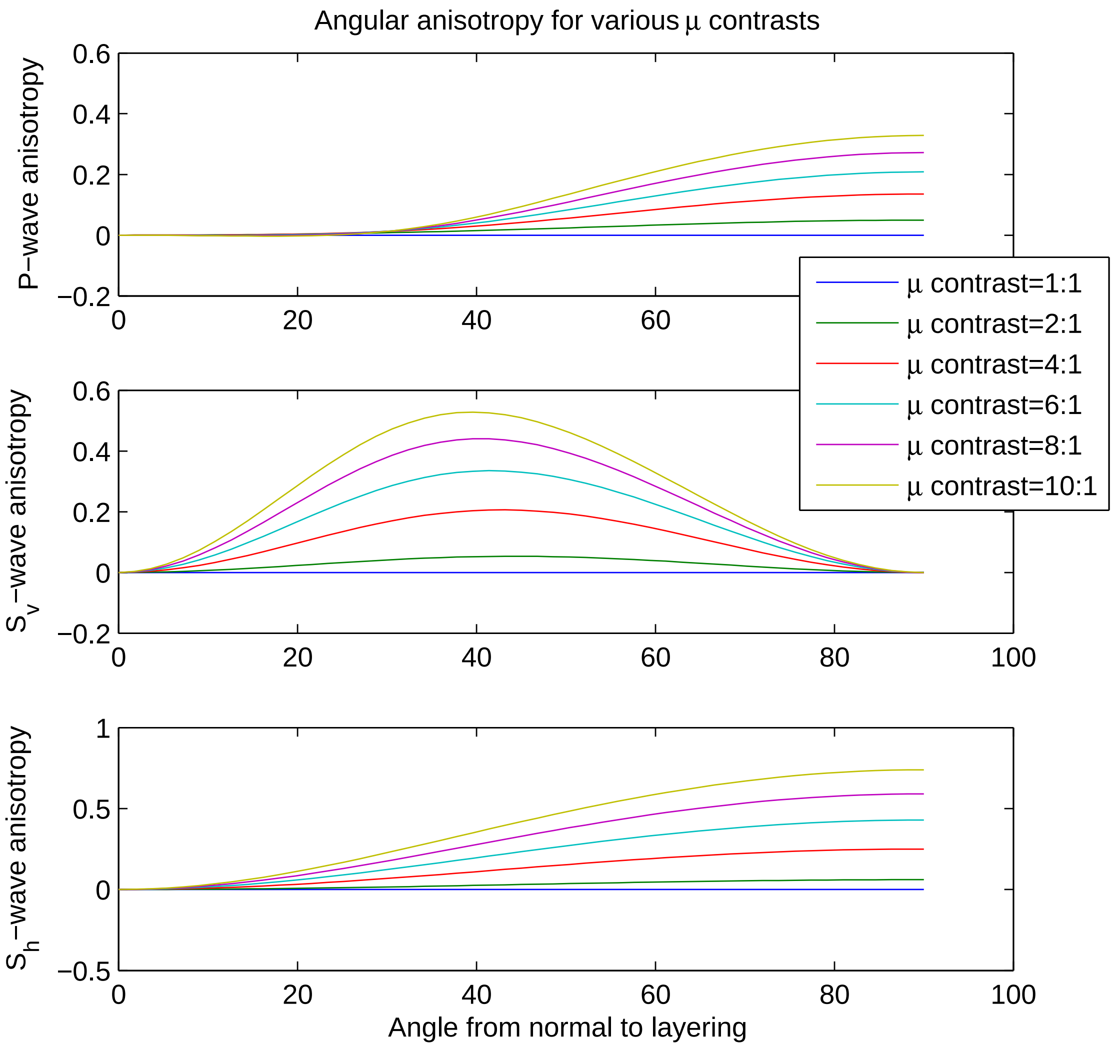


Figure 2.3: Effect of varying shear modulus contrast on angular anisotropy, with a constant bulk modulus contrast of $K_1 = 5K_2$ . The legend gives fractional contrast between layers.

Figure 2.4 shows how a variation in bulk modulus affects the maximum anisotropy. The lack of effect on anisotropy due to bulk modulus for the $S_h$ mode is expected as $S_h$ wave velocity only depends on $c_{44}$ and $c_{66}$ which from Equations 2.7 and 2.8 are only functions of the shear moduli. It is also noted that small differences in bulk modulus have a large effect on anisotropy but as the contrast gets large both $P$ and $S_v$ wave velocities approach limiting values. The same effect can be seen by examining the anisotropy as a function of angle, Figure 2.5. As with shear modulus contrast the maximum $S_v$ wave velocity can be seen shifting to shallower angles with increasing contrast.

Also considered is the effect of varying shear modulus and bulk modulus concurrently. Different lines in Figure 2.6 represent different bulk modulus contrasts, while the shear moudulus variations occur along each line from 0 at the origin to $\mu_1 = 5\mu_2$ at the terminus of each line. Here it is evident that a shear modulus contrast is required to introduce anisotropy. The major difference in introducing a bulk modulus contrast is in the character of the anisotropy indicated by the change in behavior of the $P$ vs. $S$ anisotropy.

From an examination of Equations 2.3 - 2.8 it is obvious that density contrast has no effect on the effective anisotropy, so it is not considered. The expected effect of increasing layer thickness contrast would be for the anisotropy to approach zero, as one layer becomes much thicker then the other. This can be observed in Figure 2.7.

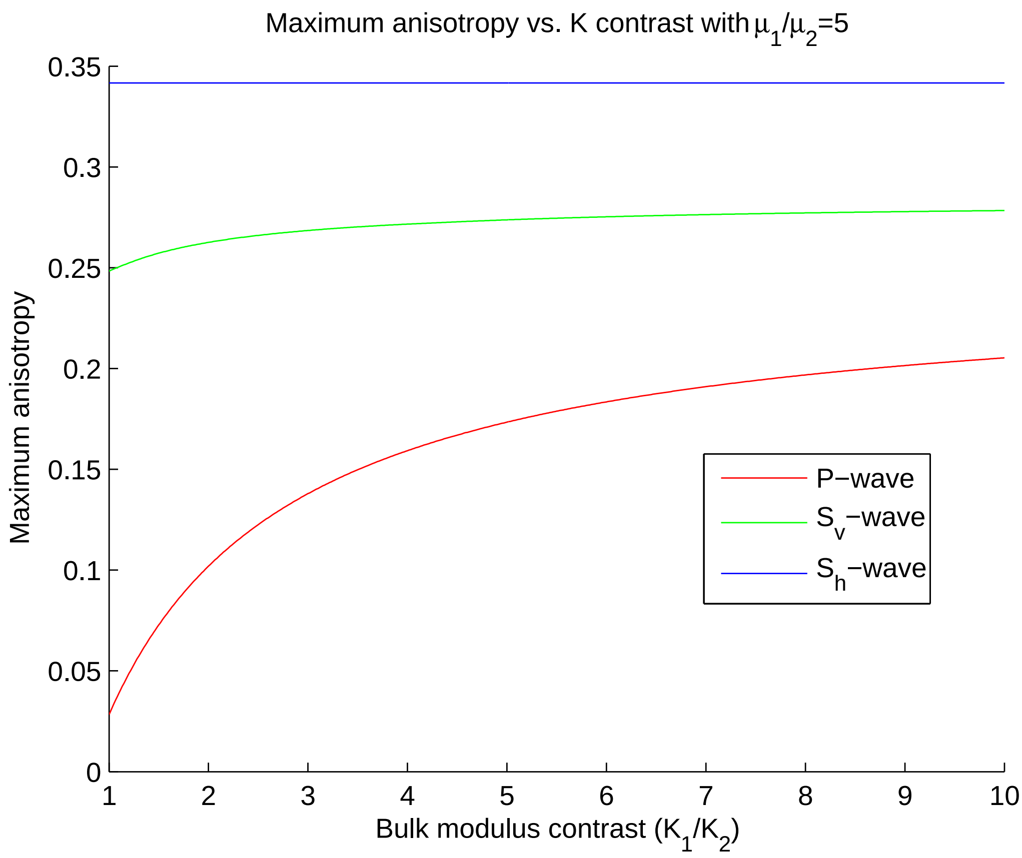


Figure 2.4: Effect of varying bulk modulus contrast on maximum anisotropy, with a constant shear modulus contrast of $\mu_1 = 5\mu_2$

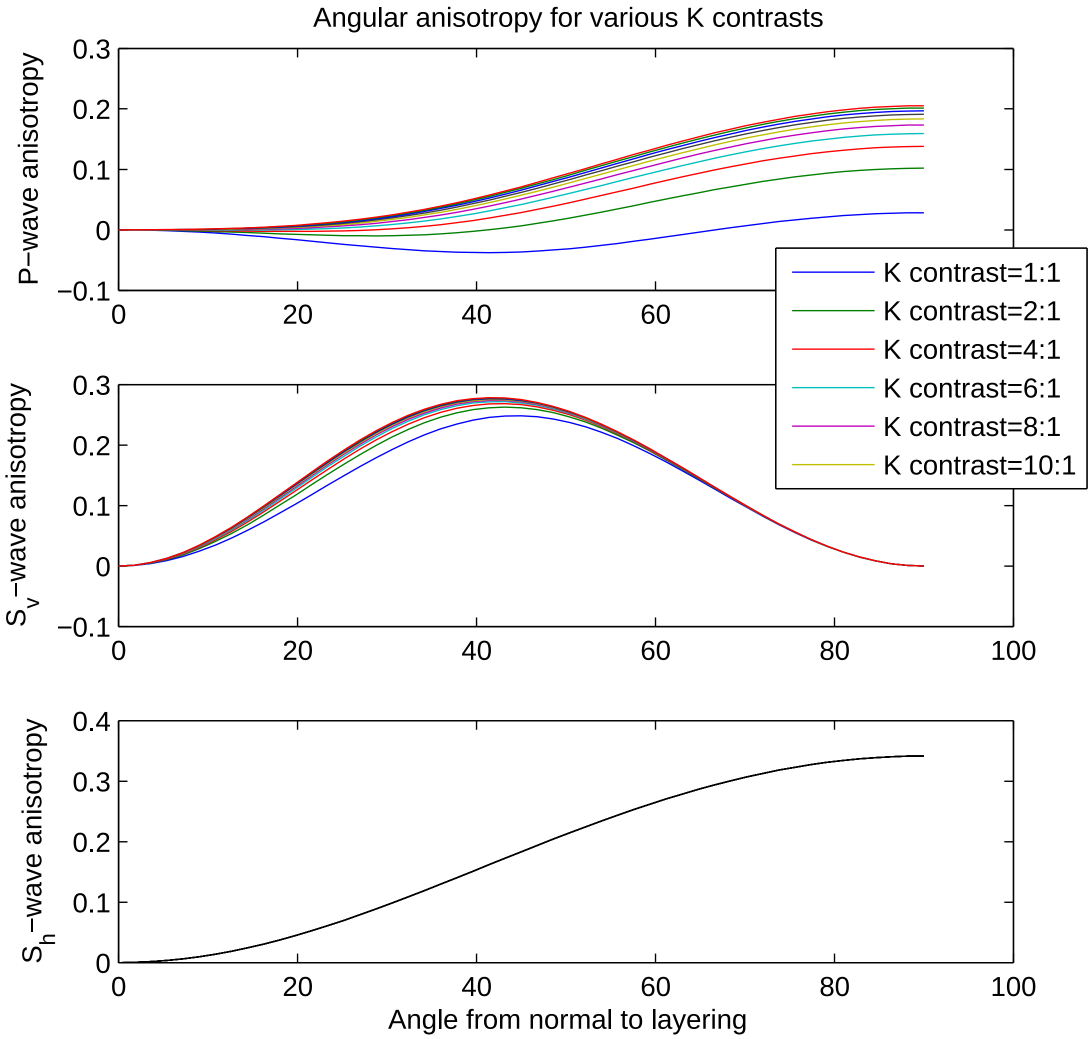


Figure 2.5: Effect of varying bulk modulus contrast on angular anisotropy, with a constant shear modulus contrast of $\mu_1 = 5\mu_2$. The legend gives fractional bulk modulus contrast.

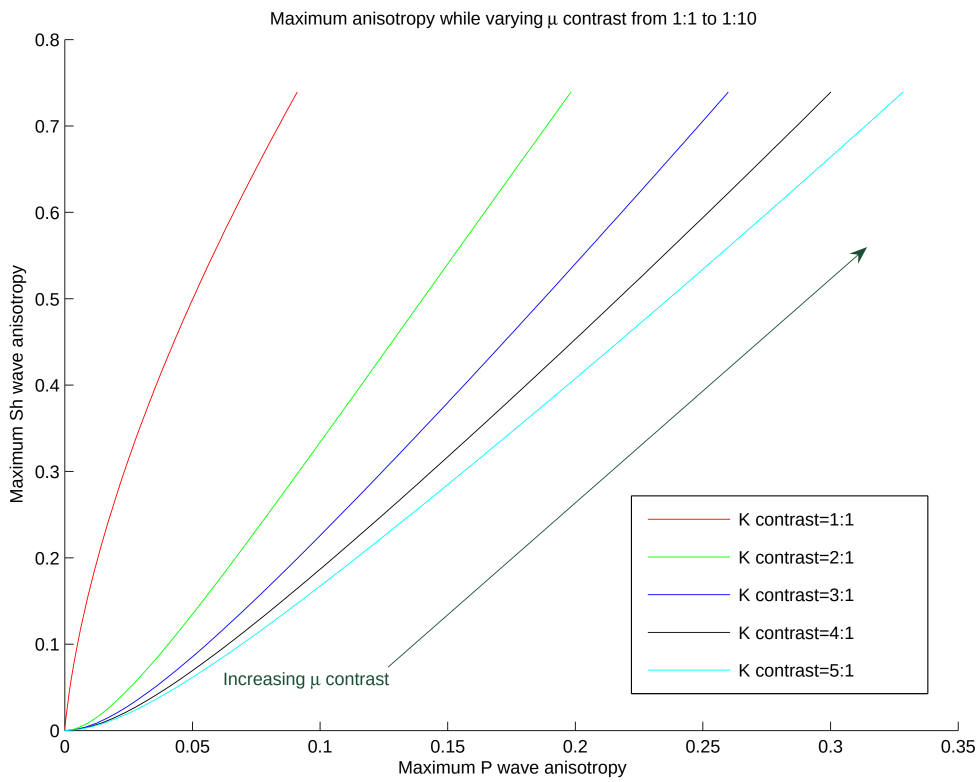


Figure 2.6: Effect of varying both bulk modulus and shear modulus simultaneously. The legend gives fractional bulk modulus contrast.

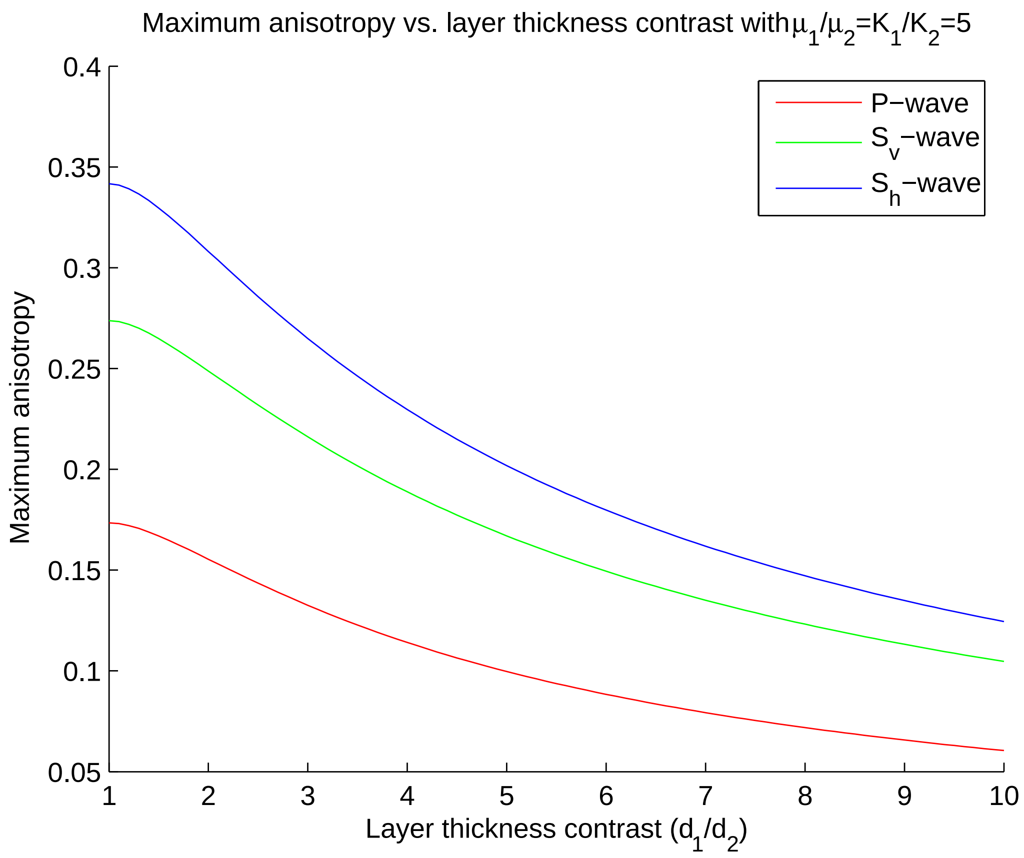


Figure 2.7: Effect of varying layer thickness contrast on maximum anisotropy, with $\mu_1 = 5\mu_2$ and $K_1 = 5K_2$.

With a better understanding of how individual parameters shape the long-wave anisotropy, the next question to be considered is: When does layer induced anisotropy become significant for real rocks?

In order to extend our analysis to real rocks, it is first necessary to define what 'real rocks' are. In exploration, inter-bedded shales and sands are common, so we shall use these as our two members. It is well known that there exists an approximately linear relation between $V_p$ and $V_s$. Various authors have also done regression analysis to demonstrate a correlation between $V_p$ and density $\rho$,(Castagna et al., 1993; Gardner et al., 1974; Wyllie et al., 1956). In order to model results close to reality the expressions given by Castagna et al. (1993) have been used as shown in Equations 2.15-2.18.

Sandstone:

$$V_s(km/s) = .8042V_p - .8559 \tag{2.15}$$

$$\rho = -.0115V_p^2 + .261V_p + 1.515 \tag{2.16}$$

Shale:

$$V_s(km/s) = .7700V_p - .8674 \tag{2.17}$$

$$\rho = -.0261V_p^2 + .373V_p + 1.458 \tag{2.18}$$

These relations are used to define a standard layered media that will be used throughout the rest of this dissertation for consistency. The properties of this standard sand-shale layered media are given in Table 2.1.

Table 2.1: Properties for a standard sand-shale periodic medium

| | Sand | Shale |
|---|---|---|
| $V_p$ ($\frac{km}{s}$) | 4.00 | 2.00 |
| $V_s$ ($\frac{km}{s}$) | 2.36 | .67 |
| $\rho$ ($\frac{gm}{cm^3}$) | 2.37 | 2.10 |
| $\lambda$ $(Gpa)$ | 11.52 | 6.50 |
| $K$ $(Gpa)$ | 20.35 | 7.13 |
| $\mu$ $(Gpa)$ | 13.24 | .95 |

Figure 2.8 shows the maximum anisotropy for a periodic medium composed of alternating shales and sands characterized by the Equations 2.15-2.18. The $P$-wave velocity of the shale is kept constant at 1.5 $km/s$ while the sand velocity is increased from 1.5 $km/s$ to 6 $km/s$. This shows significant anisotropy for reasonable constrasts between the shales and sands. Figure 2.9 looks at a faster shale over a smaller range of contrasts and Figure 2.10 considers the angular anisotropy. It's worthwhile to point out that the $S$-wave anisotropy for a system with a shale $V_p = 1.5$ $km/s$ and a sand with $V_p = 3$ $km/s$ is significantly greater than the apparently similar case of a shale $V_p = 3$ $km/s$ and a sand of 6 $km/s$. This is because the intercept for the $V_p/V_s$ relations is not zero. So a doubling of a smaller $V_p$ leads to a greater fractional change in $V_s$ than does a doubling of a larger $V_p$.

The question, at what contrast does anisotropy become significant, is addressed in Table 2.2. For this, $V_p$ for the shale was kept at 3 $km/s$ ($V_s = 1.44$ $km/s$). Velocities given, are the sand velocities necessary to get the stated amount of maximum anisotropy. From this and Figures 2.8-2.10 it is apparent that $S_h$-wave anisotropy

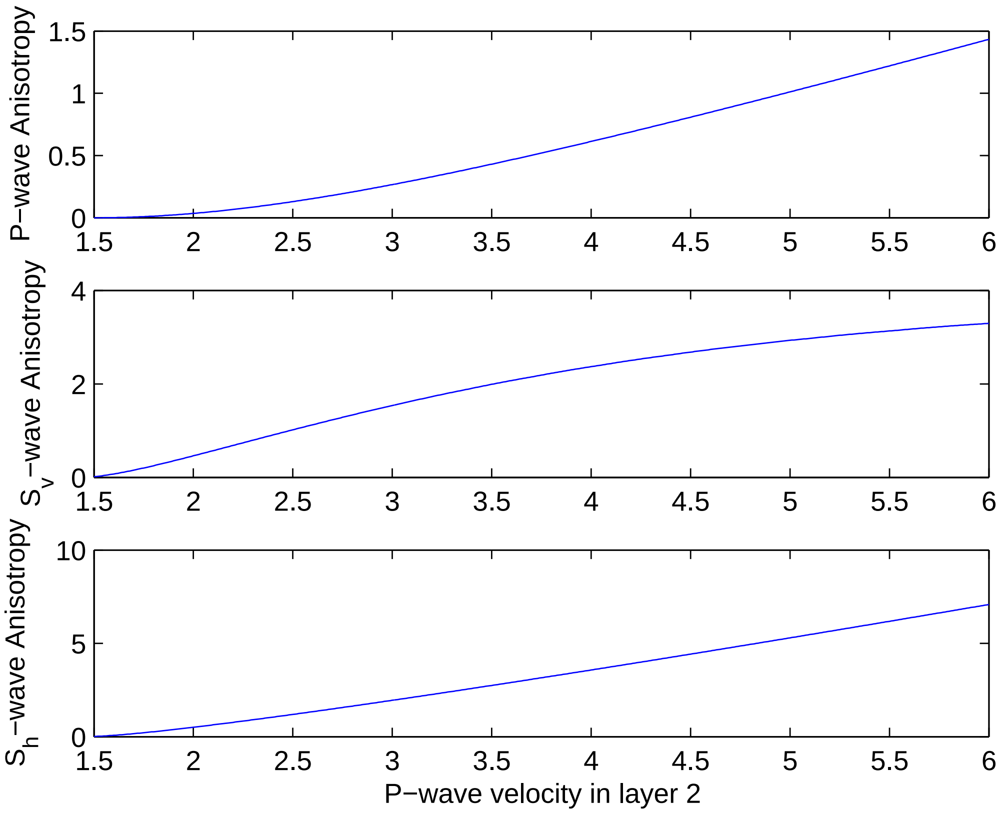


Figure 2.8: Maximum anisotropy for sand-shale system 1. Shale $P$-wave velocity is constant at 1.5 km/s while sand velocity is varied from 1.5-6 km/s.

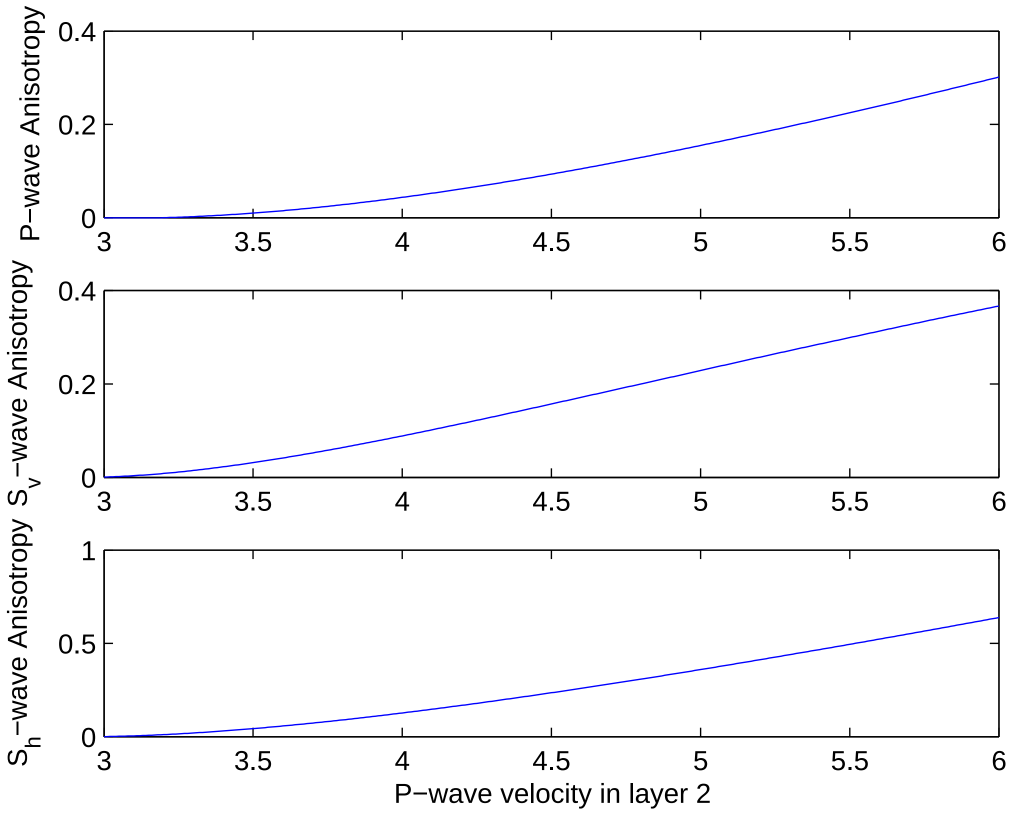


Figure 2.9: Maximum anisotropy for sand-shale system. Shale $P$-wave velocity is constant at 3 km/s while sand velocity is varied from 3-6 km/s.

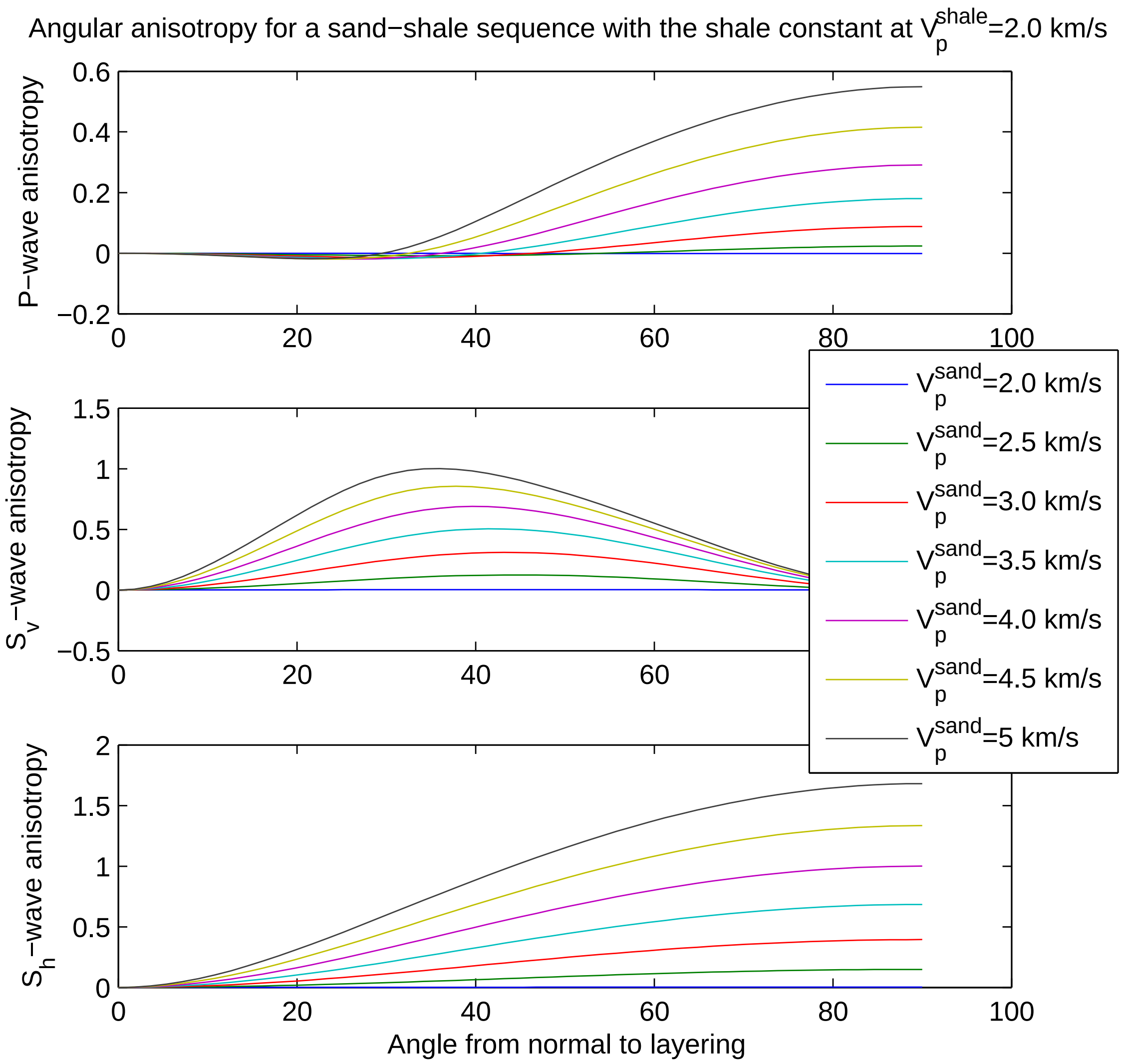


Figure 2.10: Angular anisotropy for sand-shale system. Shale $P$-wave velocity is constant at 2 km/s while sand velocity is varied from 2-5 km/s.

is most sensitive to a velocity contrast and $P$-wave anisotropy is the least sensitive, requiring almost a 2:1 velocity ratio to produce 25 percent anisotropy in this case.

Table 2.2: Maximum anisotropy and the required velocity contrast

| Maximum | Required Sand $V_p$ $(km/s)$ | | | Corresponding Sand $V_s$ $(km/s)$ | | |
|---|---|---|---|---|---|---|
| Anisotropy | $P$-wave | $S_v$-wave | $S_h$-wave | $P$-wave | $S_v$-wave | $S_h$-wave |
| .01 | 3.50 | 3.23 | 3.18 | 1.96 | 1.74 | 1.70 |
| .05 | 4.07 | 3.68 | 3.55 | 2.42 | 2.10 | 2.00 |
| .10 | 4.56 | 4.09 | 3.85 | 2.81 | 2.43 | 2.24 |
| .15 | 4.96 | 4.45 | 4.11 | 3.13 | 2.72 | 2.45 |
| .20 | 5.33 | 4.80 | 4.34 | 3.43 | 3.00 | 2.63 |
| .25 | 5.67 | 5.15 | 4.56 | 3.70 | 3.29 | 2.81 |

## 2.3 Elastic Waves:Anisotropic Constituents

Let's now expand the considerations of the previous chapter to the case where individual layers can be anisotropic. The special cases in which individual layers are transversely isotropic with different axes of symmetry will be given the most attention. The modeling in this section uses the development introduced by Schoenberg and Muir (1989).

The details of the technique are somewhat more complex then for the Backus method and will not be given here. The benefit of this approach is the ability to consider anisotropy of individual layers which may be of a general form. The only condition is that of the 'long-wave' and stationarity for which periodicity is sufficient to be satisfied. Another complication is the calculation of velocities for the case of general anisotropy. In this case the Green-Christofel tensor must be solved numerically for the velocities; the Mathematica$^{TM}$kernel was used to perform these calculations.

The first case that will be considered is that in which one layer has TI symmetry while the other is isotropic. It is obvious that there is now one more degree of freedom in the analysis, the angle that the axis of symmetry of the TI layer makes with the layering of the overall medium. In the special case that the axis of symmetry is normal to the layering it is obvious that the effective symmetry will still be VTI, as in the isotropic case. One can also examine the special case that occurs when the symmetry axis of the TI layer is parallel to the layering. The effective medium anisotropy in this case is shown to be that of orthorhombic symmetry. The general case for a TI layer oriented at arbitrary angles is also considered here.

For the initial considerations, the elasticity matrix for a TI layer will be constructed by considering the effective anisotropy of a layered media as given in the previous chapter, where one layer is a sand with $V_p = 4\frac{km}{s}$ and the other is a shale with $V_p = 2\frac{km}{s}$. The relative thicknesses are taken to be the same. The resulting effective elastic constants are then taken to represent the TI layer which is alternated with a sand isotropic layer with $V_p = 4\frac{km}{s}$. Since, in the case of general symmetries, velocity can vary with azimuth, velocities will now be represented by spheroids in three dimensions. Figure 2.11 represent the velocities for this medium in the case that the axis of symmetry for the TI layer is normal to the layering. Figure 2.12 gives the velocities in the vertical plane as a function of angle from the normal. This is simply a vertical slice through a northern quadrant of Figure 2.11.

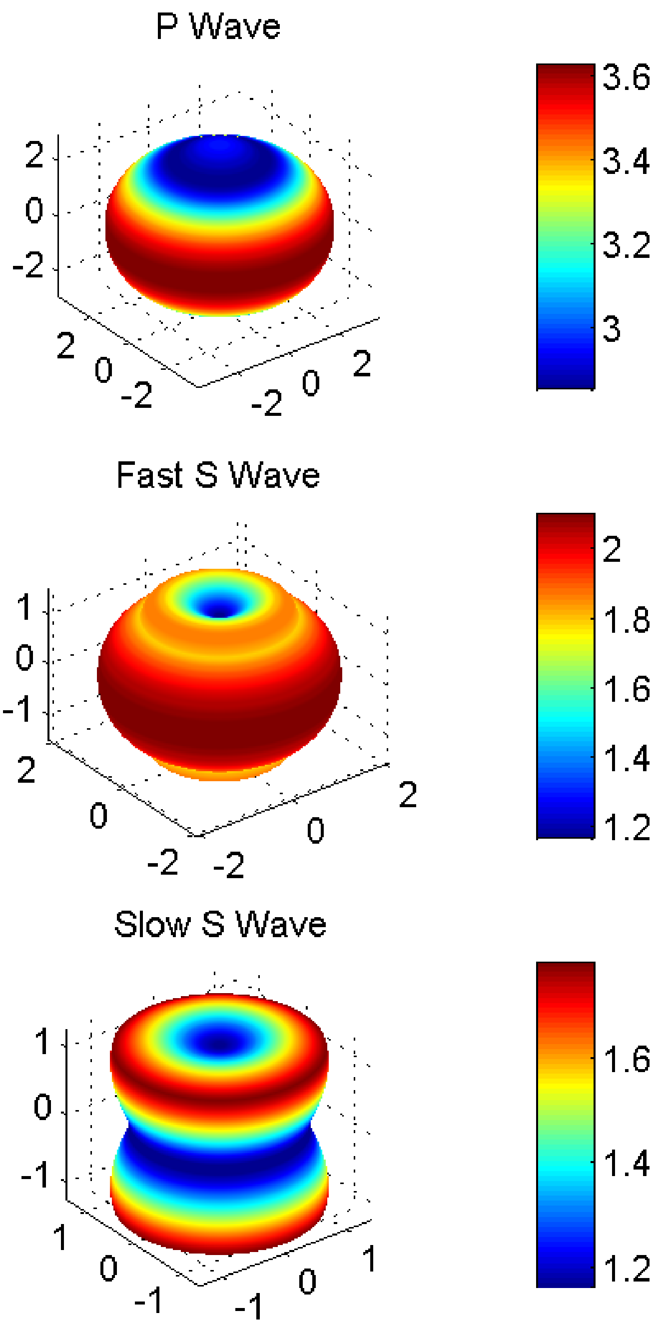


Figure 2.11: Velocity spheroids for TI axis normal to layering, magnitude of the velocity is given in km/s by the color bars

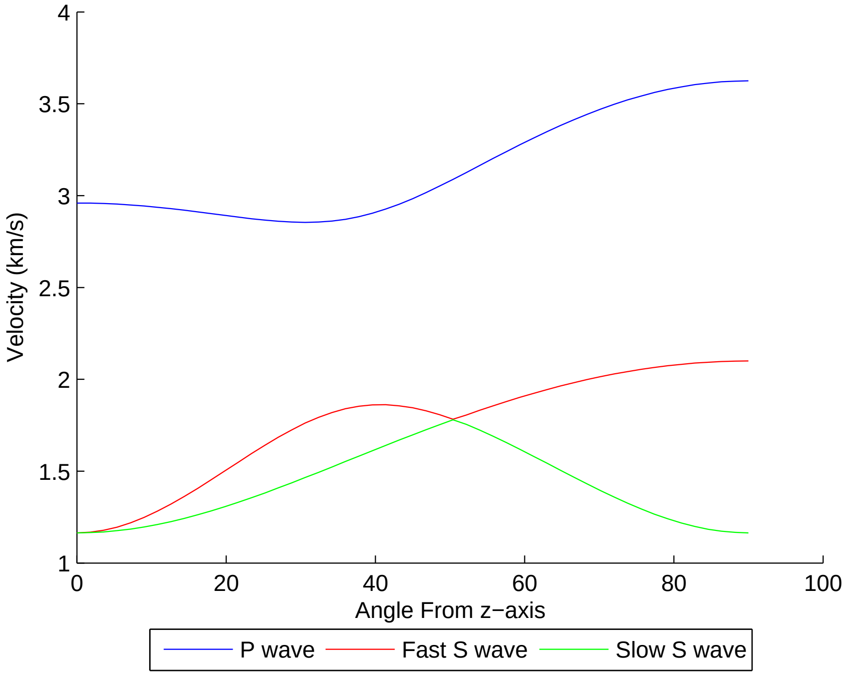


Figure 2.12: Velocity slice of vertical plane for the case with the TI axis normal to layering. Note that S-waves are defined as fast or slow, not polarization in this case.

For the general case where the axis of symmetry of the TI layer is at some angle to the layering of the medium, the elastic constants for the rotated TI medium must first be found. When the axis of symmetry is rotated about a given axis, the transformation, as given by Ting (1996) is:

$$C^* = KCK^T$$

where $C$ is the elasticity matrix in the original coordinate system, $C^*$ is the elasticity matrix after a rotation by angle $\theta$. For the special case of rotation about the y-axis $K$ is:

$$K = \begin{bmatrix} m^2 & n^2 & 0 & 0 & 0 & 2mn \\ n^2 & m^2 & 0 & 0 & 0 & -2mn \\ 0 & 0 & 1 & 0 & 0 & 0 \\ 0 & 0 & 0 & m & -n & 0 \\ 0 & 0 & 0 & n & m & 0 \\ -mn & mn & 0 & 0 & 0 & m^2-n^2 \end{bmatrix}$$

where $m = \cos\theta$ and $n = \sin\theta$.

With this definition one is free to consider the case where the TI layer has an axis of symmetry that is at some angle $\theta$ with respect to the layering. For the special case where $\theta = \frac{\pi}{2}$ the resulting anisotropy of the system is orthorhombic and, for the system under consideration, is shown in Figure 2.13. Velocity slices for each of the three orthogonal planes are shown in figure 2.14. The most important observation to make here is the distinctively different behavior of the shear wave splitting in the different symmetry planes. The shear wave velocities never touch in the z-x plane, while there are two 'kissing points'[1] in the z-y plane and one in the x-y plane.

Behavior at general angles between the two special cases that have been considered can also be explored. Figures 2.15-2.17 show the effective velocities as a function of the rotation of the TI layer for $P$-waves, fast $S$-waves and slow $S$-waves, respectively.

[1] An angle at which there is no shear wave splitting, such that the fast and slow shear wave velocities are the same is commonly referred to as the kissing point.

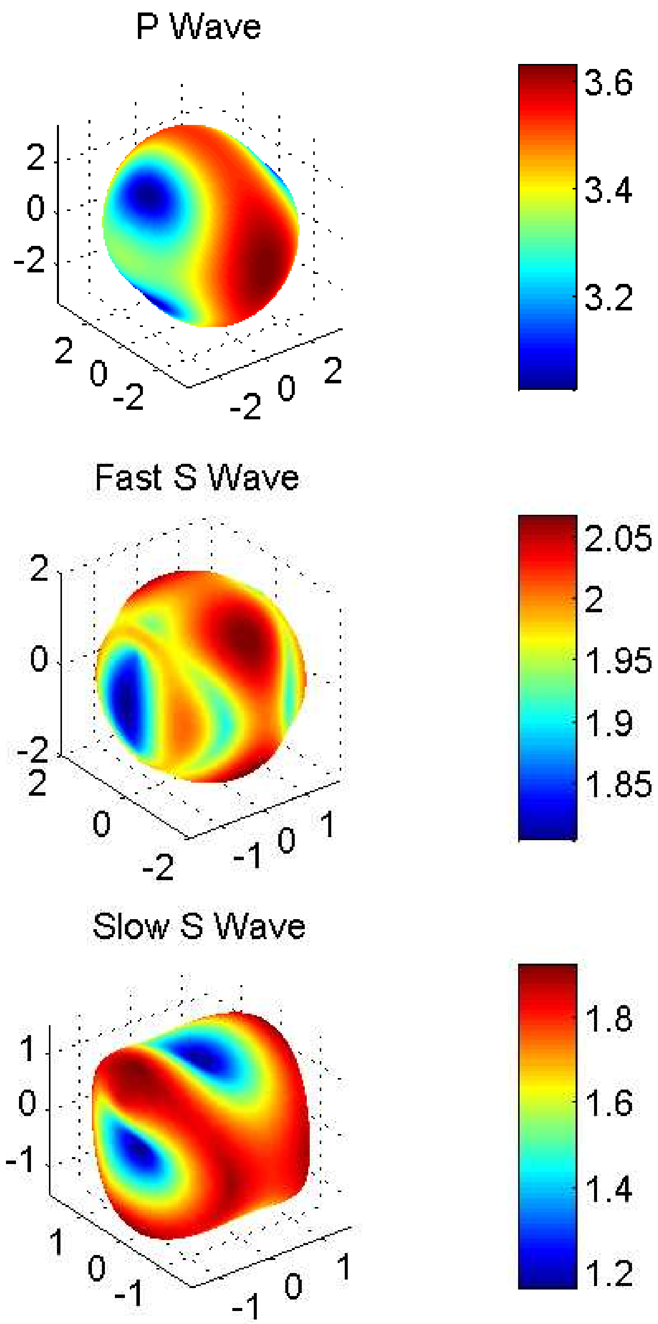


Figure 2.13: Velocity spheroids for TI axis parallel to layering, magnitude of the velocity is given in km/s by the color bars

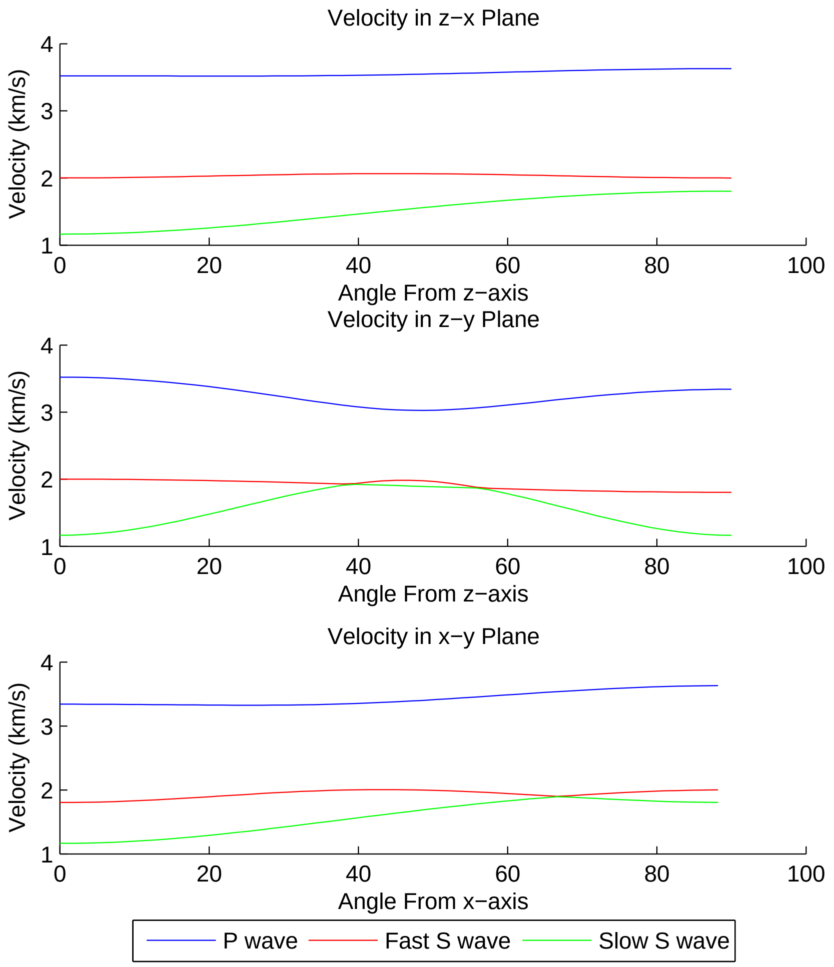


Figure 2.14: Velocity slice of vertical plane for the case with the TI axis parallel to layering.

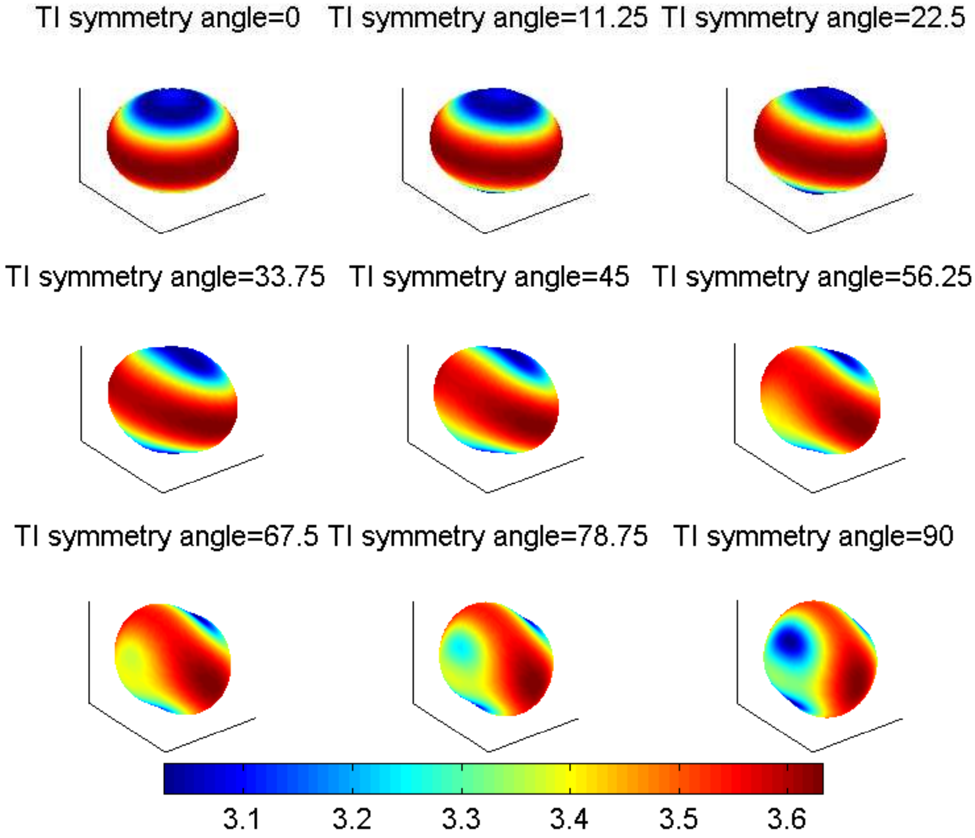


Figure 2.15: Effect on compressional wave velocity of varying the angle that the TI layer axis of symmetry makes with the layering of the medium, velocity in a given direction is given by the color bar in km/s

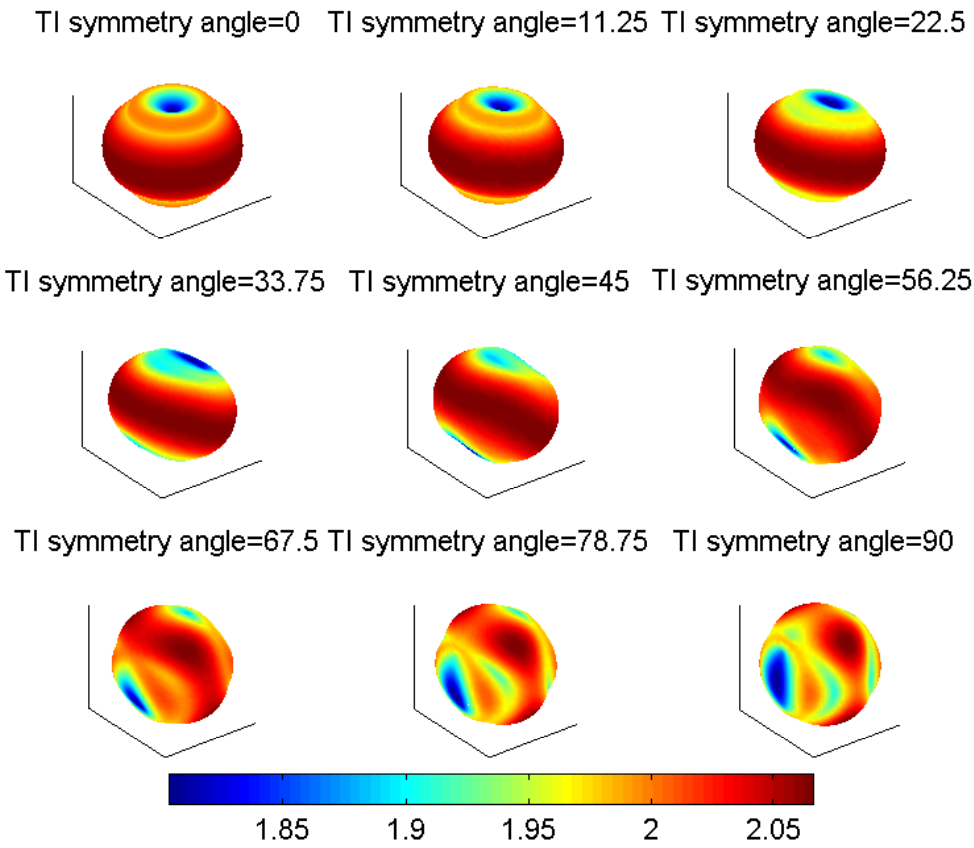


Figure 2.16: Effect on the slow shear wave velocity of varying the angle that the TI layer axis of symmetry makes with the layering of the medium, velocity in a given direction is given by the color bar in km/s

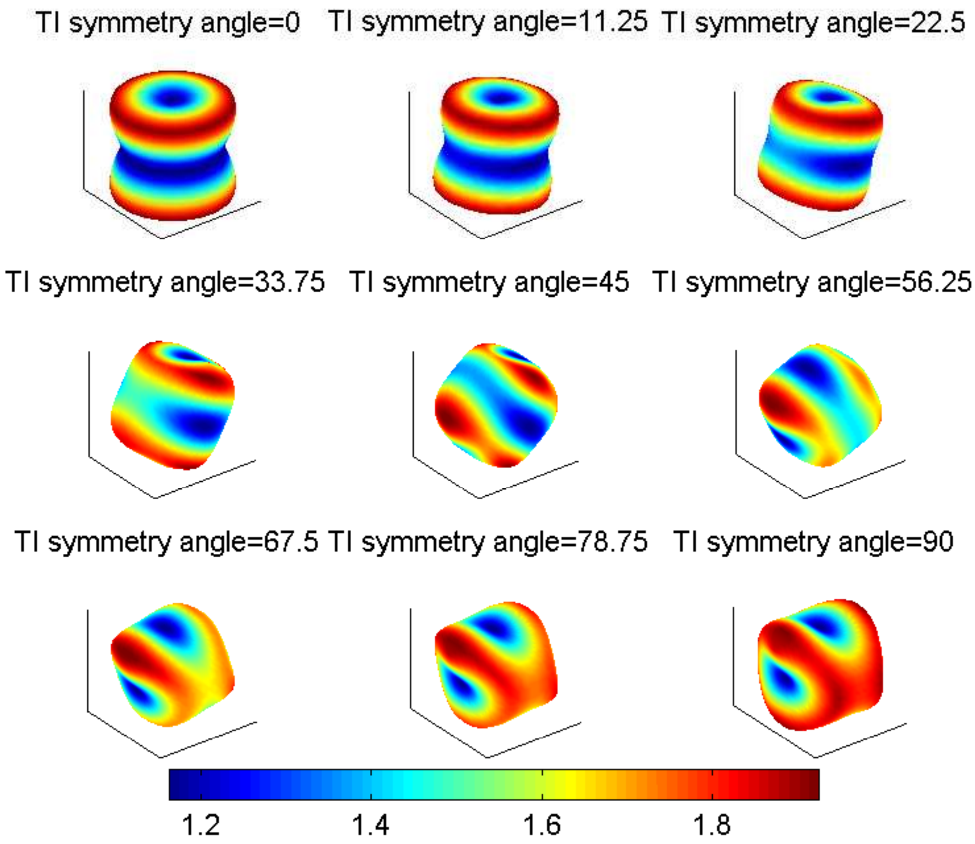


Figure 2.17: Effect on the fast shear wave velocity of varying the angle that the TI layer axis of symmetry makes with the layering of the medium, velocity in a given direction is given by the color bar in km/s

## 2.4 Electromagnetic Waves

In this section, the modeling of electromagnetic waves in a periodic media is discussed. In an identical manner to the elastic case, when considering a periodic media of alternating isotropic layers, it will behave as if it was a homogenous anisotropic media. For electromagnetic waves the term hexagonal is traditionally used in place of VTI to describe its symmetry, although physically there is no difference in the symmetry. This is because of the historical connection between EM wave propagation and crystallography. Hexagonal symmetry, which is induced by isotropic constituents much larger then the atomic scale but much smaller than the illuminating wavelength, is known as form birefringence (Born and Wolf, 1999). Electromagnetic waves in a uniaxial crystal propagate as two different modes, TE and TM. TE refers to the electric field transverse to the plane of incidence, and TM to the case with the magnetic field transverse to the plane of incidence. This can be considered analogous to two possible polarizations of the shear wave in anisotropic elastic wave propagation. Obviously there is no compressional wave in this case[2].

Rytov (1956b) derives equivalent permittivities and magnetic permeabilities for the long-wave periodic medium in the same manner as the elastic case. He uses Floquet's theorem to write a solution in periodic coefficients from which the dispersion relation is found. By taking the long-wave limit, the EM values for the equivalent VTI medium are found.

It is well known that the phase velocity for electromagnetic waves is given by:

$$v = \frac{c}{\sqrt{\epsilon\nu}} \tag{2.19}$$

where $c$ is the speed of light in a vacuum, $\epsilon$ is the relative permittivity, and $\nu$ is the relative magnetic permeability. For a more detailed understanding of where this

[2]Theoretically EM 'P-waves' can exist, but are so strongly attenuated as to be unmeasurable, the notable exception being plasmas (Landau and Lifshitz, 2003).

velocity comes from, the reader is invited to look at one of the many excellent EM text books such as, Griffiths (1999) or Jackson (1998).

The Long-wave equivalent medium values are:

$$\bar{\epsilon} = \frac{a\epsilon_1 + b\epsilon_2}{a+b} \tag{2.20}$$

$$\bar{\nu} = \frac{a\nu_1 + b\nu_2}{a+b} \tag{2.21}$$

$$\tilde{\epsilon} = \frac{\epsilon_1\epsilon_2(a+b)}{a\epsilon_2 + b\epsilon_1} \tag{2.22}$$

$$\tilde{\nu} = \frac{\nu_1\nu_2(a+b)}{a\nu_2 + b\nu_1} \tag{2.23}$$

with corresponding velocities

$$v_0 = \frac{c}{\sqrt{\tilde{\epsilon}\bar{\nu}}} \tag{2.24}$$

$$v_e = \frac{c}{\sqrt{\bar{\epsilon}\tilde{\nu}}} \tag{2.25}$$

Here $v_o$ is the so called ordinary velocity and $v_e$ is the extraordinary velocity. The corresponding velocities for the TE and TM modes are (Born and Wolf, 1999):

$$v_{TE}^2 = v_o^2$$

$$v_{TM}^2 = v_o^2 cos^2\theta + v_e^2 sin^2\theta$$

It is important to note that for the thin layered medium, $v_e > v_o$, (negative uniaxial); therefore, $v_{TM}$ is always greater or equal to $v_{TE}$ (Lekner, 1994). It can also be seen that $v_{TE} = v_{TM}$ for propagation normal to the layers and that $v_{TM}$ is at a maximum parallel to the layering. This is analagous to $S_h$ and $S_v$ elastic waves being equivalent normal to layering and $S_h$ being a maximum normal to layering. The only difference being in the $S_v$-wave which has the added complication of coupling with the $P$-wave.

Before moving to this analysis a simplification will be introduced. For most rocks, the relative magnetic permeability is very close to unity. In the common literature containing electromagnetic properties of rocks, the magnetic permeability is not even given (Olhoeft, 1989; Carmichael, 1989). Because of this, it can be said that for any two media of concern $|\epsilon_1 - \epsilon_2| \gg |\nu_1 - \nu_2|$, allowing a value of $\nu = 1$ to be assumed in this analysis.

The anisotropic behavior that arises with a contrast in permittivity between layers can be seen in Figure 2.18. There is a clear increase in anisotropy with increasing contrast. Figure 2.19 shows how the maximum anisotropy increases with increasing contrast.

Varying the layer thickness with a constant material contrast, as expected, has the same effect as the elastic case. As one layer becomes much thicker than the other the material approaches the value of the thicker layer and anisotropy decreases. This is shown in Figure 2.20.

Figure 2.21 gives the maximum anisotropy for real values. Based on published values, most rocks are assumed to lie between a velocity of $7.5e7$ $m/s$ and $1.5e8$ $m/s$, assuming the magnetic permeability for rocks is equal to that in a vacuum this gives relative electrical permittivity values from 4-16.

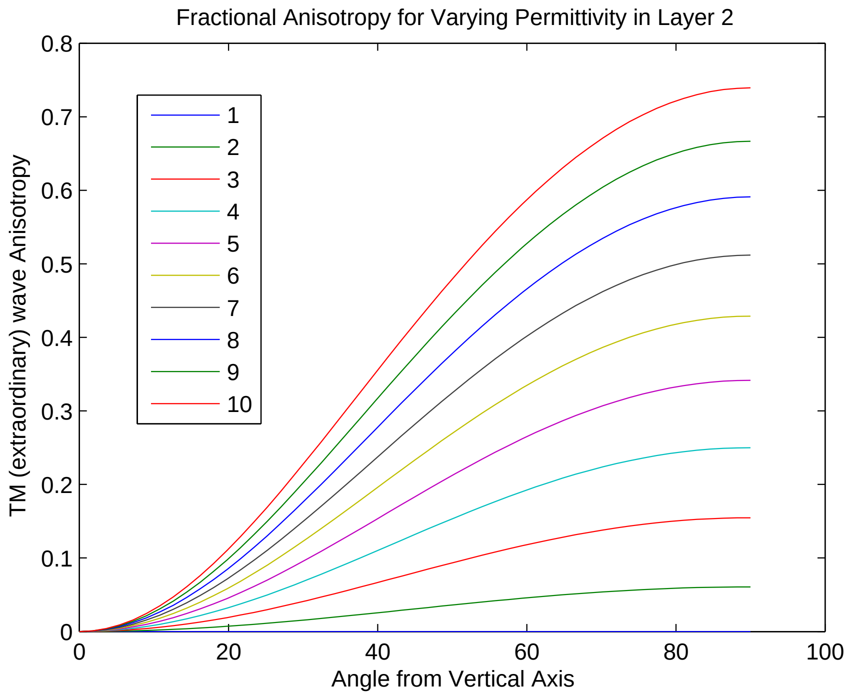


Figure 2.18: Effect of varying shear permittivity contrast on maximum anisotropy, with equal layer thickness. The legend indicates permittivity contrast between layers.

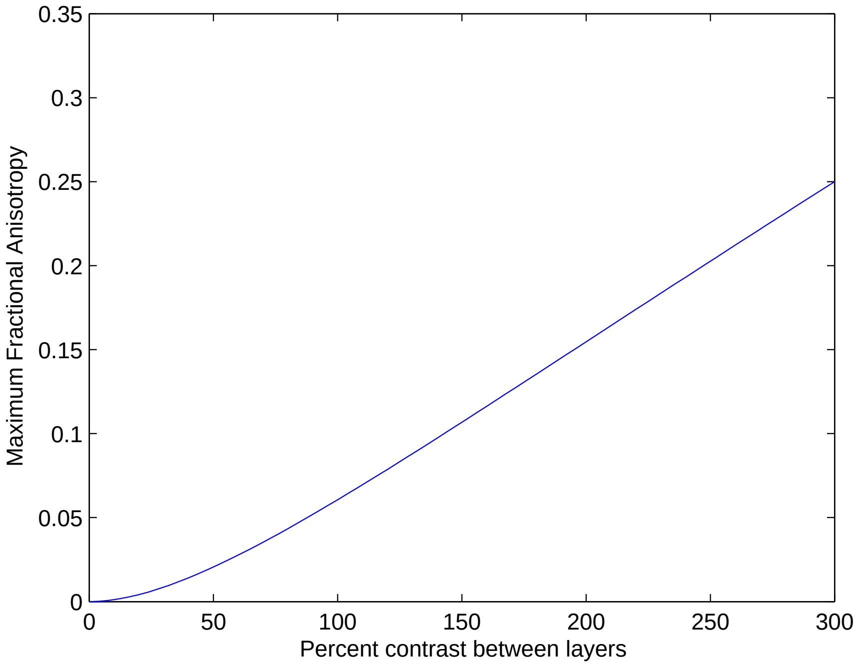


Figure 2.19: Effect of varying permittivity contrast on maximum anisotropy, with equal layer thickness.

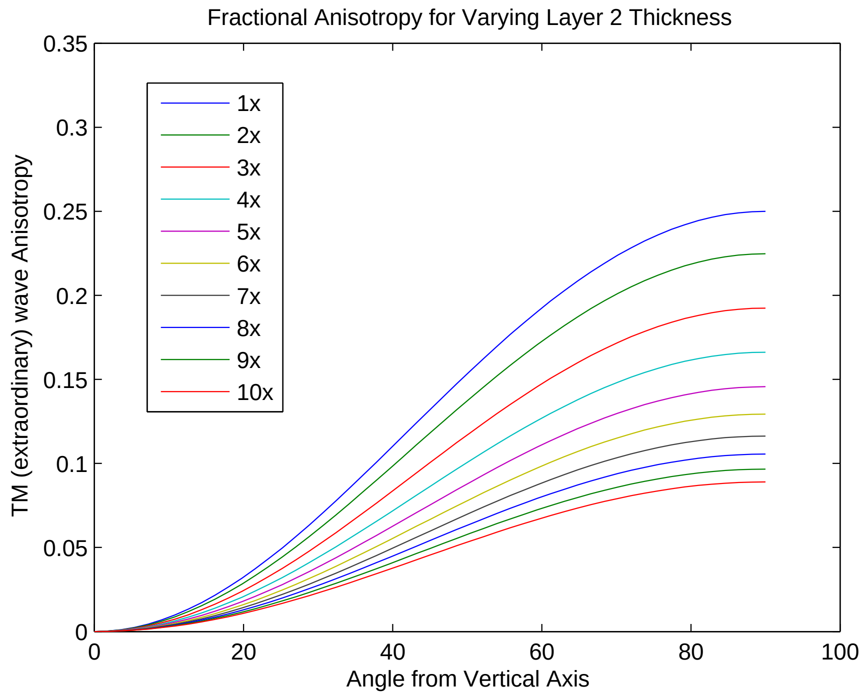


Figure 2.20: Effect of varying layer thickness on anisotropy, with a constant permittivity contrast of $\epsilon_1 = 4\epsilon_2$.

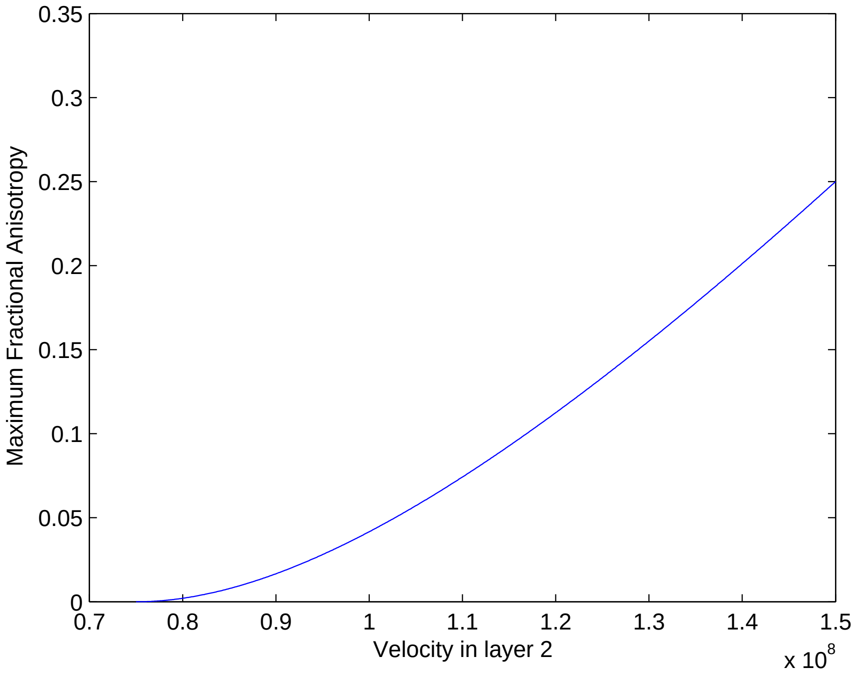


Figure 2.21: Effect of varying velocity on anisotropy.

## 2.5 Comparison of Elastic and Electromagnetic Waves

A comparison of electromagnetic and elastic waves in thin layered media shows many similarities in the degree of anisotropy for a similar contrast. Figure 2.22 compares velocity contrast to anisotropy for both the EM and elastic cases. From this there does not appear to be a difference in the amount of layer induced anisotropy for a given layer velocity contrast.

The differences that do arise are primarily due to the lack of a compressional mode in electromagnetic wave propagation. A simple way to understand this difference is to consider what is happening at a given layer boundary. An elastic shear wave with vertical polarization incident on the boundary will give rise to both compressional and shear wave reflected and transmitted modes. The same behavior occurs when a compressional wave is incident on the boundary. This gives rise to the 'coupled' nature of $P$- and $S_v$-waves in the elastic case. However, since compressional modes do not propagate in the electromagnetic case the vertically polarized (TE mode, for no $\nu$ contrast) does not exhibit this coupled behavior. The horizontally polarized shear wave and TM EM wave only give rise to identical modes upon reflection and refraction and, therefore, behave identically in both cases.

The more important differences arise when considering the property that is being seen by a given type of wave. A given change in lithology may result in a large change in elastic properties but a small change in electromagnetic properties or vice-versa. The wavelength to period ratio can also differ substantially; just as scale

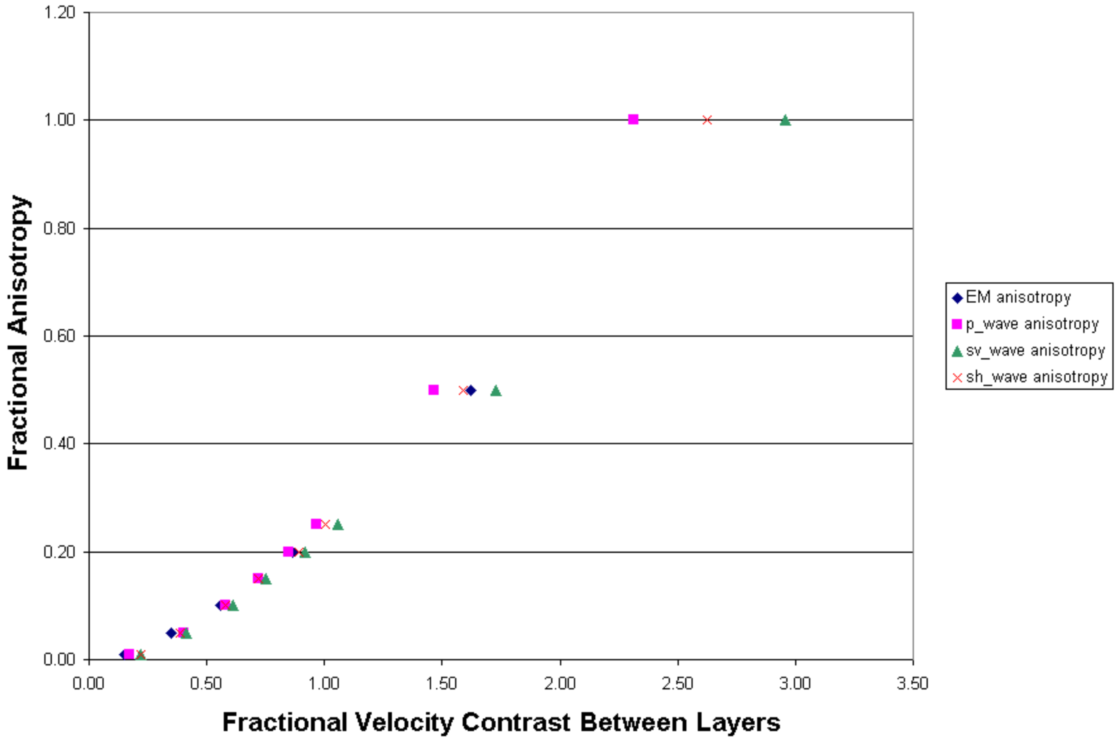


Figure 2.22: A comparison of anisotropy for both EM and elastic waves

considerations change between sonic and seismic, they also differ depending on EM frequencies. The next chapter introduces the tools needed for consideration of scale with respect to wavelength of a given mode of insonification.

# Chapter 3

# Layered Periodic Media: Frequency Dependency

Solutions to differential equations with periodic coefficients have a long history. The technique which has been used for the study of waves in periodic media is most commonly called Floquet's theory and was first published in a paper by Floquet in 1883. Other 're-discoveries' of Floquet's solutions were made by Lyaponov, and later by Bloch who considered solutions in three dimensions. Bloch is quotted by Kittel (1976) as saying:

> *When I started to think about it, I felt the main problem was to explain how the electrons could sneak by all the ions in a metal...By straight Fourier analysis I found to my delight that the wave differed from the plane wave of free electrons only by a periodic modulation.*

This chapter will provide an introduction to using Floquet's theory to quantify the dispersive behavior that results in layered media due to periodic scattering. It provides the background that will be used in the next chapter to explore how material contrasts control and affect this behavior, and what this means for real periodic materials.

## 3.1 Floquet's Solution For Isotropic Layers

### 3.1.1 Elastic Waves

The wave equation for a periodic layered, anisotropic medium is:

$$\rho(x_1)\frac{\partial^2 u_i}{\partial t^2} = \frac{\partial}{\partial x_j} C_{ijkl}(x_1)\frac{\partial u_k}{\partial x_l} \tag{3.1}$$

By virtue of the Floquet Theorem, equations for the two constituents will be considered separately, i.e., the $\rho$ and $C_{ijkl}$ dependency in the $x_1$-direction will momentarily be disregarded. This allows the elasticity constants to be moved outside the derivative, giving:

$$\rho\frac{\partial^2 u_i}{\partial t^2} = C_{ijkl}\frac{\partial}{\partial x_j}\frac{\partial u_k}{\partial x_l} \tag{3.2}$$

Here the elasticity matrix for a given layer is:

$$\begin{bmatrix} \lambda+2\mu & \lambda & \lambda & 0 & 0 & 0 \\ \lambda & \lambda+2\mu & \lambda & 0 & 0 & 0 \\ \lambda & \lambda & \lambda+2\mu & 0 & 0 & 0 \\ 0 & 0 & 0 & \mu & 0 & 0 \\ 0 & 0 & 0 & 0 & \mu & 0 \\ 0 & 0 & 0 & 0 & 0 & \mu \end{bmatrix} \tag{3.3}$$

The standard approach of breaking this into two separate parts, the so called solenoidal, and non-solenoidal parts is taken by considering the total displacement to be the sum of the gradient of a scalar potential and the curl of a vector potential,

$$\vec{u} = \nabla\phi + \nabla \times \vec{\psi}$$

or, in indicial notation:

$$u_p = \phi_{,p} + \varepsilon_{pqr}\psi_{r,q} \tag{3.4}$$

where $\epsilon_{pqr}$ is the Levi-Civita tensor, and the comma before an index indicates differentiation with respect to that index. Wave propagation in the $u_1$-direction is considered first. By substituting in $C_{ijkl}$, and using the identity above, the wave equation becomes:

$$\rho\frac{\partial^2}{\partial t^2}(\phi_{,i} + \varepsilon_{iqr}\psi_{r,q}) = C_{ijkl}\frac{\partial}{\partial x_j}\frac{\partial}{\partial x_l}(\phi_{,k} + \varepsilon_{kqr}\psi_{r,q}) \tag{3.5}$$

$$\rho\frac{\partial^2}{\partial t^2}(\phi_{,1}+(\psi_{3,2}-\psi_{2,3}))=(\lambda+2\mu)\phi_{,111}+\mu(\psi_{3,211}-\psi_{2,311}) \tag{3.6}$$

Using the definition $\psi_1^* = \psi_{3,2} - \psi_{2,3}$ and generalizing to three dimensions the equation of motion in an isotropic system becomes:

$$\rho\frac{\partial^2}{\partial t^2}(\frac{\partial\phi}{\partial x_i}+\psi_i^*)=\frac{\partial^2}{\partial x_i^2}((\lambda+2\mu)\frac{\partial\phi}{\partial x_i}+\mu\psi_i^*) \tag{3.7}$$

It is clear here that $\psi_i^*$ is the $i^{th}$ component of the curl of a solenoidal vector potential with zero divergence. Separate equations for the so called $P$- and $S$-waves are found by considering zero curl or zero divergence, respectively.

$$\rho\frac{\partial^2}{\partial t^2}\frac{\partial\phi}{\partial x_i}=(\lambda+2\mu)\frac{\partial^2}{\partial x_i^2}\frac{\partial\phi}{\partial x_i} \tag{3.8}$$

$$\rho\frac{\partial^2\psi_i^*}{\partial t^2}=\mu\frac{\partial^2\psi_i^*}{\partial x_i^2} \tag{3.9}$$

By recognizing that the $i^{th}$ derivative can be removed from the equation for the scalar potential it can be written:

$$\rho\frac{\partial^2\phi}{\partial t^2}=(\lambda+2\mu)\frac{\partial^2\phi}{\partial x_i^2} \tag{3.10}$$

Due to the symmetry of the layered media, it is clear that the problem may be completely characterized by considering wave propagation constrained to any given vertical plane. For simplicity then this analysis will be restrained to the $x_1$-$x_2$ plane, which will be referred to as the z-y plane. The problem is now such that two separate cases can be considered: the first in which the displacement field is in the $z$-$y$ plane and the second in which the displacement is orthogonal to the $z$-$y$ plane. The first case corresponds to $P$- and $S_v$-waves, while the second corresponds to $S_h$-waves. The derivation for the first case was given by Sve (1971) and is replicated here with some deviations and clarifications; the most prominent being the explicit consideration of the component wave numbers, $k_z$ and $k_y$ which leads to a more intuitive understanding of the periodic scattering implicit in the Floquet solution. The solution for the second case using the same approach is also given.

For the first case the following solutions will be considered,

$$\phi = f_j(z)e^{i(k_z z + k_y y - \omega t)} \tag{3.11}$$

$$\psi_x = g_j(z)e^{i(k_z z + k_y y - \omega t)} \tag{3.12}$$

where $k_z$ and $k_y$ are the $z$- and $y$-components of the wave vector $\mathbf{k}$ such that $k_z = |k| \cos\theta$ and $k_y = |k| \sin\theta$. Here, $\theta$ is the angle from the $z$-axis. The subscript $j$ refers to the solution in the $j^{th}$ layer. In accordance with Floquet's theorem $f_j(z)$ and $g_j(z)$ are periodic with a period $d$ equal to the medium such that $f_j(z) = f_j(z+d)$ and $g_j(z) = g_j(z+d)$. The necessity for only providing a solution for $\psi_3$ will be clarified later.

For the first case, isotropic layers are considered such that there are only two independent elastic constants in each layer, $\lambda + 2\mu$ and $\mu$, corresponding to the compressional and shear waves, respectively.

Substituting Equations 3.11 and 3.12 into Equations 3.10 and 3.9 yields second order differential equations for the periodic coefficients $f_j(z)$ and $g_j(z)$. These equations have the following solutions:

$$f_j(z) = A_j e^{-iz(k_z - \sqrt{\frac{\omega^2}{c_{lj}^2} - k_y})} + B_j e^{-iz(k_z + \sqrt{\frac{\omega^2}{c_{lj}^2} - k_y})} \tag{3.13}$$

$$g_j(z) = C_j e^{-iz(k_z - \sqrt{\frac{\omega^2}{c_{tj}^2} - k_y})} + D_j e^{-iz(k_z + \sqrt{\frac{\omega^2}{c_{tj}^2} - k_y})} \tag{3.14}$$

where $c_{tj}$ and $c_{lj}$ are the isotropic shear and compressional wave velocities, respectively.

Further intuition into the Floquet solution can be gained by considering these periodic coefficients. First $\frac{\omega}{c_j} = k_j$ the wavenumber in layer $j$. $k_y$ can also be rewritten as:

$$k \sin\theta = \frac{\omega}{c_{eff}} \sin\theta = \omega p$$

where $c_{eff}$ is the velocity of the Floquet wave and $p$ is the horizontal slowness. I avoid calling $p$ the ray parameter because in this case $c_{eff}$ is a phase velocity. Now consider the wave propagating in layer $j$ with:

$$k_y = \omega p = \omega \frac{\sin\theta_j}{c_j}$$

where $\theta_j$ is the angle of propagation in layer $j$. It is now clear that the square root in the exponent can be written as

$$\omega(\frac{1}{c_j^2} - \frac{\sin\theta_j{}^2}{c_j^2}) = \frac{\omega}{c_j}(1 - \sin\theta^2) = \frac{\omega}{c_j}\cos\theta_j = k_{zj}$$

where $k_{zj}$ is recognized as the z component of the wave vector in layer $j$. This allows for rewriting the solutions for the periodic coefficients as:

$$f_j(z) = A_j e^{-iz(k_z - k_{zlj})} + B_j e^{-iz(k_z + k_{zlj})} \quad (3.15)$$

$$g_j(z) = C_j e^{-iz(k_z - k_{ztj})} + D_j e^{-iz(k_z + k_{ztj})} \quad (3.16)$$

It is now clear that the effective 'Floquet wave' is characterized by the combination of upward and down going plane waves characterized by vertical wave numbers $k_{z(l,t)j}$ in the individual layers. While this is obvious for vertical 'Floquet waves' it must be stressed that $k_{z(l,t)i} \neq 0$ in at least one of the layers for the case of horizontally traveling 'Floquet waves'.

For this system to apply, certain boundary conditions must be met. Both the amplitudes of the displacements and stresses must be continuous across the boundary between any two layers. So, the solutions for the displacement and stresses must converge as one approaches a boundary from opposite sides. If we arbitrarily place the $z$ origin at the boundary this gives the following conditions:

$$u_z(0) = u_z^*(0)$$

$$u_y(0) = u_y^*(0)$$

$$u_z(d_1) = u_z^*(-d_2)$$

$$u_y(d_1) = u_y^*(-d_2)$$

$$\sigma_{zy}(0) = \sigma_{zy}^*(0)$$

$$\sigma_{yy}(0) = \sigma_{yy}^*(0)$$

$$\sigma_{zy}(d_1) = \sigma_{zy}^*(-d_2)$$

$$\sigma_{yy}(d_1) = \sigma_{yy}^*(-d_2)$$

where Hooke's law in isotropic medium gives the stress as $\sigma_{ij} = \lambda\delta_{ij}\varepsilon_{kk} + 2\mu\varepsilon_{ij} = \lambda\delta_{ij}u_{k,k} + \mu(u_{i,j} + u_{j,i})$ where $i$ and $j$ correspond to the x-,y-, and z-directions in this case. The displacements are found using equation 3.4, such that:

$$u_z = \phi_z + \psi_{x,y} - \psi_{y,x}$$

$$u_y = \phi_y + \psi_{z,x} - \psi_{x,z}$$

$$u_x = \phi_x + \psi_{y,z} - \psi_{z,y} = 0$$

Since it is clear that for displacements constrained to the $z$-$y$ plane $\psi_{i,x} = 0$, it is only necessary to consider the solution for $\psi_x$.

Using the above boundary conditions gives eight equations with eight unknowns. In order for a non-trivial solution to the above system to exist, the determinant of the coefficient matrix must vanish, which is the same as stating that the rows must be linearly dependent. For ease of representation this 8x8 matrix is represented by the following 4 8x2 submatrices composed of columns 1 and 2, 3 and 4, 5 and 6, and 7 and 8, respectively.

$$\begin{bmatrix} -k_{zl1} & k_{zl1} \\ k_y & k_y \\ -e^{-\imath k d_1 (k_z + k_{zl1})} k_{zl1} & e^{-\imath k d_1 (k_z - k_{zl1})} k_{zl1} \\ -e^{-\imath k d_1 (k_z + k_{zl1})} k_y & e^{-\imath k d_1 (k_z - k_{zl1})} k_y \\ 2 k_y k_{zl1} \mu_1 & -2 k_y k_{zl1} \mu_1 \\ -k_y^2 \lambda_1 - k_{zl1}^2 (\lambda_1 + 2\mu_1) & -k_y^2 \lambda_1 - k_{zl1}^2 (\lambda_1 + 2\mu_1) \\ 2 e^{-\imath k d_1 (k_z + k_{zl1})} k_y k_{zl1} \mu_1 & -2 e^{-\imath k d_1 (k_z - k_{zl1})} k_y k_{zl1} \mu_1 \\ -e^{-\imath k d_1 (k_z + k_{zl1})} (k_y^2 \lambda_1 + k_{zl1}^2 (\lambda_1 + 2\mu_1)) & -e^{-\imath k d_1 (k_z - k_{zl1})} (k_y^2 \lambda_1 + k_{zl1}^2 (\lambda_1 + 2\mu_1)) \end{bmatrix}$$

$$
\begin{bmatrix}
-k_y & k_y \\
-k_{zt1} & k_{zt1} \\
-e^{-\imath k d_1(k_z+k_{zt1})}k_y & -e^{-\imath k d_1(k_z-k_{zt1})}k_y \\
-e^{-\imath k d_1(k_z+k_{zt1})}k_{zt1} & -e^{-\imath k d_1(k_z-k_{zt1})}k_{zt1} \\
(k_y^2-k_{zt1}^2)\mu_1 & (k_y^2-k_{zt1}^2)\mu_1 \\
-2k_yk_{zt1}\mu_1 & 2k_yk_{zt1}\mu_1 \\
e^{-\imath k d_1(k_z+k_{zt1})}(k_y^2-k_{zt1}^2)\mu_1 & e^{-\imath k d_1(k_z-k_{zt1})}(k_y^2-k_{zt1}^2)\mu_1 \\
-2e^{-\imath k d_1(k_z+k_{zt1})}k_yk_{zt1}\mu_1 & 2e^{-\imath k d_1(k_z-k_{zt1})}k_yk_{zt1}\mu_1
\end{bmatrix}
$$

$$
\begin{bmatrix}
-k_{zl2} & k_{zl2} \\
k_y & k_y \\
-e^{-\imath k d_1(k_z+k_{zl2})}k_{zl2} & e^{-\imath k d_1(k_z-k_{zl2})}k_{zl2} \\
-e^{-\imath k d_1(k_z+k_{zl2})}k_y & e^{-\imath k d_1(k_z-k_{zl2})}k_y \\
2k_yk_{zl2}\mu_1 & -2k_yk_{zl2}\mu_1 \\
-k_y^2\lambda_1-k_{zl2}^2(\lambda_1+2\mu_1) & -k_y^2\lambda_1-k_{zl2}^2(\lambda_1+2\mu_1) \\
2e^{-\imath k d_1(k_z+k_{zl2})}k_yk_{zl2}\mu_1 & -2e^{-\imath k d_1(k_z-k_{zl2})}k_yk_{zl2}\mu_1 \\
-e^{-\imath k d_1(k_z+k_{zl2})}(k_y^2\lambda_1+k_{zl2}^2(\lambda_1+2\mu_1)) & -e^{-\imath k d_1(k_z-k_{zl2})}(k_y^2\lambda_1+k_{zl2}^2(\lambda_1+2\mu_1))
\end{bmatrix}
$$

$$
\begin{bmatrix}
k_y & k_y \\
k_{zt1} & -k_{zt1} \\
e^{\imath k d_2(k_z+k_{zt2})} k_y & e^{\imath k d_2(k_z-k_{zt2})} k_y \\
e^{\imath k d_2(k_z+k_{zt2})} k_{zt2} & -e^{\imath k d_2(k_z-k_{zt2})} k_{zt2} \\
(k_y^2 - k_{zt2}^2)\mu_2 & (k_y^2 - k_{zt2}^2)\mu_2 \\
-2k_y k_{zt2}\mu_2 & 2k_y k_{zt2}\mu_2 \\
e^{2\imath k d_2(k_z+k_{zt2})}(k_y^2 - k_{zt2}^2)\mu_2 & e^{\imath k d_2(k_z-k_{zt2})}(k_y^2 - k_{zt2}^2)\mu_2 \\
-2e^{\imath k d_2(k_z+k_{zt2})} k_y k_{zt2}\mu_2 & 2e^{\imath d_2(k_z-k_{zt2})} k_y k_{zt2}\mu_2
\end{bmatrix}
$$

Solving for the conditions under which this determinant is zero will give the dispersion relation that must be satisfied for the given plane wave solutions for $P$- and $S_v$-waves to exist in the periodically layered media. It can be shown that, in the case of propagation normal or parallel to the layers, the above will reduce to separate fourth order determinants for $P$- and $S_v$-waves.

Solving for the dispersion relation for $S_h$ waves is done in the same manner. In this case, however, it is recognized that the displacement is only due to the vector potential, $\psi$, and is only in the $n_x$ direction.

$$u_z = \psi_{x,y} - \psi_{y,x} = \psi_{x,y} = 0$$

$$u_y = \psi_{z,x} - \psi_{x,z} = -\psi x, z = 0$$

$$u_x = \psi_{y,z} - \psi_{z,y}$$

which allows consideration of the solution

$$u_x = \psi_{y,z} - \psi_{z,y} = g(z)e^{i(k_z z + k_y y - \omega t)}$$

Note that this condition always holds for an isotropic medium; this is why it is common to see the two separate equations for compressional and shear waves written as functions of the displacements and not the potentials. It is also why the vector potential is often represented as a scalar when it is actually a vector.

Taking the boundary conditions for continuity of stress and displacement gives the following:

$$\begin{bmatrix} 1 & 1 & -1 & -1 \\ e^{-\imath d_1(k_z+k_{z1})} & e^{-\imath d_1(k_z-k_{z1})} & -e^{\imath d_2(k_z+k_{z2})} & -e^{\imath d_2(k_z-k_{z2})} \\ -k_{z1}\mu_1 & k_{z1}\mu_1 & k_{z2}\mu_2 & -k_{z2}\mu_2 \\ -e^{-\imath d_1(k_z+k_{z1})}k_{z1}\mu_1 & e^{-\imath d_1(k_z-k_{z1})}k_{z1}\mu_1 & e^{\imath d_2(k_z+k_{z2})}k_{z2}\mu_2 & -e^{\imath d_2(k_z-k_{z2})}k_{z2}\mu_2 \end{bmatrix}$$

The solution given for $P$- and $S_v$-waves is similar to that given by Sve (1971) with the exception of notational differences. The solution for $S_h$-waves is numerically identical to that given by Helbig (1984) in which he used propagator matrices to find the dispersion relation for $S_h$-waves. By taking the real part of the determinant of the preceding set of equations, the compact expression given by Helbig (1984)[1] is found. Unfortunately, no discrete form exists for the coupled $P$- and $S_v$-waves, and

[1]A typographical error in Helbig's paper is corrected here

the $8 \times 8$ determinant must be calculated numerically. The discrete form for $S_h$-waves is:

$$\cos k_z(d_1 + d_2) = \cos k_{z1} d_1 \cos k_{z2} d_2 - \frac{1}{2}\left(\frac{m_1}{m_2} + \frac{m_2}{m_1}\right) \sin k_{z1} d_1 \sin k_{z2} d_2 \tag{3.17}$$

where,

$$m_i = \sqrt{\rho_i \mu_i} \cos \beta_i = \sqrt{\rho_i \mu_i} \frac{k_{zi}}{k_i}$$

and,

$$\beta_i = \arccos \frac{k_{zi}}{k_i}$$

is the angle of incidence in layer $i$. This expression is easily solved for $k_z(k_y, \omega)$ by recognizing that $k_{zi} = \sqrt{k_i^2 - k_y^2}$ and $k_i = \frac{\omega}{c_i}$.

The two above results now completely characterize the dispersive wave propagation in a layered media at all general angles. It can be shown that in the long wave case the above dispersion relations give the same solution as those given by Backus averaging and solution of the Green-Christoffel tensor for general directions of propagation.

An examination of the dispersion relation given by the Floquet solution can give an intuitive picture of the behavior of waves in a periodic medium. First, the equation that is found by consideration of continuity of shear stresses across the boundary located at the origin gives row three of the matrix. The factor in this equation, $\frac{k_{zi}}{k}\mu_i$,(the factor $\frac{1}{k}$ was removed in the proceeding expression), can alternatively be expressed as:

$$C_{eff}\sqrt{\mu_i\rho_i}\cos\theta_i = C_{eff}I_i\cos\theta_i$$

where $I_i$ is the impedance. This expression is clearly a stress, as the impedance is defined as stress divided by velocity. It is clear that in the determinant, $C_{eff}$ can be removed, making this condition one of impedance matching of the vertical component of the plane waves in the separate layers.

In consideration of the Floquet solution let's again examine why there is no anisotropy if there is not a shear wave contrast. This effect was first mentioned in Section 2.2 with regard to the Backus solution. An examination of the Floquet solution will demonstrate this, but first I shall make a few comments. I started by writing the solution for the displacement as a sum of a scalar potential and a vector potential. This is a mathematical identity, Helmholtz's theorem, and can be used for any medium, regardless of anisotropy or inhomogeneity. The only necessary conditions are given by Arfken (1970):

$$[\nabla\cdot\vec{u}]_\infty = 0$$

$$[\nabla\times\vec{u}]_\infty = 0$$

However, it is easily shown, by performing the substitution into the general wave equation, that only the isotropic and homogeneous case will lead to a separation into two separate equations. In the general case the $P$- and $S$-waves are coupled and this operation will not result in separate equations for the scalar and vector potentials. Another point to note is that, in the case of liquids where the shear modulus is zero, the vector potential is zero and the displacement field is only due to the scalar potential, hence no anisotropy. The point that was just made is that if the displacement is considered to be the sum of a vector and scalar potential, that anisotropy is associated with the vector potential and obviously not with the scalar potential. Anisotropy is a dependence on direction, and by definition a scalar does not depend on direction. So, even if you have an inhomogeneous scalar potential, it is not sufficient to give anisotropy, and can only be observed in the vector potential.

It is important to recognize that there is no contradiction in this interpretation scheme. The $P$ wave can still be anisotropic, it is simply being recognized that anisotropy is due to the vector potential not the scalar potential, or in other words the coupled behavior of the scalar and vector fields means that the $P$ wave in an anisotropic media is dependent on both the scalar and vector potential. Hence, it can be anisotropic.

These observations can be used to consider the Floquet solution in a periodic media and what happens if there is no shear modulus contrast between layers. If there is no shear modulus contrast, the velocity $c_{t1}$ in layer 1 will be equal to $c_{t2}$ in layer 2, and therefore $k_{zt1} = k_{zt2}$. This means that the solution for the vector potential in layer 1 is equal to the solution in layer 2. Since each layer is isotropic (isotropic vector potential) and it is now seen that this vector potential is equal in both layers, it is obvious that the total vector potential for the equivalent medium is also represented by this isotropic vector potential, hence no anisotropy. Obviously by doing the converse, holding $\lambda + 2\mu$ constant in both layers, the scalar potential is now homogenous. However, because the vector potential may vary across the layers, there still may be anisotropy.

### 3.1.2 Electromagnetic Waves

The similarity between the Floquet solution for shear elastic waves and electromagnetic waves allows us to skip the details of the derivation of the theory for electromagnetic waves. Instead this section will stress what is unique about the electromagnetic waves in the periodic layered media.

The discrete solutions, which are structurally identical to Equation 3.17 are:

$$\cos k_z(d_1 + d_2) = \cos k_{z1}d_1 \cos k_{z2}d_2 - \frac{1}{2}\left(\frac{k_{z2}}{k_{z1}} + \frac{k_{z1}}{k_{z2}}\right) \sin k_{z1}d_1 \sin k_{z2}d_2 \qquad (3.18)$$

for the TE mode, and,

$$\cos k_z(d_1 + d_2) = \cos k_{z1}d_1 \cos k_{z2}d_2 - \frac{1}{2}\left(\frac{n_1^2 k_{z2}}{n_2^2 k_{z1}} + \frac{n_2^2 k_{z1}}{n_1^2 k_{z2}}\right) \sin k_{z1}d_1 \sin k_{z2}d_2 \quad (3.19)$$

for the TM mode, where $n_i$ is the index of refraction (Gu and Yeh, 1996).

The obvious difference when compared to elastic waves is that the TE mode here is structurally identical to the TM mode, as opposed to the more complicated elastic case where the $S_v$ mode was coupled with the $P$-wave leading to a more complex behavior.

## 3.2 Dispersion of Waves Propagating in a Periodic Layered Media

Wave propagation in periodic structures is an extensively researched and documented area of study in solid state physics. The most comprehensive early work in this field is that of Brillouin (1946). The most important contribution of his work is the demonstration of the presence of stop-bands, which occur at the boundaries between the so-called 'Brillouin zones'. These are frequency bands at which waves are only attenuated and not propagated in periodic structures. Brillouin zones are also sometimes referred to as Bragg zones in honor of the solid state physicist Felix Bragg. Brillouin also demonstrated that to fully describe wave behavior in a periodic media one needs only to consider wave numbers within the range:

$$-\frac{\pi}{d} \leq k \leq \frac{\pi}{d}$$

where $d$ is the period of the medium and $k$ is the wave number. As an illustration of this, the first case to be considered is for waves propagating normal to the periodic layered medium, recognizing that the solution is identical to Brillouin's consideration of waves in a one-dimensional lattice.

For wave propagation normal to isotropic layers, $k_y = 0$ and Equation 3.17 reduces to the form given by Rytov (1956a):

$$\cos k(d_1 + d_2) = \cos k_1 d_1 \cos k_2 d_2 - \frac{1 + \chi^2}{2\chi} \sin k_1 d_1 \sin k_2 d_2 \tag{3.20}$$

where

$$\chi = \frac{v_2 \rho_2}{v_1 \rho_1}$$

and

$$k_i = \frac{\omega}{v_i}$$

It is recognized that $v_i$ is either the shear or compressional wave velocity in layer $i$, depending on which is being considered. In this form $k$ can be found as an explicit function of frequency making it the simplest case to consider.

For the case of my standard sand and shale model (Table 2.1) with $d_1 = d_2$ the frequency-wave number spectrum for the full domain of real solutions is shown in Figure 3.1. The stop-bands are those frequency bands at the edges of the Brillouin zones for which there exists no solution. The black lines in Figure 3.1 represent the isotropic wave velocities of the individual layers. The red and green lines represent the long wave and ray velocities, respectively. An examination of this figure or Equation 3.20 illustrates Brillouin's condition of periodicity. It can also be observed that the dispersion relation is even such that: $\omega(k) = \omega(-k)$. This allows us to fully describe the dispersion relation by considering only those wave numbers such that $0 \leq k \leq \frac{\pi}{d}$. This is referred to as the reduced zone scheme (Lee and Yang, 1973; Lee, 1975; Ziman, 1972) and is shown in Figure 3.2.

Moving to the extended zone scheme allows us to evaluate the phase velocities in the normal way where $v = \frac{\omega}{k}$ (Lee and Yang, 1973). This is shown in Figure 3.3

Using the extended zone scheme from the calculated dispersion relation it is now possible to examine how the phase velocity varies with frequency and wave number.

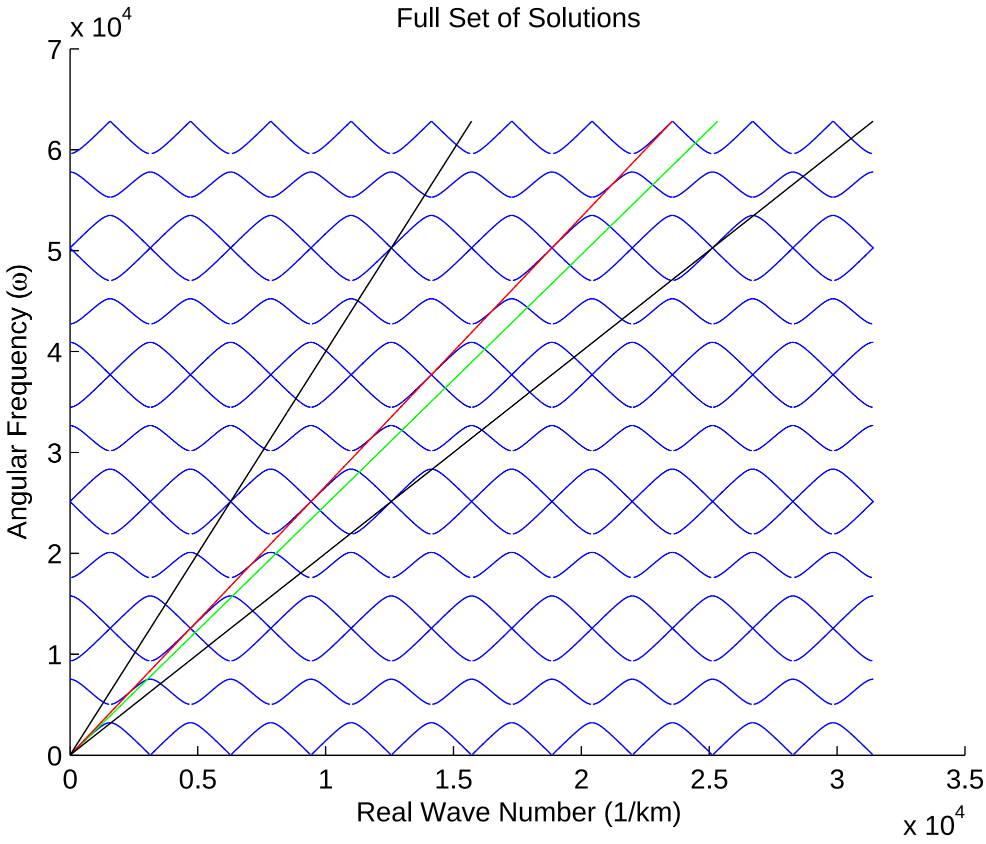


Figure 3.1: Entire frequency spectrum for alternating sand ($v_p = 4\frac{km}{s}$) and shale ($v_p = 2\frac{km}{s}$)

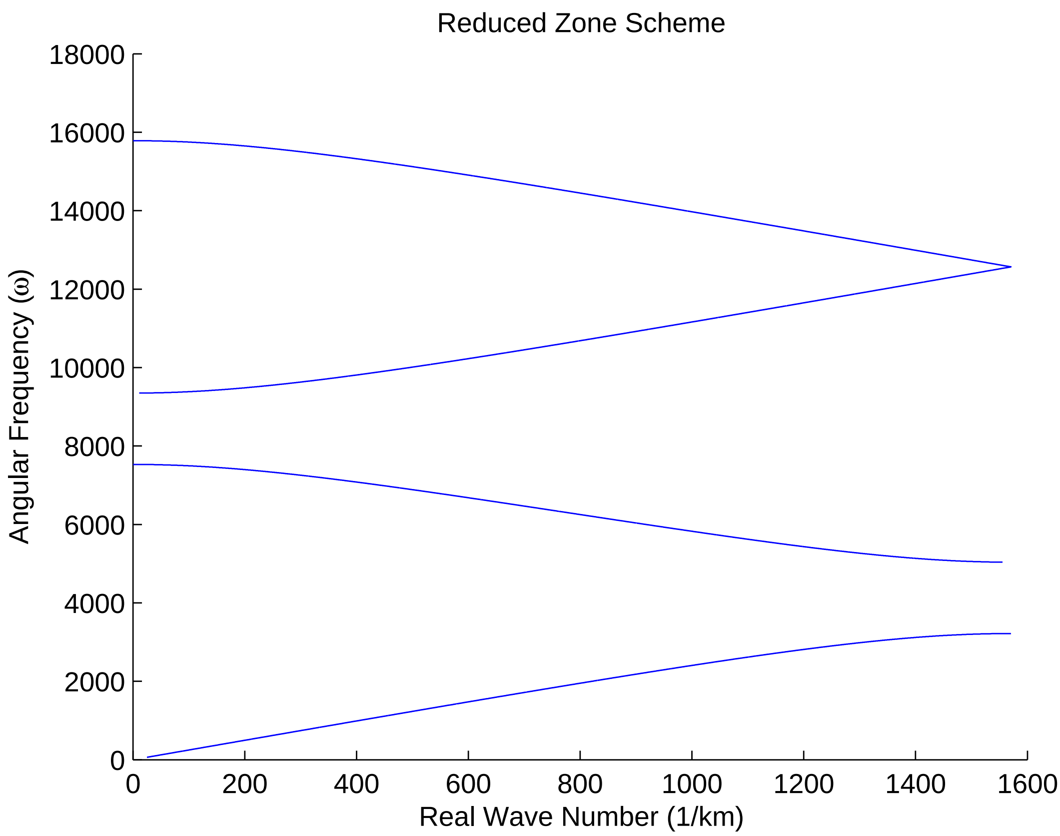


Figure 3.2: Reduced zone frequency spectrum for alternating sand ($v_p = 4\frac{km}{s}$) and shale ($v_p = 2\frac{km}{s}$)

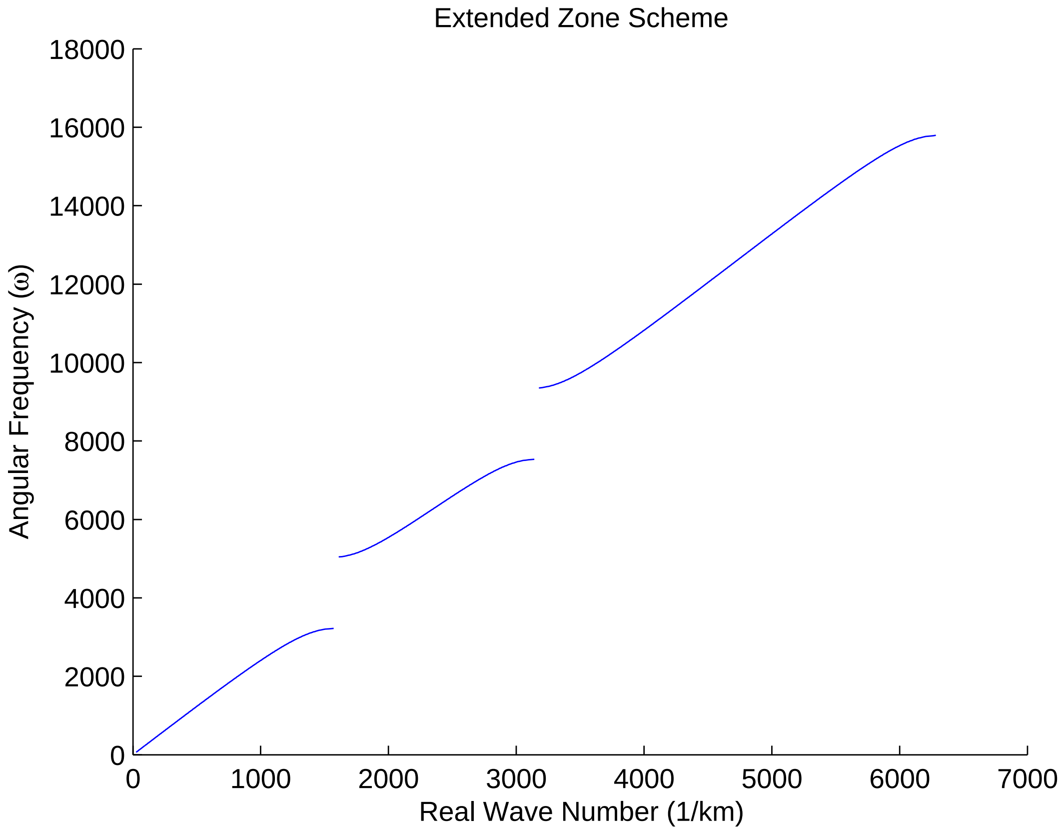


Figure 3.3: Extended zone frequency spectrum for alternating sand ($v_p = 4\frac{km}{s}$) and shale ($v_p = 2\frac{km}{s}$)

Figure 3.4 shows the velocity as a function of frequency and Figure 3.5 shows the velocity as a function of wavelength divided by the period of the medium ($\frac{\lambda}{d}$). To illustrate the convergence to both the long wave and high frequency velocities in those cases, the corresponding long wave (EMT) and high frequency (ray) velocities are also plotted. Figure 3.6 is taken to much shorter wavelengths, clearly demonstrating that in the short wave limit the Floquet solution does indeed converge to the velocity expected from ray theory.

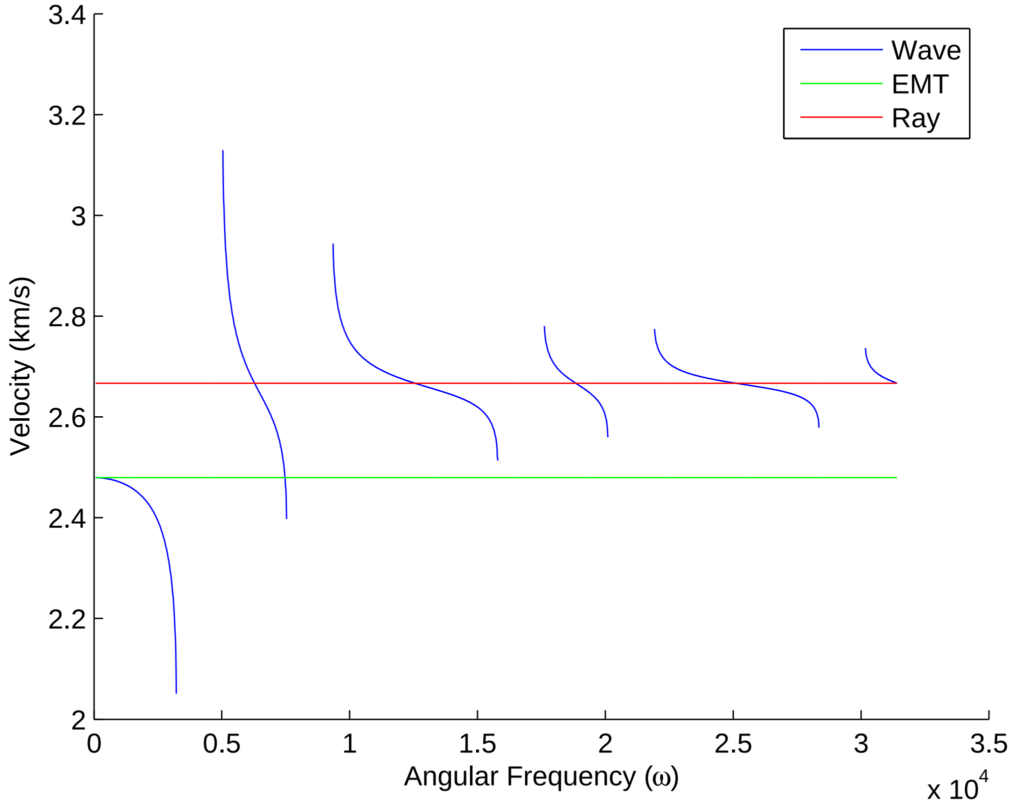


Figure 3.4: $\omega$ vs. velocity with propagation normal to layers for alternating sand ($v_p = 4\frac{km}{s}$) and shale ($v_p = 2\frac{km}{s}$)

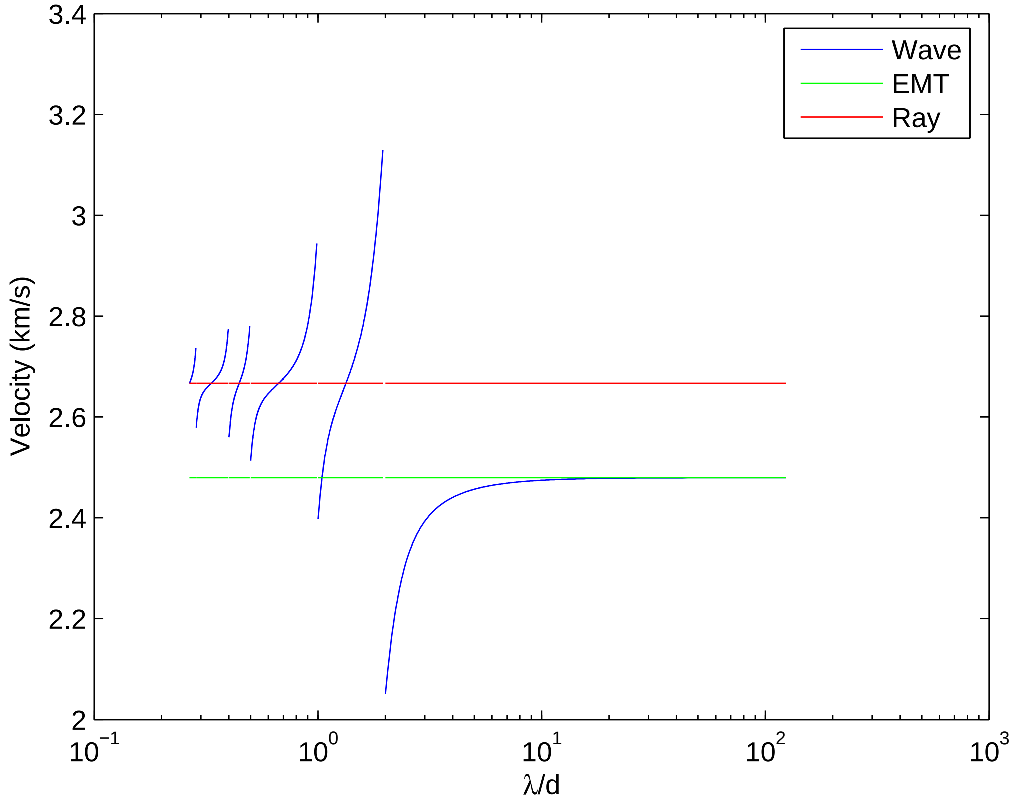


Figure 3.5: $\frac{\lambda}{d}$ vs. velocity with propagation normal to layers for alternating sand ($v_p = 4\frac{km}{s}$) and shale ($v_p = 2\frac{km}{s}$)

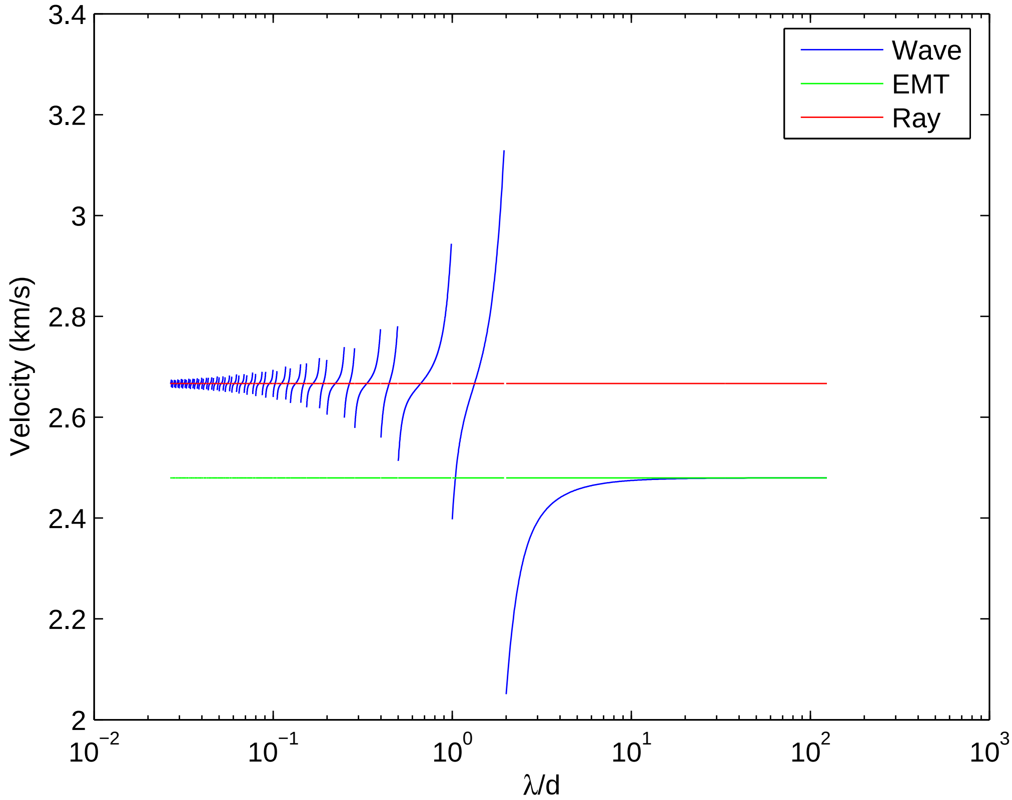


Figure 3.6: $\frac{\lambda}{d}$ vs. velocity with propagation normal to layers for alternating sand ($v_p = 4\frac{km}{s}$) and shale ($v_p = 2\frac{km}{s}$), small $\lambda$

## 3.3 Dispersion at General Angles of Propagation

The discussions, so far, have related to the case of wave propagation that is normal to the layering, $k_y = 0$. In order to characterize waves propagating at general angles it is now necessary to consider solutions such that $k_y \neq 0$. Computationally this problem becomes much more intensive. Helbig (1984) suggests an efficient representation of the dispersion relation for this general case. Lines of constant frequency are plotted on the $k_z - k_y$ plane. The phase velocity is then represented by the vector $\mathbf{k}$ from the origin where the velocity at a certain frequency is in the direction $\hat{\mathbf{k}}$ and has a magnitude $\frac{\omega}{|\mathbf{k}|}$. Group velocity is given by a normal to a given frequency contour, where the magnitude is equal to $\frac{d\omega}{dk}$. Presumably, due to lack of computing power, Helbig (1984) only provides an example extending to the first Brillouin zone. Figure 3.7 provides this representation for elastic $S_h$-waves the standard sand-shale model through the first three Brillouin zones. The sharp discontinuities represent the locations of the Brillouin zones. In an isotropic media, concentric semi-ellipses would be expected; deviations from ellipses in this figure represent the dispersion and anisotropy. An important observation that can be made by looking at this representation over multiple Brillouin zones is the presence of gaps in the Brillouin zones that can be connected by a single $\mathbf{k}$ vector. This represents a critical angle at which there is no dispersion. This effect and its material controls are explored in much greater detail in Chapter 4.

By tracing a vector through a given angle using the representation given in Figure 3.7 the standard dispersion relation, extended zone scheme, can be found. Figure 3.8 illustrates this at four general angles of propagation. As shallower shallower angles are approached the occurrence of Brillouin zones gradually decreases. Obviously from Figure 3.7 there are no Brillouin zones for propagation parallel to the layering, although there is still dispersion.

Figure 3.9 shows the dispersion relation for elastic wave propagation both normal and parallel to the layering. In the long-wave, effectively anisotropic case the

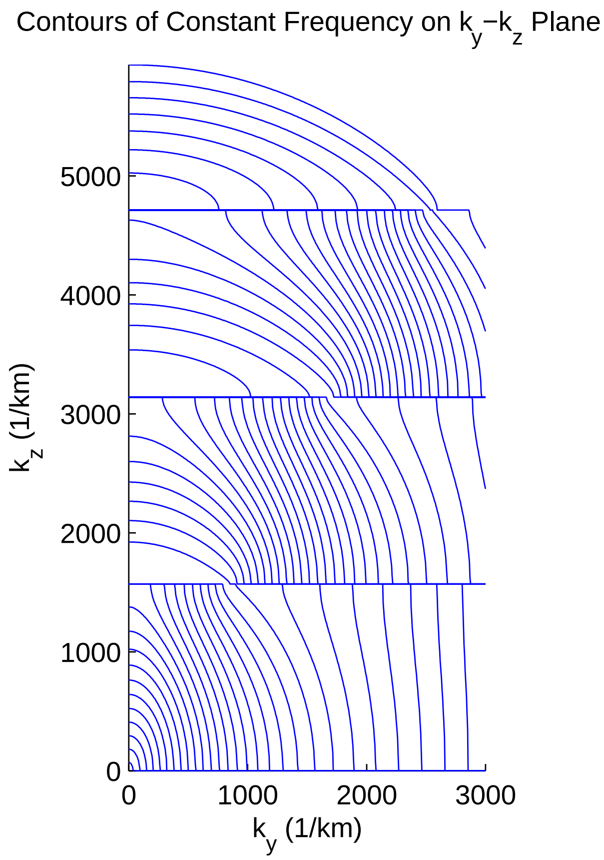


Figure 3.7: Lines represent contours of equal frequency on the $K_y - K_z$ plane.

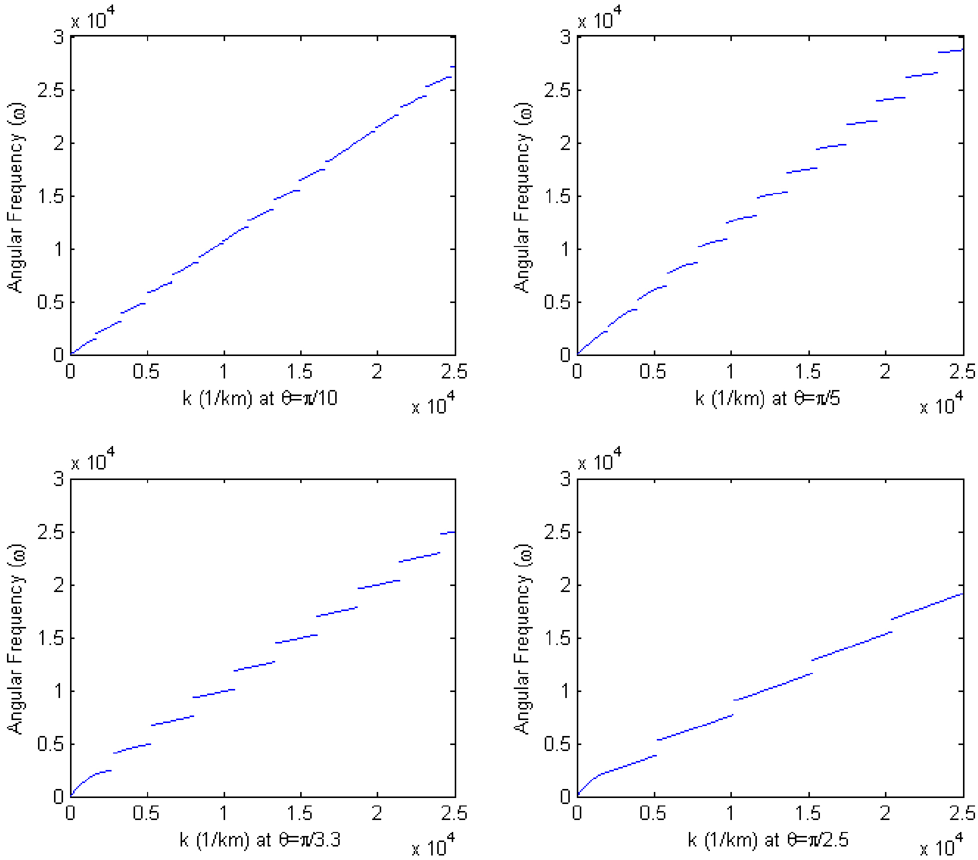


Figure 3.8: Dispersion relations for $S_h$-waves at different general angles of propagation

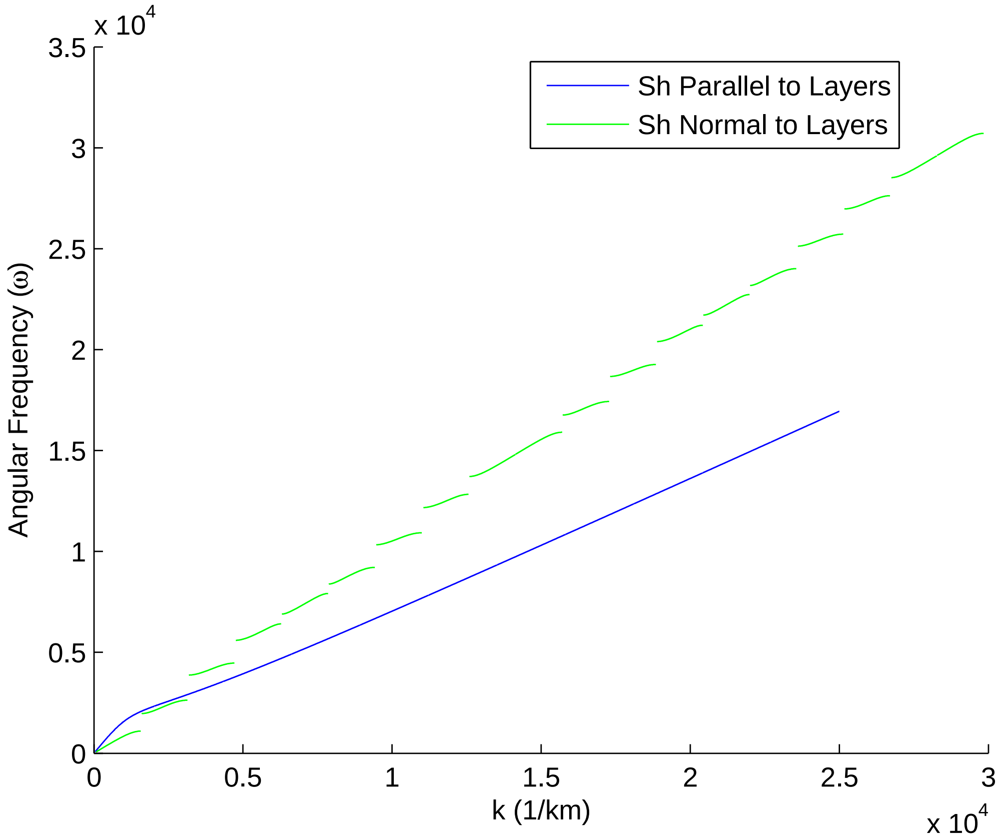


Figure 3.9: Dispersion relations for $S_h$-waves parallel and normal to layers

velocity is clearly greater for propagation parallel to the layering. However, past the first Brillouin zone for normal wave propagation, the velocity is greater for wave propagation normal to the layering. This is also illustrated in Figure 3.10 which shows velocity vs. the wavelength to material period ratio.

For electromagnetic waves, propagation at general angles offers a contrast to that of elastic waves. While the TM EM wave behaves identical to $S_h$-waves for a given magnitude of contrast, the TE mode behaves distinctly different from the coupled

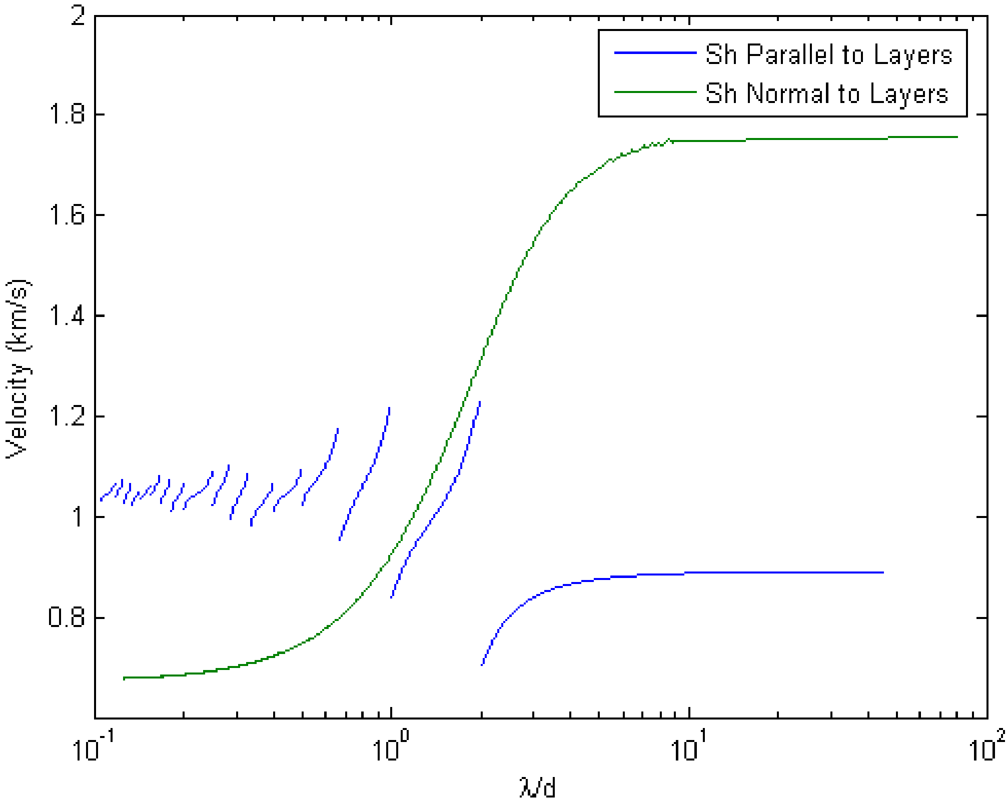


Figure 3.10: Wavelength-period ratio vs. velocity for normal and parallel shear wave propagation

elastic $S_v$ mode. Figure 3.11 shows the dispersion relation for both TE and TM polarization, propagating parallel to the layering. Note the lack of dispersion in the TE mode. It is also apparent that the phase and group velocities of the TE and TM mode approach each other as the frequency gets very large, as should be expected.

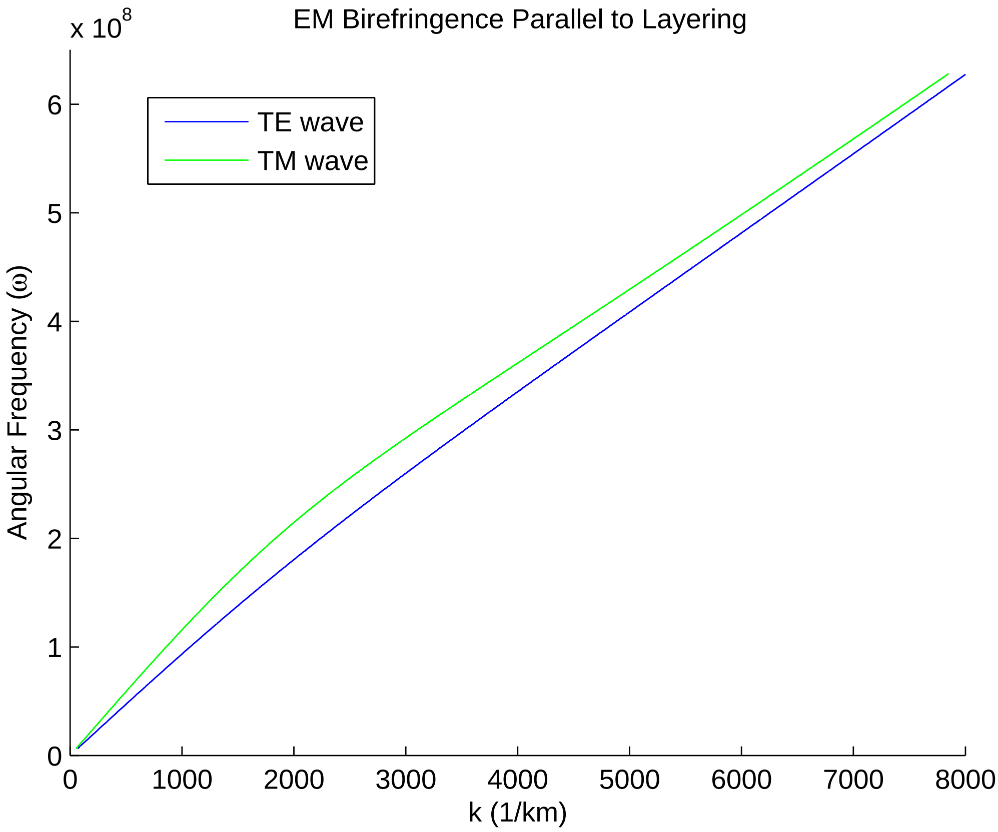


Figure 3.11: TE and TM waves propagating parallel to layering

## 3.4 Comments on the Floquet Solution for Anisotropic Layers

Several authors have given approaches to find the dispersion relation for layered media when the individual layers are themselves anisotropic (Nayfeh, 1991; Braga, 1992; Potel et al., 1995; Wang and Rokhlin, 2002). In this section, a general overview of the complications that are encountered are presented, as well as a suggested approach that follows the general procedure given for isotropic layers.

In the traditional approach for isotropic layers, separate equations for the shear and compressional waves are considered. As mentioned, however, in a general anisotropic media, considering the displacement as a sum of a gradient of a scalar and the curl of a vector, will not in general result in two separate equations for shear and compressional waves. Hence, it is necessary to begin with the equation for a general anisotropic medium, Equation 3.2. It is recognized that this can be written as three coupled scalar equations:

$$\rho\frac{\partial^2 u_1}{\partial t^2} = C_{1jkl}\frac{\partial}{\partial x_j}\frac{\partial u_k}{\partial x_l}$$

$$\rho\frac{\partial^2 u_2}{\partial t^2} = C_{2jkl}\frac{\partial}{\partial x_j}\frac{\partial u_k}{\partial x_l} \tag{3.21}$$

$$\rho\frac{\partial^2 u_3}{\partial t^2} = C_{3jkl}\frac{\partial}{\partial x_j}\frac{\partial u_k}{\partial x_l}$$

which, for a layered periodic medium, has solutions according to Floquet theory of the form:

$$u_1 = F[x_3]e^{ik(n_j x_j - ct)}$$

$$u_2 = G[x_3]e^{ik(n_j x_j - ct)} \tag{3.22}$$

$$u_3 = H[x_3]e^{ik(n_j x_j - ct)}$$

where $F[x_3], G[x_3]$, and $H[x_3]$ are periodic with the same period as the medium, and $n_j$ are the direction cosines defining the direction of wave propagation. Substituting solutions 3.22 into Equations 3.21 results in a set of three coupled second order differential equations for the periodic coefficients $F[x_3], G[x_3]$, and $H[x_3]$. A solution in both layers will result in twelve unknown constants. In this case, consideration of the continuity of displacements and stresses across the boundaries will result in twelve equations. The dispersion relation for the case of general anisotropic layers can then be found by considering the cases in which this twelfth order determinant goes to zero.

As an example, consider the special case of waves propagating normal to the layering, $n_1 = n_2 = 0$ and $n_3 = 1$. For orthorhombic or VTI layer symmetry the solutions are:

$$F[x_3] = Ae^{-ikx_3(1-\alpha)} + Be^{-ikx_3(1+\alpha)}$$

$$G[x_3] = Ce^{-ikx_3(1-\beta)} + De^{-ikx_3(1+\beta)}$$

$$H[x_3] = Qe^{-ikx_3(1-\gamma)} + Re^{-ikx_3(1+\gamma)}$$

where,

$$\alpha = c\sqrt{\frac{\rho}{C_{55}}}$$

$$\beta = c\sqrt{\frac{\rho}{C_{44}}}$$

$$\gamma = c\sqrt{\frac{\rho}{C_{33}}}$$

As in the isotropic case, similar solutions are found for each layer. Note that these solutions are of the same form as those given in Sub-Section 3.1.2 for isotropic layers, with different notation to emphasize the elastic constants, as opposed to velocities.

From these solutions it is obvious that there are three possible solutions for wave propagation normal to the layering for orthorhombic media. For a VTI medium (and isotropic) $C_{44} = C_{55}$. Therefore, it is obvious that normal to VTI layers there are only two solutions, the pure compressional wave given by $u_3$ and the pure shear wave given by $u_1$ or $u_2$.

In this case of propagation along a symmetry axis, $S$-waves can be considered independent of $P$-waves. Since this wave motion is uncoupled, $\hat{u}_2 \cdot \hat{k} = \hat{u}_1 \cdot \hat{k} = 0$, I can let $u_3 = 0$ such that only displacements in the $u_1$- and $u_2$-directions are being considered. The conditions that must be satisfied are the continuity of the displacements $u_1$ and $u_2$ across the boundary as well as the shear stresses $\sigma_{13}$ and $\sigma_{23}$ From these boundary conditions a system of eight equations and eight unknowns is found whose determinant must vanish for a solution to exist. Of course for the case being considered here, the shear waves could also be considered independently as 2 fourth-order determinants, which will be equal in the case of VTI and isotropic layers. The solution for $P$-waves would follow the same approach. This was a special case which exploited symmetry to simplify the problem. Propagation at general angles, would require the solution of the full twelfth-order determinant.

## 3.5 Synthetic Seismograms in Layered Periodic Media

To fully understand the effect of the dispersion relations obtained in the preceding chapters, the effect of a given wave propagating through the layered periodic medium will now be considered. These theoretical results are obtained for both the simplest case of wave propagation normal to the layers in an isotropic system and for propagation parallel to the layering. In the former case my results are shown to agree with the behavior of published experimental results.

In the previous chapter, dispersion relations were obtained for the periodic layered media of the form $k(\omega)$. It will be demonstrated how this can be used via the theory of Green's functions for inhomogeneous differential equations to produce synthetic seismograms. For a given ODE of the form:

$$\mathcal{L}u(\mathbf{r}) = p(\mathbf{r})$$

where $\mathcal{L}$ is a linear differential operator, and given a solution to the homogeneous equation, $G(\mathbf{r}, \mathbf{r}')$, such that:

$$\mathcal{L}G(\mathbf{r}, \mathbf{r}') = \delta(\mathbf{r} - \mathbf{r}')$$

then the solution to the inhomogeneous equation is given by:

$$u(\mathbf{r}) = \int G(\mathbf{r}, \mathbf{r}')p(\mathbf{r}')d\mathbf{r}'$$

Recognizing that the solution for $k$ is an effective condition that must be satisfied for waves to propagate through the entire medium we consider a green's function solution to the standard wave equation in the frequency domain of the form:

$$G(\mathbf{r}, \mathbf{r}', \omega) = e^{-ik(\omega)|\mathbf{r}-\mathbf{r}'|}$$

Considering a plane wave source at $r_0$, the source term $p(\mathbf{r}', \omega)$ becomes:

$$p(\omega)\delta(\mathbf{r}' - \mathbf{r_0})$$

Leading to the expression for the displacement at a point $\mathbf{r}$ due to a point source at $\mathbf{r_0}$:

$$u(\mathbf{r}, \omega) = \int G(\mathbf{r}, \mathbf{r}', \omega)p(\omega)\delta(\mathbf{r} - \mathbf{r}')d\mathbf{r}'$$

$$= G(\mathbf{r}, \mathbf{r_0}, \omega)p(\omega) = p(\omega)e^{-ik(\omega)|\mathbf{r}-\mathbf{r_0}|}$$

This is clearly a phase shift between positions $\mathbf{r}$ and $\mathbf{r_0}$, and according to the definition of Fourier transforms this corresponds to a time shift in the time domain for a traveling pulse due to a point source located at $\mathbf{r_0}$:

$$p(t - t_0) \Leftrightarrow p(\omega)e^{-i\omega t_0}$$

With the recognition that $\omega = kc = k\frac{d}{t_0}$ and $d = |\mathbf{r} - \mathbf{r_0}|$ this is clearly the same relation we derived using a Green's function solution.

Knowing the dispersion relation for a given periodic media, creating synthetic seismograms reduces to the following steps. First, define the source pulse in the time domain, and perform a Fourier transform of the pulse. Multiply each frequency component by the corresponding phase shift $e^{-\imath k(\omega)d}$, then perform the inverse Fourier transform.

Simulations were performed for the standard sand-shale model used in previous chapters. The wavelet used was a Gaussian windowed sign,

$$p(t) = \sin{(\omega_0 t)}e^{\frac{-2\omega_0^2 t^2}{n^2}}$$

where $\omega_0 = 2\pi f_0$ is the center frequency and $n$ is the number of cycles. For these simulations the values used where $f_0 = 50$hz and $n = 4$. This pulse was then propagated over a distance of 500 meters first considering compressional waves only, Figure 3.12, and then both compressional and shear waves, Figure 3.13. In both figures the sand and shale layer thicknesses are equal, but the period is varied from the bottom to the top where the periods are: .2m, 2m, 10m, 30m, 90m, 150m, and 300m respectively. Also shown in Figure 3.14 is a figure reproduced from Marion and Coudin (1992) which shows results from an experiment conducted with alternating plastic and steel layers. This shows identical behavior to that given in the simulations for a sand-shale periodic media.

It is apparent that dispersion begins to appear in the slower $S$-wave at smaller periods then the $P$-wave. The dispersion for both appears to be strongest in the range of 30-90m. These effects are further examined in the next section.

Figure 3.15 gives the dispersion relation for a pulse traveling parallel to the layering. Note that the dispersion of the pulse is restrained to a much smaller range of material periods. An examination of Figure 3.9 shows that the dispersive region for parallel waves occurs only over a single small range of frequencies.

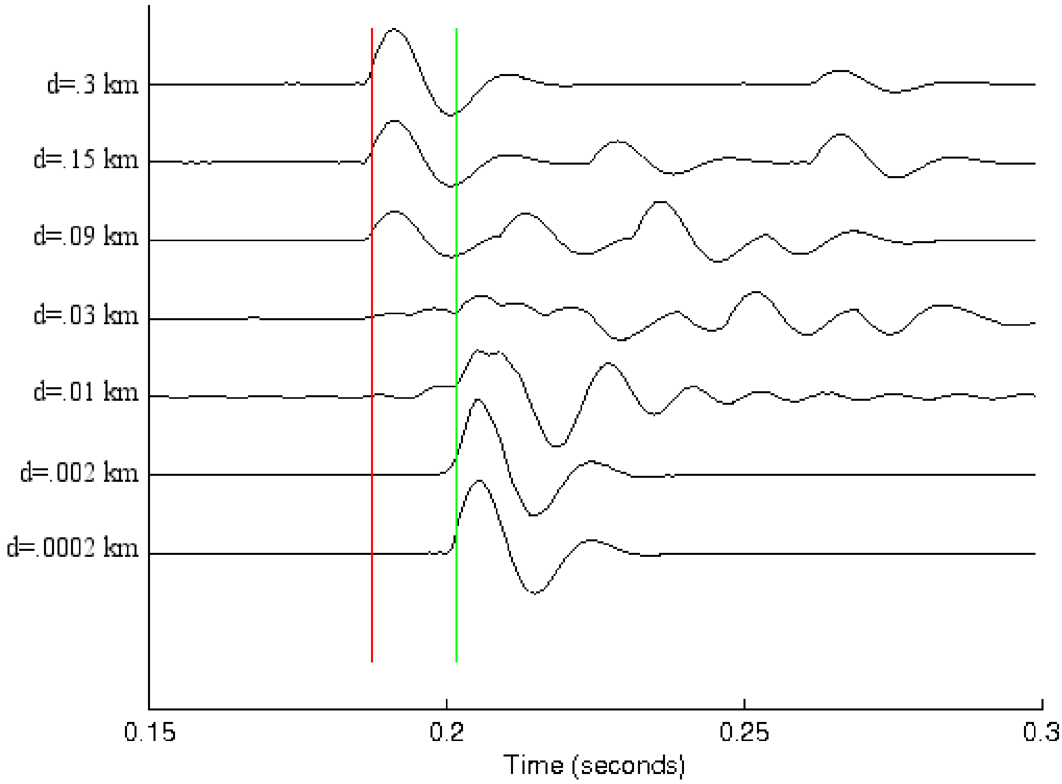


Figure 3.12: P-wave propagating through a Sand-Shale medium of different periods with a dominant wavelength in the long-wave approximation of $\lambda_0 = .050$km.

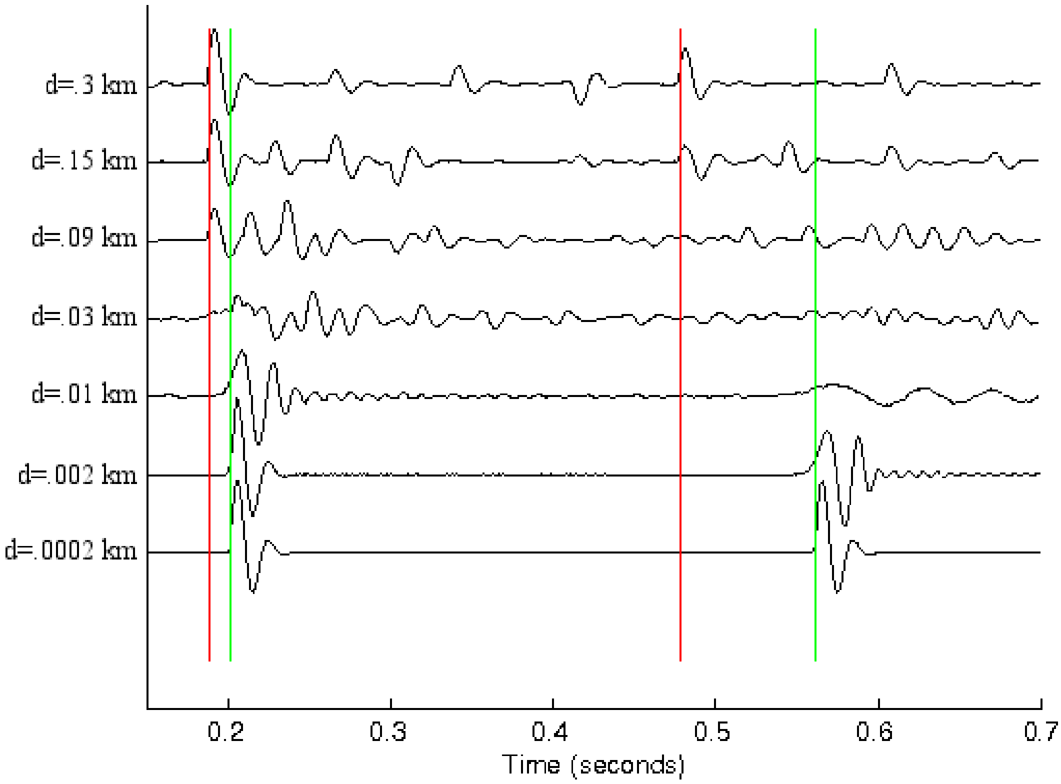


Figure 3.13: P- and S-waves propagating through a Sand-Shale medium of different periods with dominant wavelengths in the long-wave approximation of, $\lambda_0 = .050$km for the P-wave and $\lambda_0 = .018$km for the S-wave.

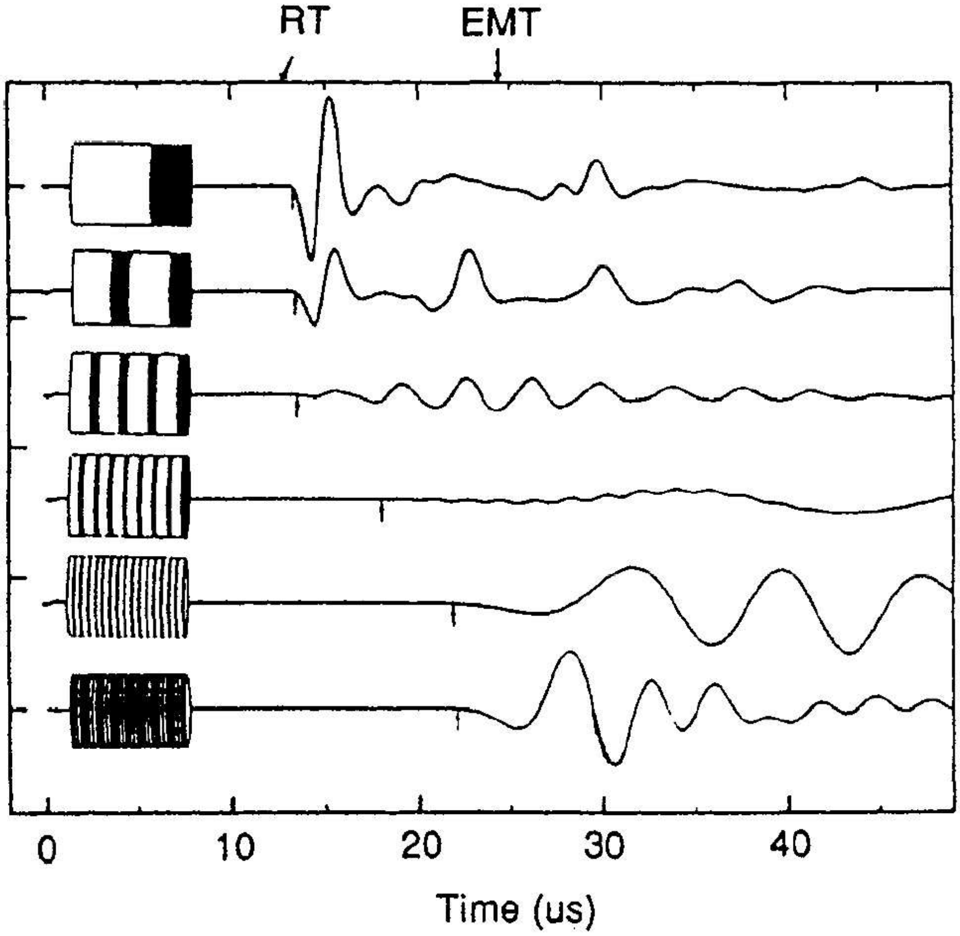


Figure 3.14: Experimental dispersion in a plastic-steel media, reproduced from Marion and Coudin (1992)

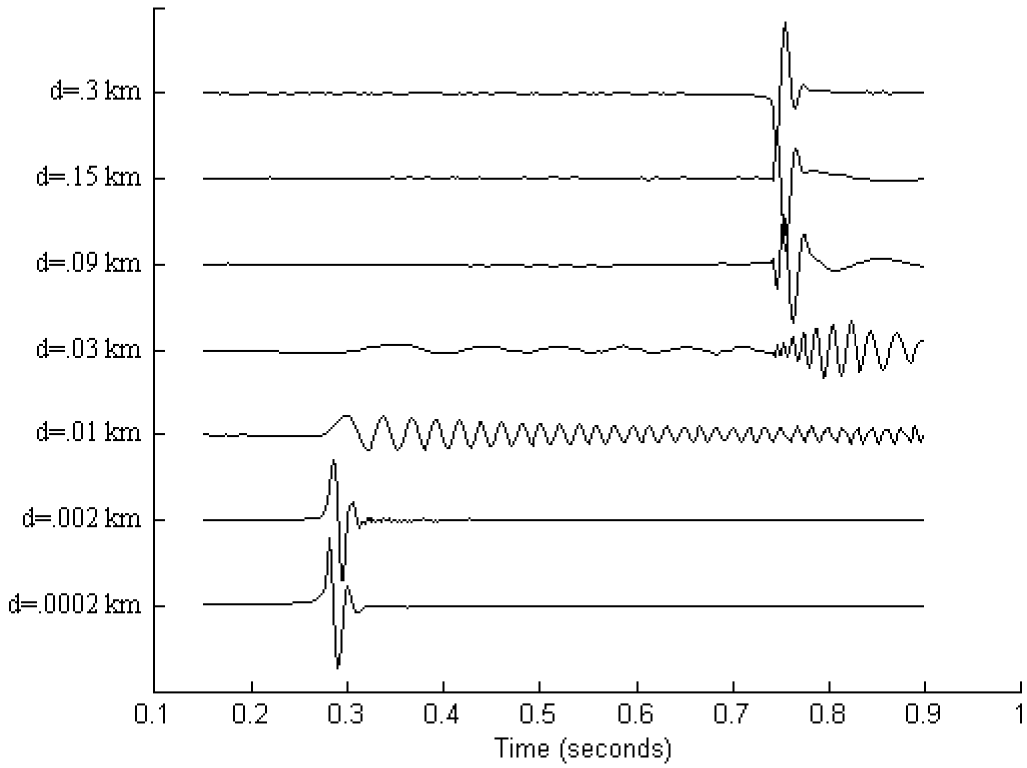


Figure 3.15: $S_h$-wave propagating parallel to layering

# Chapter 4

# Frequency-Dependency and Material Contrasts

## 4.1 Quantification of Dispersion based on Material Contrasts

As was examined in Chapter 2 when an insonifying wavelength is much greater than the period of the medium, the medium behaves as an effectively anisotropic medium that is not dependent on frequency. Chapter 3 examined the dispersion of a wave that occurs when the long-wave condition does not hold. The question that arises is: What is the wavelength at which dispersion becomes significant? Helbig (1984) suggested through numerical simulations that the dispersion becomes significant when the wavelength is three times the spatial period of the medium, $\frac{\lambda}{d} = 3$. Experimental and numerical simulations by Marion et al. (1994) put the ratio at near ten times. Carcione et al. (1991) stresses the importance of this limit on the impedance of the materials and numerically finds values of eight for a glass-epoxy media and six for a sand-limestone media. This dependency on the impedance of the layers was further stressed in papers by Hovem (1995) and Mukerji et al. (1995).

Another important observation that is both demonstrated experimentally, (Melia and Carlson, 1984) and numerically, (Carcione et al., 1991) is the dependence of the $\frac{\lambda}{d}$ ratio on the fraction of each component. The highest ratio for dispersion occurs at equal proportions of each component. This is similar to the effect of component proportions for the long-wavelength case that was shown in section 2.2.

In this chapter expansions on these earlier observations will be carried out by carefully considering the effect of material contrasts. Also, of particular importance is my consideration of fractured rocks and their fluid inclusions in the next chapter. While this was mentioned briefly by Hovem (1995), it has only recently been considered in any detail by Grechka (2003).

The first point that must be established is the threshold at which the dispersion is considered to be significant. For practical purposes, experimentalists are concerned with the point at which a wavelet becomes distorted from its long-wave form. Carcione et al. (1991) considers this problem by looking at the semblance between a dispersed pulse and the long wave pulse. Because wavelet shape and spectrum can vary, which will effect its dispersion, this is not a good technique to use for a thorough quantitative analysis. I do consider this technique first, however, to establish a more standard guide for what constitutes the dispersive propagation regime for a given medium.

The results from Chapter 3.3 will be used here to examine the dispersion. Following the convention used by Carcione et al. (1991) the following definitions are used:

$$\lambda_{long} = \frac{v_{long}}{f_0}$$

where $\lambda_{long}$ is the wavelength in the long wave case at frequency $f_0$, which is the center frequency of the wavelet. The ratio of wavelength to spatial period is:

$$R = \frac{\lambda_0}{d}$$

The fractional semblance is:

$$S = \frac{\sum(a_i + b_i)^2}{2\sum(a_i^2 + b_i^2)}$$

Varying the period of the media gives the semblance as a function of $R$, and for the case from Chapter 3.3 is shown in Figure 4.1. The two particular cases of $S = .97$ and $S = .85$ are shown in Figures 4.2 and 4.3, respectively.

Carcione (Carcione et al., 1991) uses the value of $S = .97$ to define the $R$ value at which dispersion begins to become significant. The problem with this approach is the definition of $\lambda_{long}$ which uses the pulse center frequency, $f_0$. It is obvious that the point at which a given wavelet enters the dispersive regime is not only dependent on the center frequency but also the pulse width. A wavelength to period ratio based on the dispersion relation is established. Instead of considering a wavelet, a single frequency is considered. The dispersion in this case is not given by the semblance but

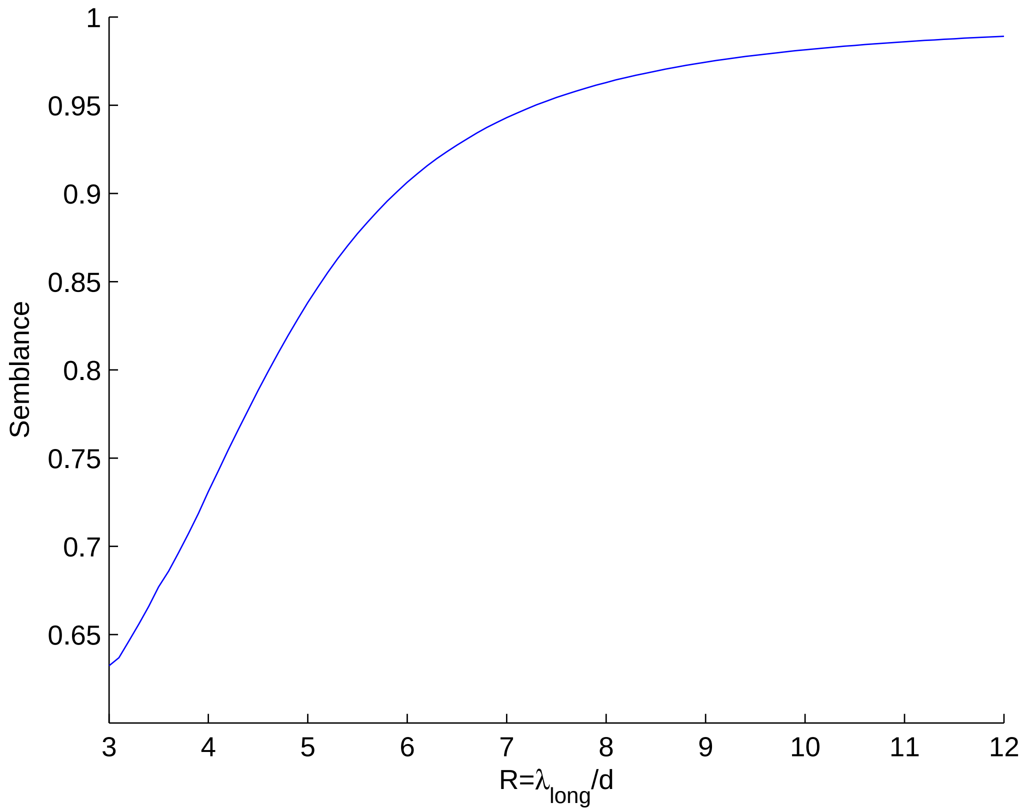


Figure 4.1: Semblance as a function of R for the standard sand-shale media

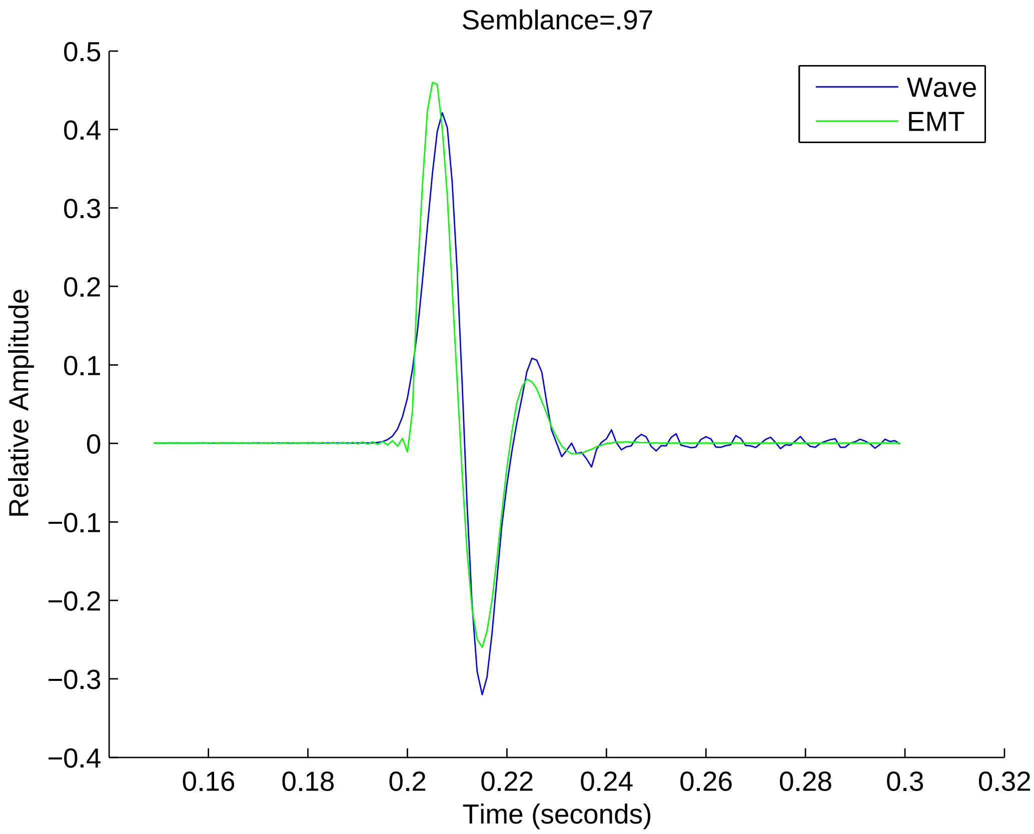


Figure 4.2: $S = .97$ for the standard sand-shale media

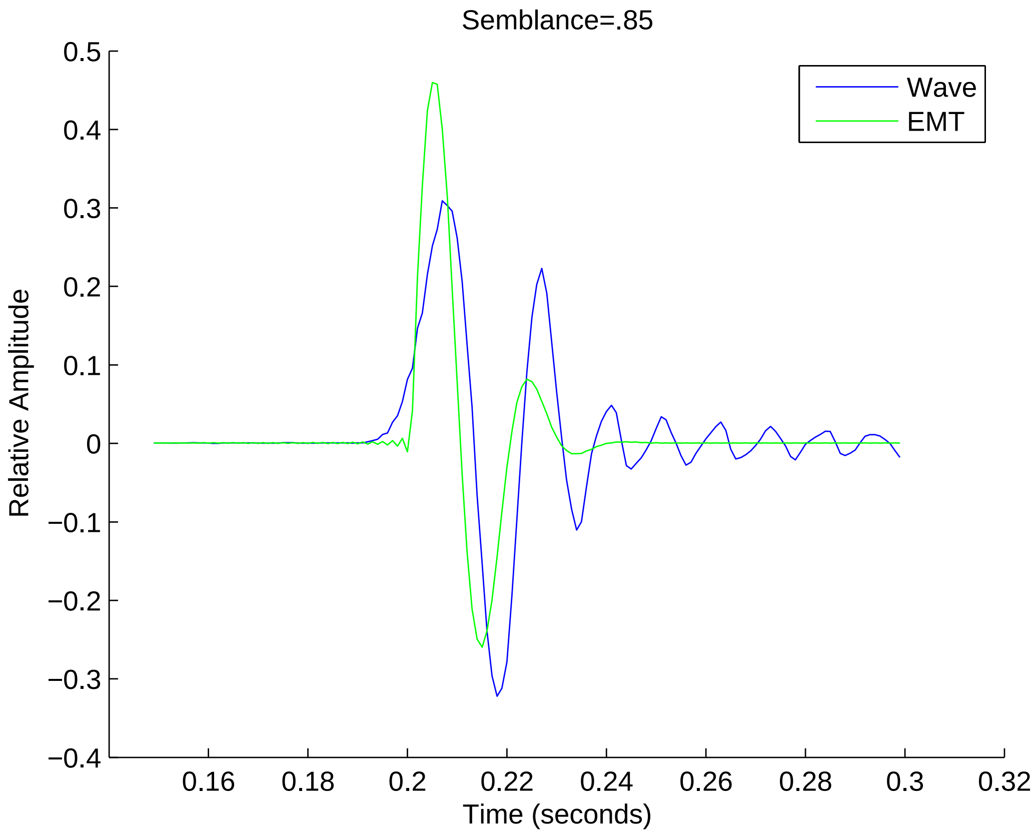


Figure 4.3: $S = .85$ for standard sand-shale media

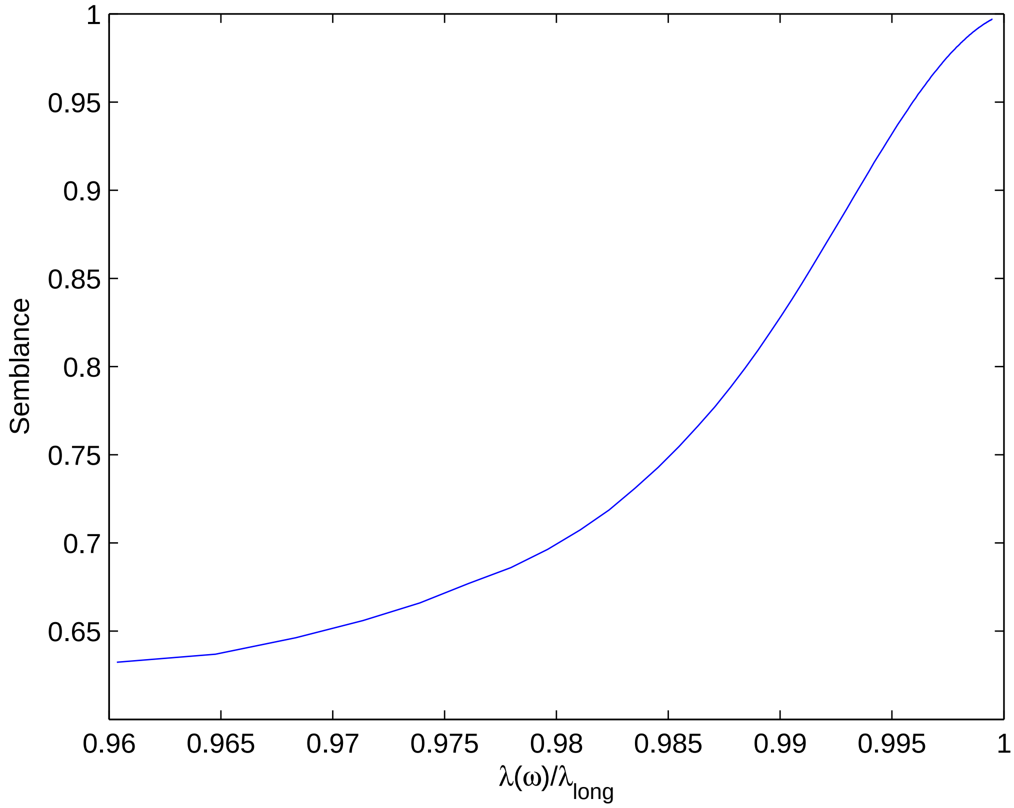


Figure 4.4: $\frac{\lambda(\omega)}{\lambda_{long}}$ vs Semblance for Sand-Shale

by the ratio of the long-wave wavelength and the wavelength given by the dispersion relation for a given spatial period and frequency.

$$\frac{\lambda(\omega)}{\lambda_{long}} = \frac{k_{long}}{k(\omega)}$$

To establish an applicable threshold, Figure 4.4 plots this ratio vs. the semblence for the sand-shale media as given in Figure 4.1 for a fixed frequency of $f = f_0 = 50$hz.

It is obvious from Figure 4.4 that a small change in $k(\omega)$ away from the long wave value results in a pulse that undergoes dramatic dispersion. With $\frac{\lambda(2\pi f_0)}{\lambda_{long}} = .99$, the semblance for the given wavelet with respect to the undispersed wavelet is $S = .83$. For a wavelet with a given center frequency, the lower frequencies are well into the dispersive regime by the time the center frequency enters the dispersive regime. Based on this, a value of $\frac{k_{long}}{k(\omega)} = .99$ will be used for comparing the effects of material contrasts and determining the long wave limit.

This discrepancy partially accounts for the dramatic difference in results between those given by Helbig (1984), who only considers the dispersion relation and the subsequent papers that considered experimental or numerical wavelets traveling through a given media. The value of .99 still results in a much larger dispersion then what Carcione et al. (1991) considered dispersive for a wavelet, however, it is only being used in the following section to make relative comparisons of the material contrasts and dispersion. For a given experiment the bandwidth of the pulse must be taken into consideration when establishing what the absolute value of the long-wave limit will be.

## 4.2 Theoretical Results for Material Contrasts

Based on results by various authors it is apparent that the wavelength at which dispersion becomes significant is strongly influenced by both impedance contrast and relative layer thicknesses (Carcione et al., 1991; Melia and Carlson, 1984; Hovem, 1995; Mukerji et al., 1995). In this section I thoroughly examine these dependencies to quantify this relation.

Figures 4.5 and 4.6 explore separately the effect of varying the shear modulus or bulk modulus independently. For each case the total impedance contrast,($\rho V$), is also plotted. Figure 4.7 is identical except it examines the effect of varying only the density contrast.

From these plots it is obvious that any change in material property, ($\mu$, $K$ or $\rho$) will lead to a change in R. Hence, it is obvious that any change in impedance, which is a function of these parameters, will result in a change in $R$. While it may be intuitively obvious, it is important to point out how this differs from the case of material contrast and long-wave anisotropy as discussed in Chapter 2.

For anisotropy to exist, it was demonstrated that there must be a contrast in shear modulus between the layers. A contrast in bulk modulus and/or density alone was not sufficient to produce anisotropy. As was discussed, this is a direct effect coming from the nature of shear modulus which is associated with the vector potential. While anisotropy is a function of the direction associated with the wave vector $k$, dispersion is related to its magnitude. Dispersion is seen for any material contrast regardless of the type, where anisotropy required a contrast in shear modulus. So, it can be said that while a periodic layered media may not exhibit effective anisotropy, it will always be dispersive.

As an additional consideration, $R$ has been plotted for the standard sand-shale media in Figure 4.8. In this case the shale $V_p$ was held constant at $1.5\frac{km}{s}$ while the sand $V_p$ was varied from $1.5 - 6\frac{km}{s}$. $R$ becomes dramatically larger for small

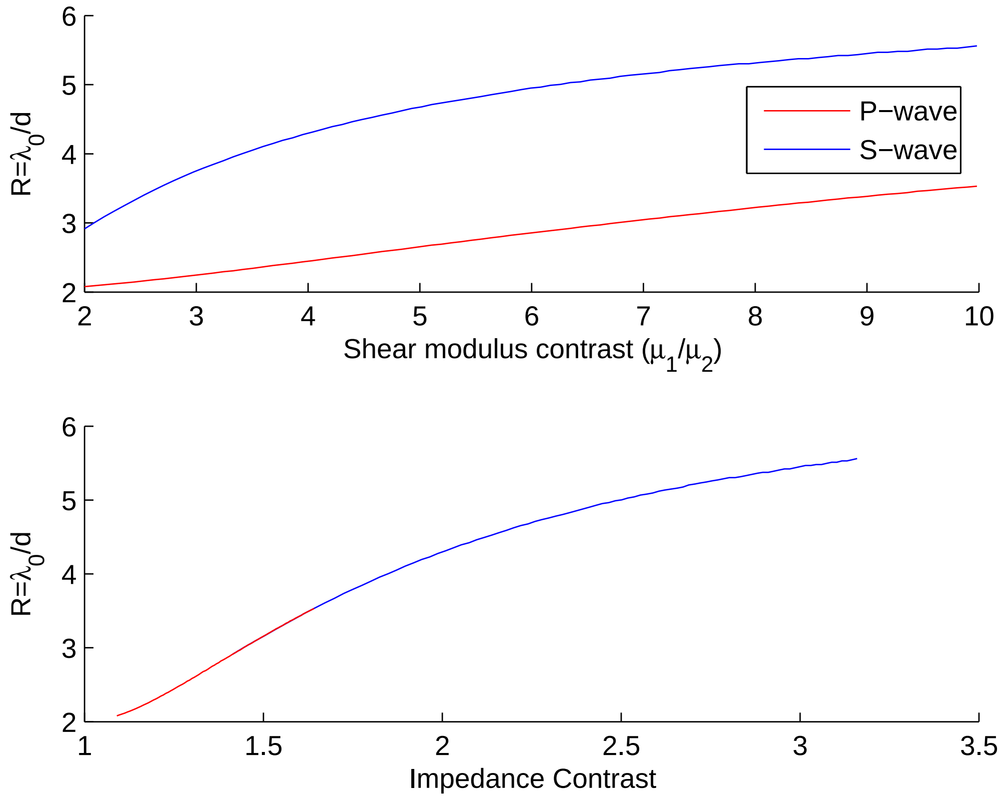


Figure 4.5: Shear modulus contrast and the onset of dispersion. No other material contrast

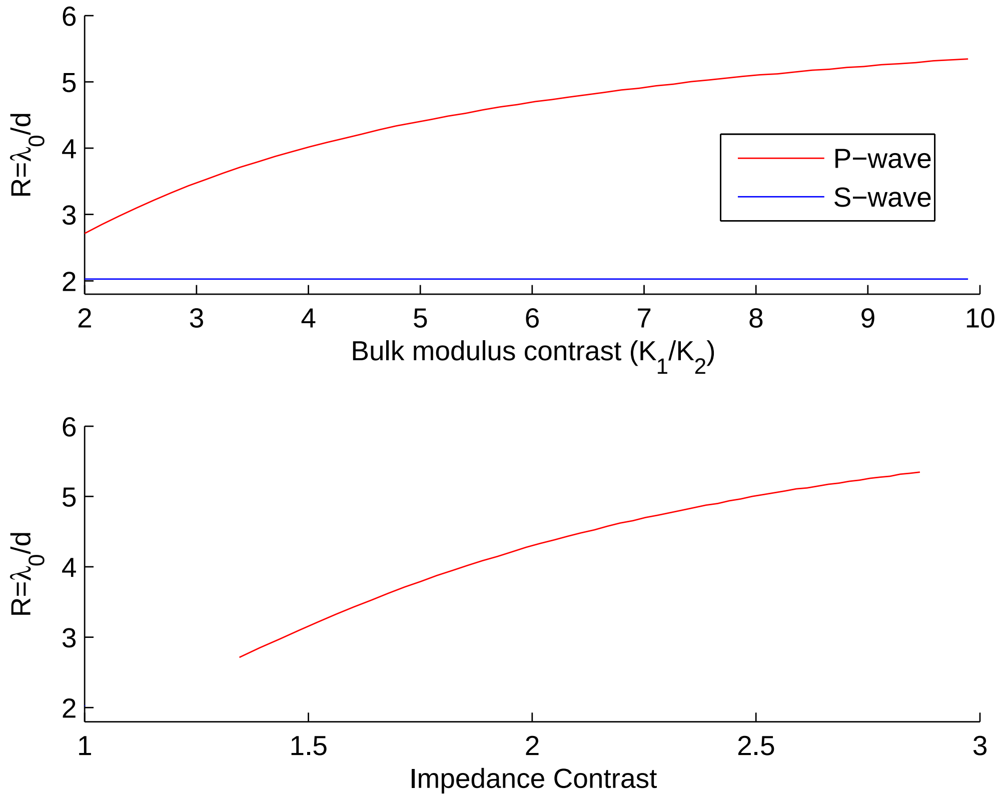


Figure 4.6: Bulk modulus contrast and the onset of dispersion. No other material contrast

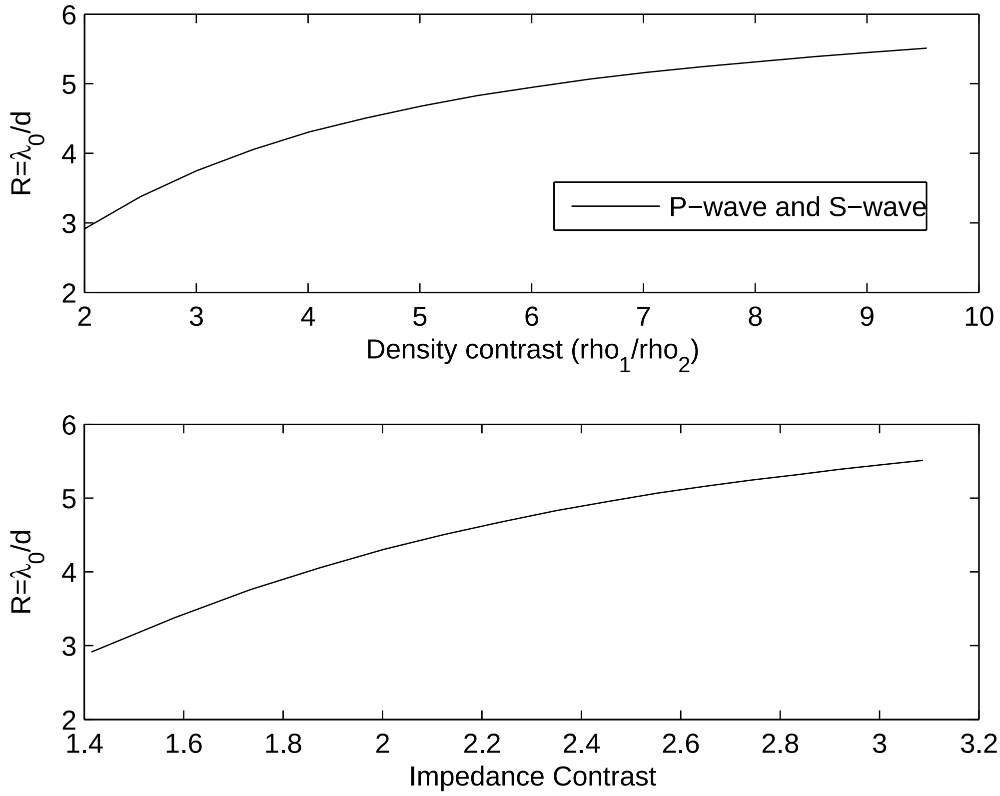


Figure 4.7: Density contrast and the onset of dispersion. No other material contrast

contrasts, but increases much less as the contrast continues to increase. It is also notable that $R$ is always greater for the $S$-wave in this case.

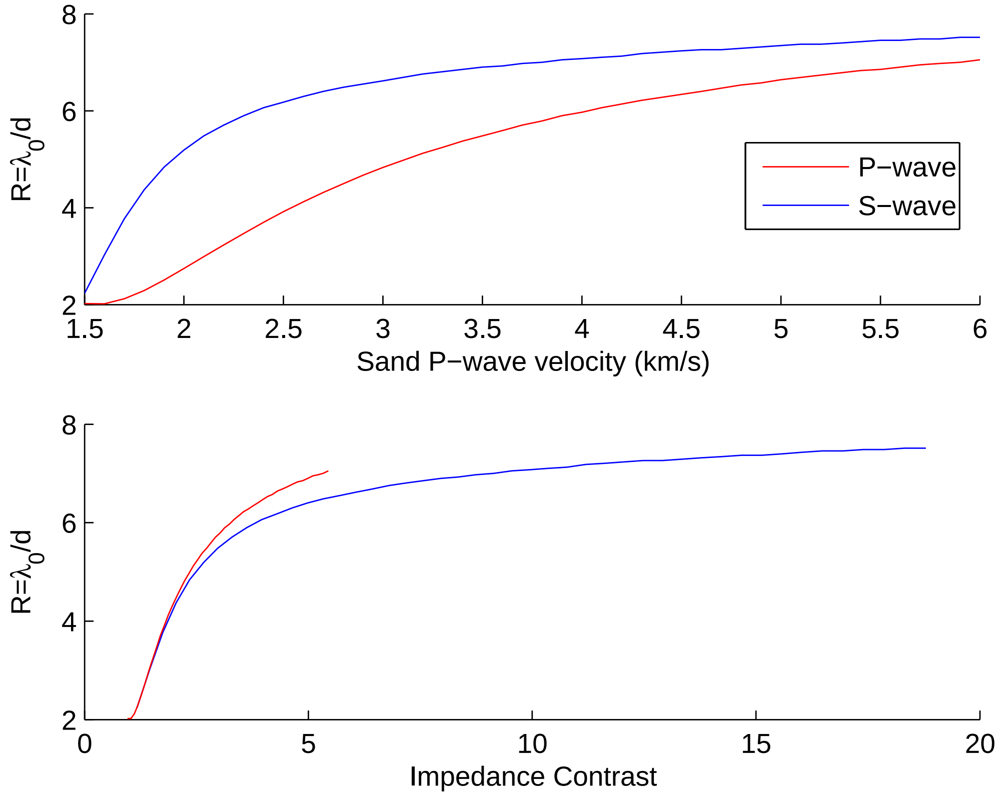


Figure 4.8: Sand-shale and the onset of dispersion

### 4.2.1 Stop-Band Thickness and Impedance Contrast

Two major effects of the scattering in periodic media are the dispersion and occurrence of stop-bands in which waves are attenuated due to destructive interference.

The characteristics of the Brillouin zones and stop-bands are controlled by two factors, the relative fraction of constituents, and the impedance contrast between those constituents. Figure 4.9 shows how the thickness of the first four stop-bands are controlled by impedance contrast for $P$-waves propagating normal to the layering. Both layers are of equal thickness with one layer being held constant with $V_p = 2\frac{km}{s}$ the second layer starts with all identical properties, but has one parameter ($\mu, K$, and $\rho$) varied for each of the subplots giving the stated impedance contrast. The thickness of each layer is held constant at 1 meter. Obviously the stop-band widths are to be examined relative to each other as the actual width depends on the period of the media.

The most important observation is that the character of the stop-bands remains virtually independent of which material property is being changed. However, there is a significant difference in the absolute behavior when a change in density as opposed to the elastic constants leads to the impedance contrast. A given impedance contrast caused by elastic constant contrast will lead to larger stop-bands then if that same impedance contrast is attributable to a density contrast.

Figure 4.10 shows the stop-bands vs. impedance contrast for an alternating sand-shale sequence. The shale is maintained at a constant $V_p = 1.5\frac{km}{s}$ while the sand is varied to give the corresponding impedance contrast. The thickness of each layer is 1 meter. An examination of this figure reveals that the disappearance of stop-bands always occurs at integer or half-integer impedance contrasts. Upon closer

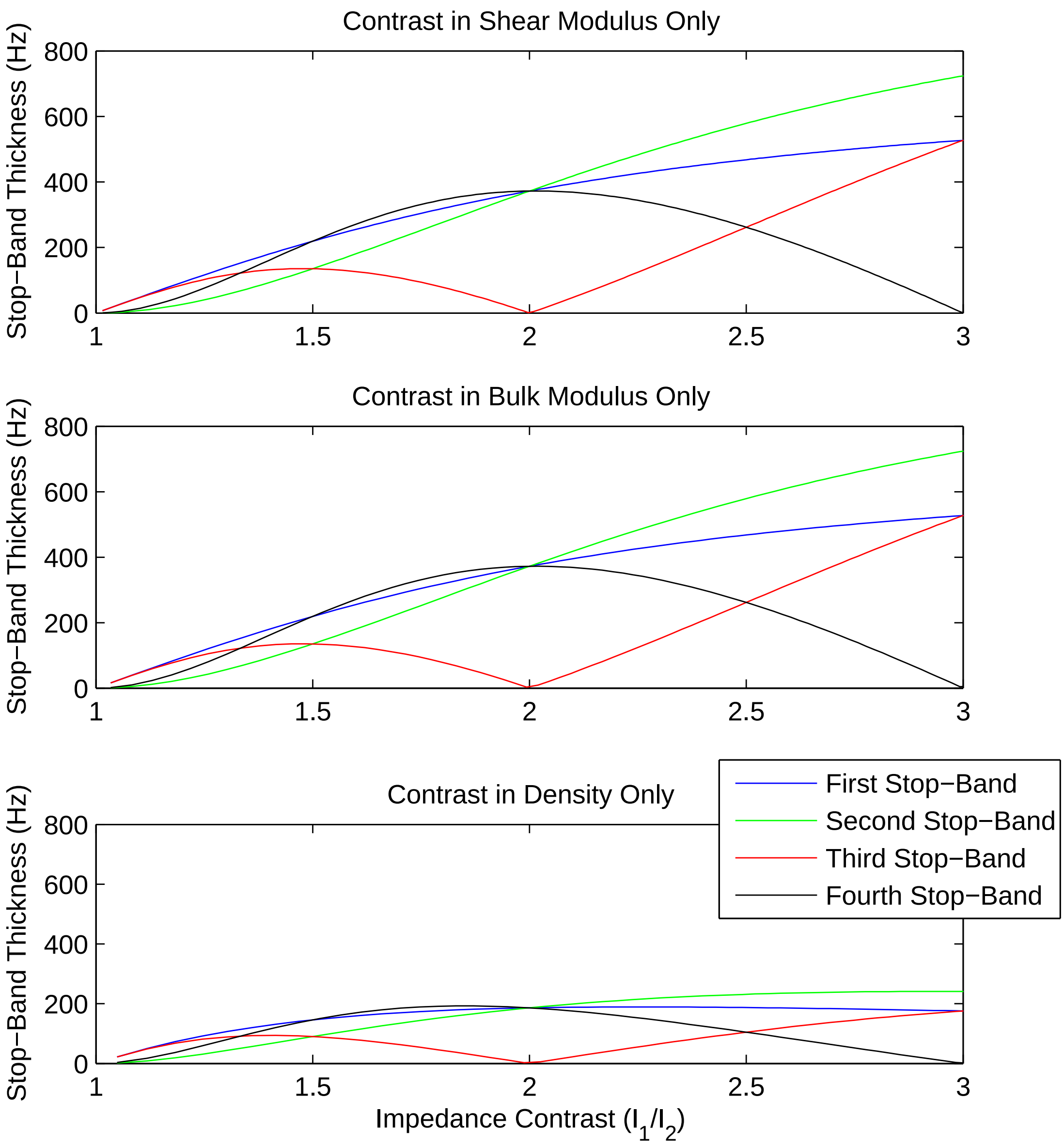


Figure 4.9: Thicknesses of the stop-bands are a function of the impedance contrast

examination a condition for the disappearance of band-gaps can be seen. When the following condition is satisfied the band-gap will go to zero:

$$m_i = \frac{\omega d_i}{c_i \pi} \tag{4.1}$$

When all $m_i$ are integer values at a given frequency the stop-band at the edge of the $p^{th}$ Brillouin zone will close, where $p = \sum_i m_i$.

This is a simple extension of the physics that leads to the appearance of band-gaps. To satisfy the conditions requiring continuity of stresses and displacements when the Floquet wave is a harmonic of the period of the medium (edge of a Brillouin zone), vertical wave numbers in each layer must be harmonics of those layers or the Floquet wave must have an imaginary part (scattering attenuation).

Another condition for the disappearance of stop-bands has been given by Shul'ga (1982) and Manzanares-Martinez and Ramos-Mendieta (2000).

$$\sin\theta_b = \sqrt{(\frac{\mu_1\rho_1}{\mu_2\rho_2} - 1)(\frac{\mu_1^2}{\mu_2^2} - 1)^{-1}} \tag{4.2}$$

For wave propagation at this so called 'elastic Brewster angle'[1] all stop bands go to zero. This is manifested as a line through points where frequency contours are continuous across Brillouin zones in Figure 3.7. Figure 4.11 shows the disappearance of the stop-bands for the standard sand-shale medium at an angle of about $28^o$ to the layering, corresponding to the expected elastic Brewster angle.

[1]While this effect does occur when the reflected and refracted waves are orthogonal as with the traditional EM Brewster angle, it must be emphasized that the physics are different.

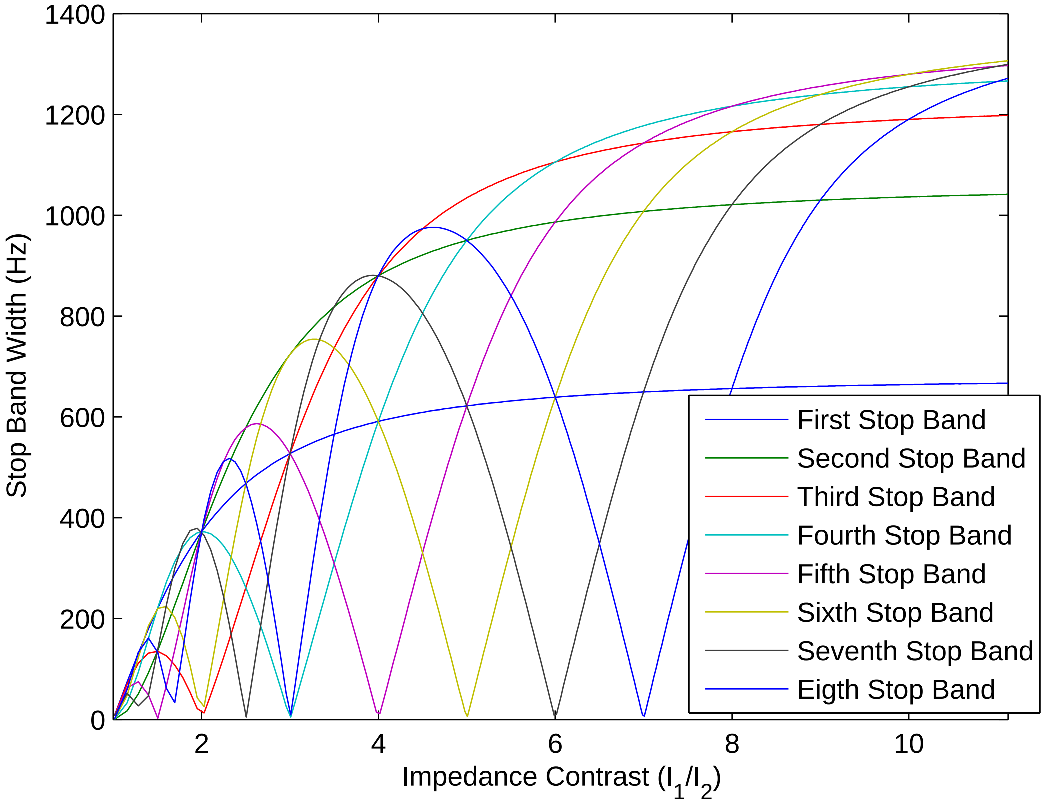


Figure 4.10: Thicknesses of the stop-bands are a function of the impedance contrast for a sand-shale medium

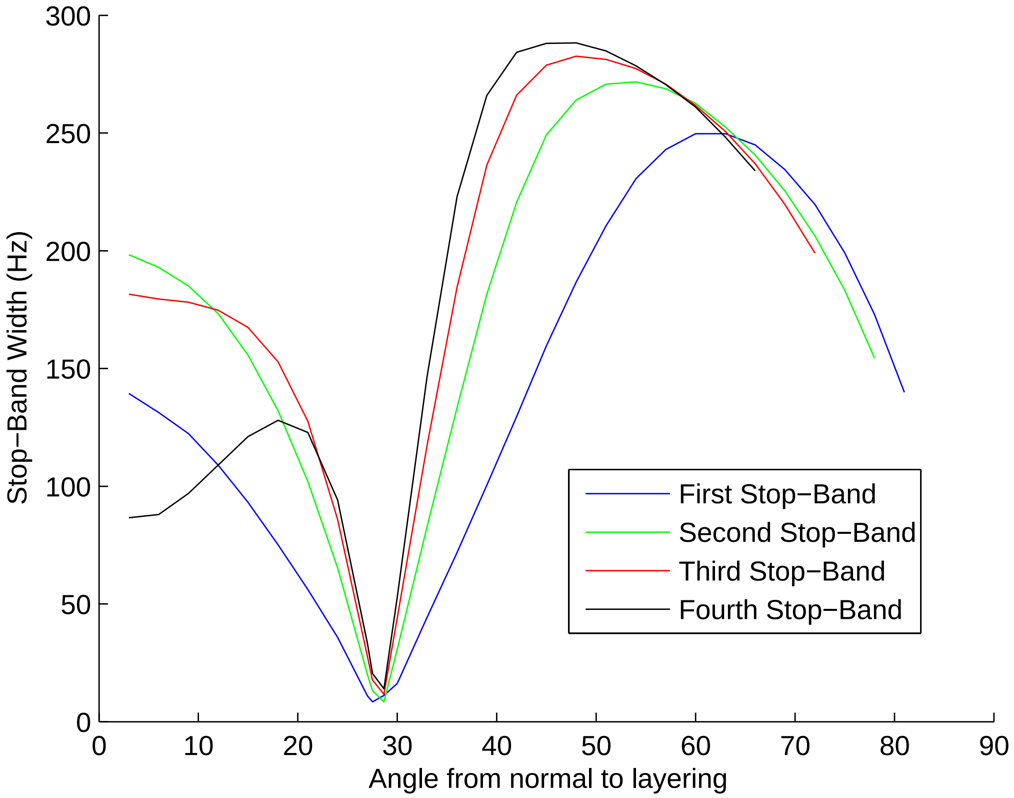


Figure 4.11: Thicknesses of the stop-bands are a function of angle of incidence for a sand-shale medium

# Chapter 5

# Fractured Thin Layered Periodic Media

## 5.1 The Problem

The preceding chapters have demonstrated how layering of geologic materials leads to anisotropy and dispersion. In most cases the anisotropy was demonstrated to be of VTI symmetry. The one exception was that shown in Section 2.3 where the effect of anisotropic layers was considered. The case where at least one layer was HTI was found to lead to orthorhombic symmetry. Orthorhombic symmetry commonly arises in two other cases. One is due to principal stress directions, the other closely related causes are aligned vertical fractures or inclusions. In this chapter, the latter's effect on anisotropy in a layered environment are considered.

Effective media theory for inclusions and fractures is, as well, if not better documented in the literature than for layered media. However, the case in which both are considered in unison is much more sparse. Theoretical considerations in which cracks are considered in superposition with thin layering where studied by Gelinsky and Shapiro (1997); Schoenberg and Helbig (1997); Bakulin et al. (2000), although

Grechka (2003) points out an error in this approach (this is considered in more detail in the next section). The only experimental considerations of this problem are those that consider the orthorhombic symmetry due to a phenolic laminate (Rumpker et al., 1996; Mah and Schmitt, 2001) and Hood and Mignogna (1994) who considers a laminate of glass and epoxy that is sliced vertically and and reglued with epoxy. The most realistic experiment is that of Assad (2005) who considers vertical rubber inclusions in a layered background.

## 5.2 Validity of Approach

In order to simulate fractures or inclusions in a thin layered media there appear to be two possible approaches, as illustrated in figure 5.1. The first approach would be to start with the two distinct layers, calculate separately their effective elastic constants with the inclusions and then proceed to the effective layered case with these two effective constituents. The other approach would be to calculate the effective elastic constants of the layered media and then calculate the effective constants with the inclusions.

First it must be stressed that these approaches are expected to produce different results. Effective media theory assumes that the inclusions are in an unbounded media, i.e. there is no consideration of the effect of boundaries on the inclusions. This leads to different results for both approaches and also is why both techniques are technically incorrect if the goal is to consider cracks which penetrate between layers. Grechka (2003) encounters this error while considering vertical cracks in a

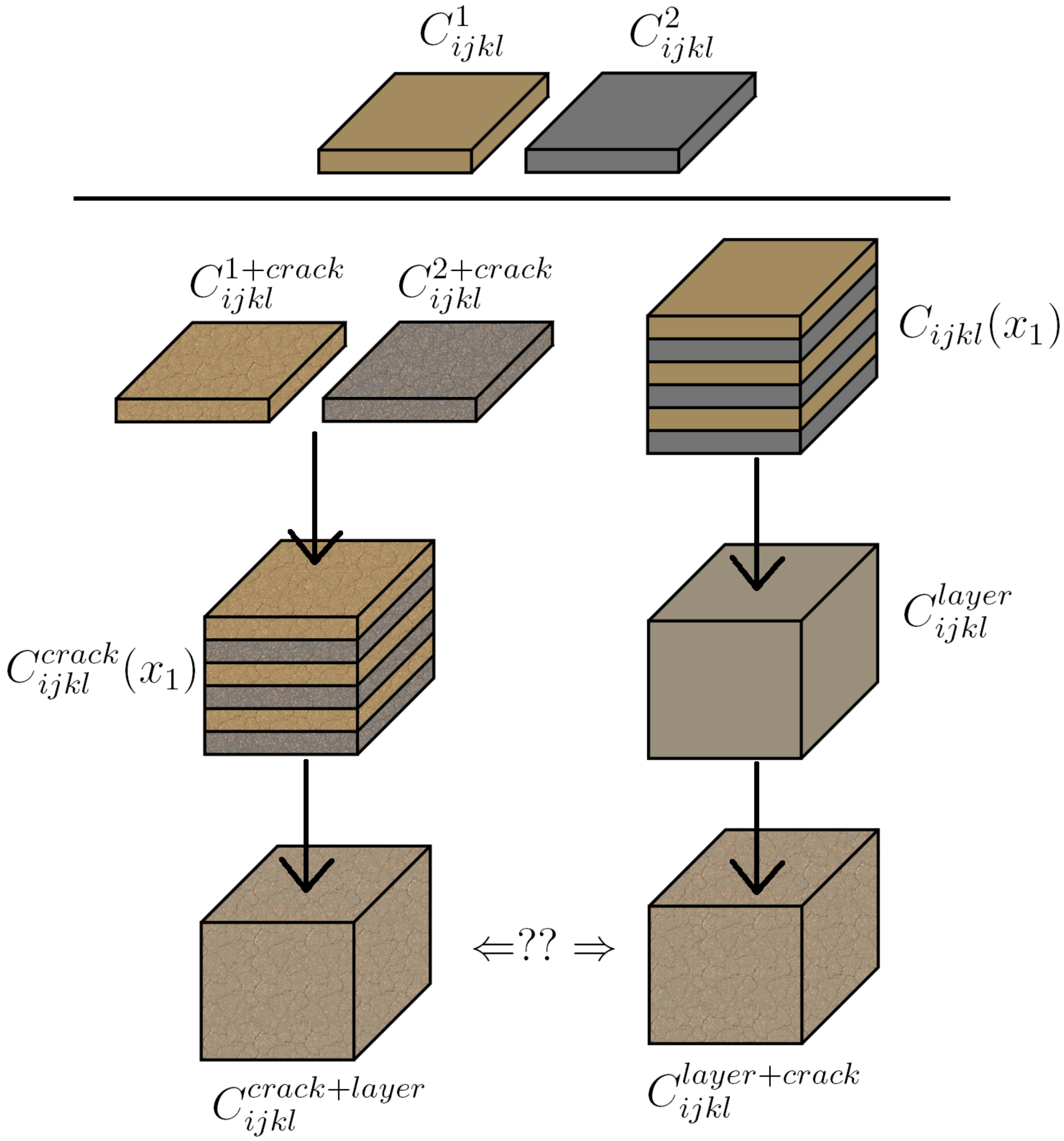


Figure 5.1: Two possible approaches to the fractured EMT problem

layered media and comparing the theoretical results to numerical simulations in 2-D. His published results show little actual error in these two approaches, but he stresses that further simulations showed increasing contrast between layers or cracks led to greater error. This is expected because, as the stress field around an inclusion or fracture increases, its effect on the stress between layers increases and vice-versa. Grechka (2003) does point out that the elastic constants $C_{44}$ and $C_{55}$ are equivalent for both approaches and give the appropriate EMT values.

In the subsequent simulations both of the above approaches are used to simulate different situations. The first case in which inclusions are considered separately in different layers is obviously appropriate as long as we consider the case where the fractures are much smaller then the thickness of the layer, i.e. micro-cracks. Here, the second case will be used to model fractures which may be larger then the layer thickness. To justify this latter approach I first consider EMT for the experimental results published by Hood and Mignogna (1994).

Hood and Mignogna (1994) considered a layered media consisting of alternating glass plates and epoxy. They first make velocity measurements of this effective TI media, then they cut the media vertically and glue it back together using epoxy and make measurements of what is then an effective orthorhombic medium. They then compare their experimental results to theoretical results based on Schoenberg (1980, 1983) which models cracks as layers of weakness. They note that the thin epoxy layers may not fulfill the conditions of Schoenberg's linear slip deformation assumptions, but they still get reasonable results. Here, a different approach to modeling their data is taken, in order to illustrate the rigorousness of using a sequence of two averaging approaches for modeling reality.

First, the initial layered media is considered using the approach of Schoenberg and Muir (1989) as used in chapter 2. The isotropic glass properties are given as:

$$V_p = 5.37\frac{km}{s}, V_s = 3.37\frac{km}{s}, \rho = 2.51\frac{kg}{m^3}$$

and the epoxy as:

$$V_p = 2.24\frac{km}{s}, V_s = .956\frac{km}{s}, \rho = 1.08\frac{kg}{m^3}$$

The thickness of the glass is $4 \times 10^{-4}$m. The thickness of the epoxy is given as an average found by considering the total thickness of the glass plates before and after the epoxy layers were added. The average thickness is $8.38 \times 10^{-6}$m It is clear that this average layer thickness is sufficient for accurately finding the effective media behavior if we consider the conditions of Backus averaging. The layering was required to be stationary, for which we use periodicity to satisfy this condition as simply as possible. If the exact layer thickness's were not known, the medium could be considered a random, but stationary medium still allowing for the calculations of effective properties. What would be expected, however, are for the perturbations in epoxy layer thickness to average out giving the same result as using an average thickness.

The experimental results given by Hood and Mignogna (1994) as well as my theoretical results are given in Table 5.1. These results are also plotted in Figure 5.2, and match the orthorhombic behavior shown in Figure 2.14. The important observation to make is that even with the large contrast between the glass and epoxy, using two sequential averaging approaches introduces no more error then already appears in the experiment after the first averaging. Also note that the error in $C_{44}$ and $C_{55}$ is no less then the errors in the other constants. Since we expect these constants to always be correct for sequential averaging in orthorhombic media it appears little extra error has been introduced by this approach. With these observations, using this averaging approach to simulate effective behavior of the fractured layered media is justified.

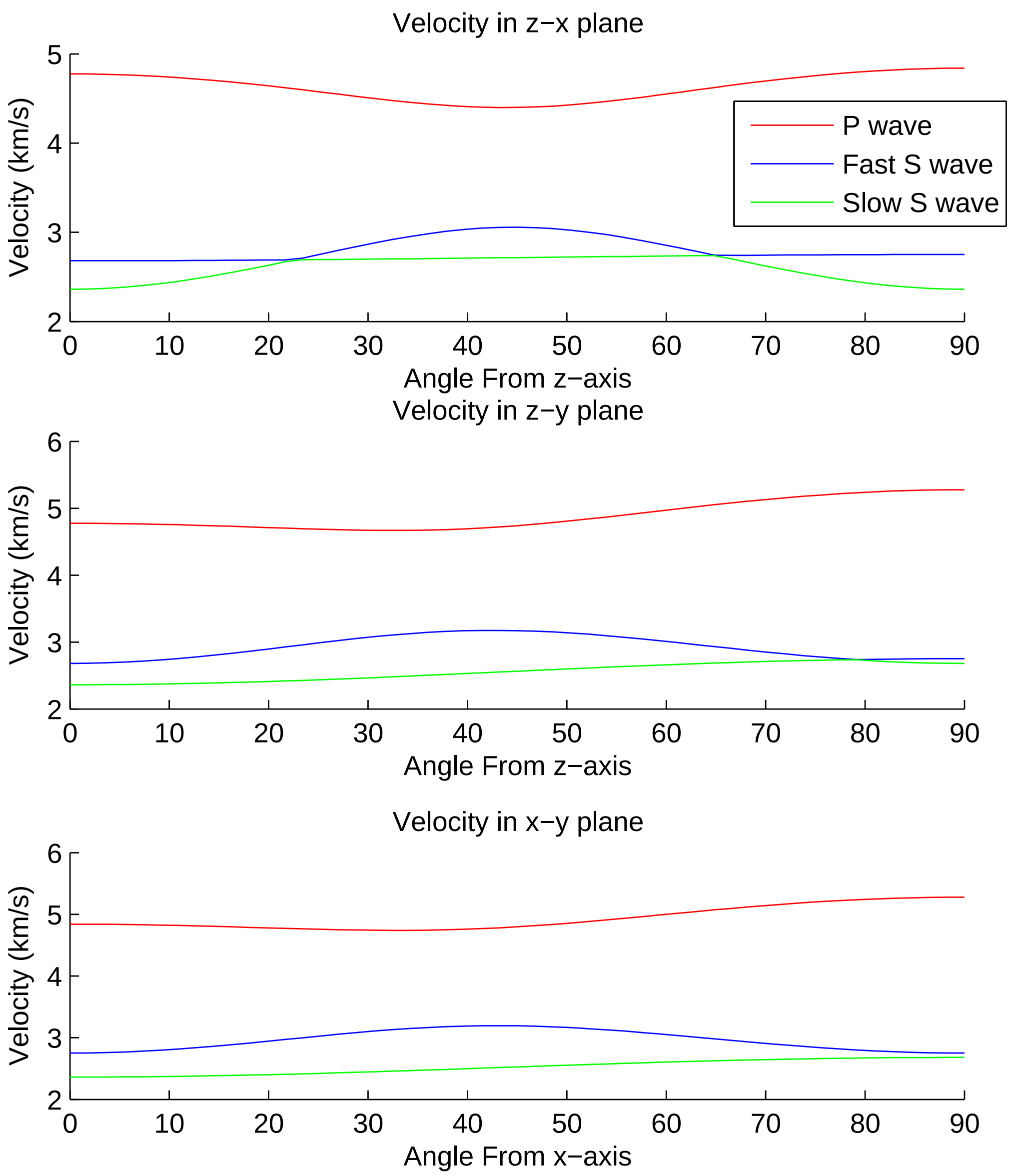


Figure 5.2: Anisotropy from calculations for model from Hood and Mignogna (1994)

Table 5.1: Model results from Hood and Mignogna (1994) data

| | Measured from Layered (Hood and Mignogna, 1994) (Gpa) | Calculated (Gpa) | Percent Error | Measured from orthorhombic medium (Gpa) | Calculated (Gpa) | Percent Error |
|---|---|---|---|---|---|---|
| $C_{11}$ | 7.89 | 7.06 | 11.1 | 6.44 | 5.81 | 10.2 |
| $C_{22}$ | 7.89 | 7.06 | 11.1 | 7.62 | 6.91 | 9.78 |
| $C_{33}$ | 6.97 | 5.77 | 18.0 | 6.64 | 5.66 | 16.0 |
| $C_{44}$ | 2.13 | 1.81 | 16.1 | 2.06 | 1.78 | 14.7 |
| $C_{55}$ | 2.13 | 1.81 | 16.1 | 1.65 | 1.38 | 17.4 |
| $C_{66}$ | 2.83 | 2.79 | 14.2 | 1.94 | 1.88 | 3.20 |
| $C_{12}$ | – | 1.47 | – | – | 1.25 | – |
| $C_{13}$ | – | 1.28 | – | – | 1.10 | – |
| $C_{23}$ | – | 1.28 | – | – | 1.23 | – |

## 5.3 Effective Anisotropy of Fractured Layered Periodic Media

A question that is of primary importance to the study of anisotropic media is: what can anisotropy tell us about fluid content? This is the question which will be addressed in this section. A fractured layered media is modeled and the effective anisotropy that results for both gas and liquid filled penny-shaped fractures is considered.

For all purposes, the standard sand-shale model that has been used in the previous chapters is considered here. It is assumed that the wavelength of insonification is much greater then both the period of the media as well as the size of the fractures. The effective media behavior caused by fractures is calculated using pre-existing software that employs the General Singular Approximation (Bayuk and Chesnokov, 1997). In addition $V_p/V_s^{max}$ ratios are considered as they have previously been demonstrated to be useful in a fractured isotropic background (Bayuk and Chesnokov, 1997).

The first model, Figures 5.3 and 5.4, compares the effect of averaging order as illustrated in Figure 5.1. For this case the fractures have an aspect ratio of 1 : 100 with a total fractional volume porosity, of .01. The crack content is defined with the properties in Table 5.2. All fractures are parallel to each other with their major axis orthogonal to the layering, lying in the $y-z$ plane. In the figures, the column labeled 'isotropic background' has the fractures calculated before layering and the other column labeled 'layered background' has the effective layering anisotropy calculated first.

In this figure it is apparent that the absolute behavior of the gas or oil filled inclusions is indistinguishable between averaging order. The relative behavior between gas and oil using one averaging approach does differ from the other approach. Again this simulation supports using this sequential averaging approach, because of the lack of difference in the absolute behavior between the two orders of averaging. Subsequent simulations will use the 'micro-crack' approach of averaging fractures before layering. This is expected to introduce less error, then the 'large-crack', layering before fractures approach. Although the difference between the two approaches is seen to not be very dramatic, it is still important to stress this distinction.

Table 5.2: Inclusion properties for modeling of fractures

| Inclusion | K (Gpa) | $\mu$ (Gpa) | $\rho$ |
|---|---|---|---|
| Gas | 1.39 | 0 | .8 |
| Oil | .000175 | 0 | .007 |
| Water | 2.25 | 0 | 1 |

Before examining the effect of material controls on this anisotropy, first the effect of having fractures and layering as opposed to having just fractures will be examined, i.e. what effect does layering introduce in the effective anisotropy already present due to vertical fractures. Figures 5.5 and 5.6 show the effect of gas and oil filled inclusions in a isotropic and layered background. The primary effect of layering on the $V_p/V_s^{max}$ ratio is an exaggeration of the contrast between the gas and fluid ratios.

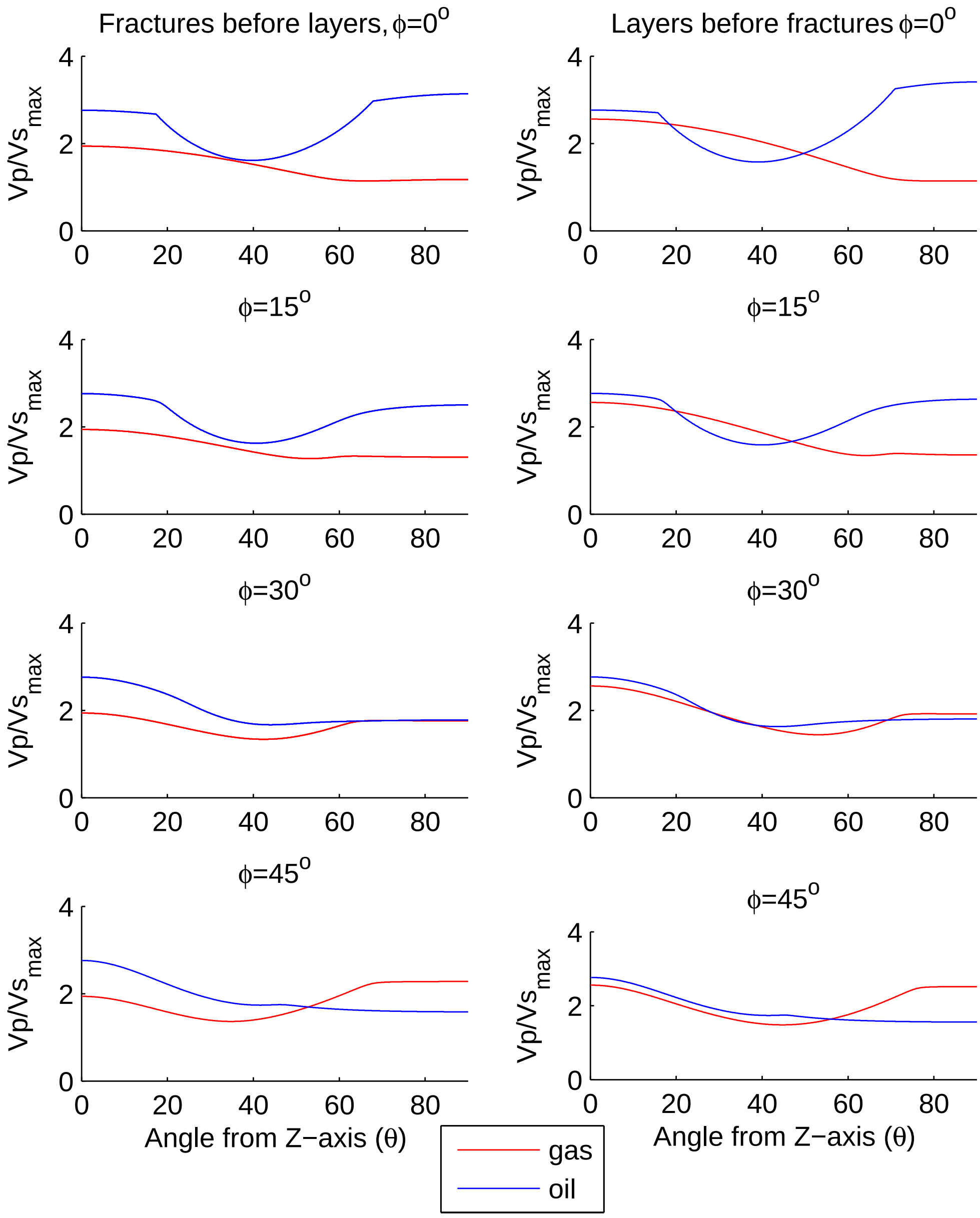


Figure 5.3: Comparison of cracks before or after layering $0^o$-$45^o$ azimuth

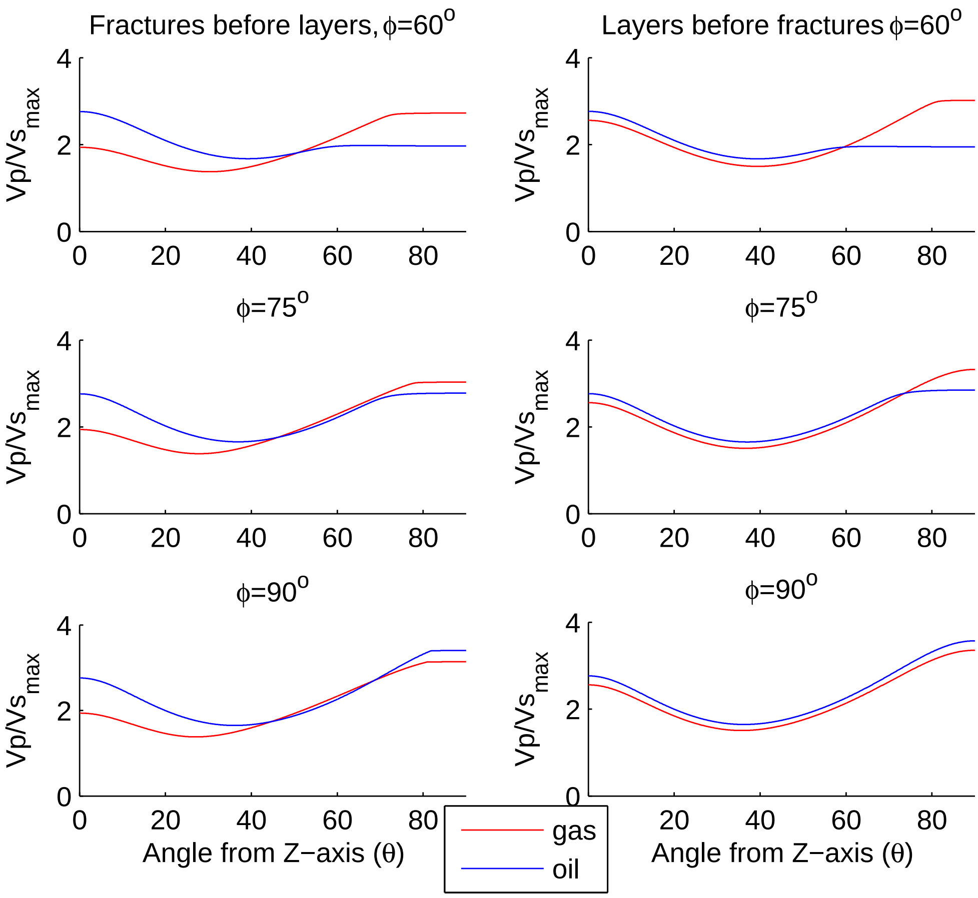


Figure 5.4: Comparison of cracks before and after layering $60^o$-$90^o$ azimuth

As already seen this difference in behavior is still most dramatic at a zero degree azimuth, and disappears as the azimuth goes to ninety degrees.

Variations in the porosity appear to have little effect on these differences between gas and liquids. The difference doesn't significantly decrease until the porosity approaches .05%. Differences in porosity are shown in Figure 5.7. Figure 5.8 shows the effect of different aspect ratios. There is a dramatic difference between liquid and gas at very small aspect ratios. This difference only disappears at very large aspect ratios.

The inclusion of vertical fractures in an otherwise isotropic rock has previously been shown to lead to anisotropy which can be used to distinguish gas from liquid inclusions (Bayuk and Chesnokov, 1997). The same approach is used here to demonstrate that the effective anisotropy caused by the addition of layering is orthorhombic, and that there is an increase in the difference of the $V_p/V_s^{max}$ ratio with the addition of layering.

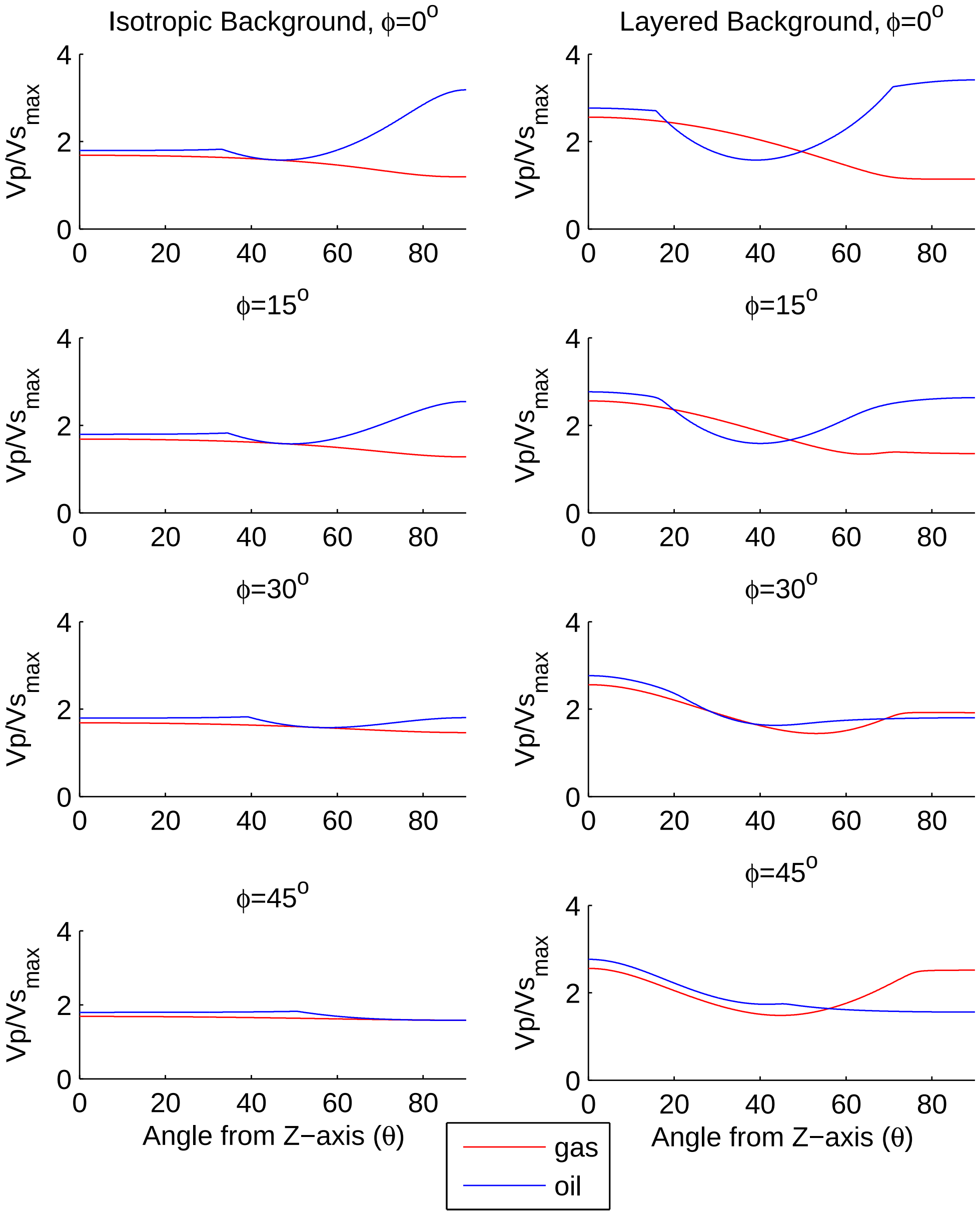


Figure 5.5: Comparison of cracks in isotropic vs. layered media $0^o$-$45^o$ azimuth

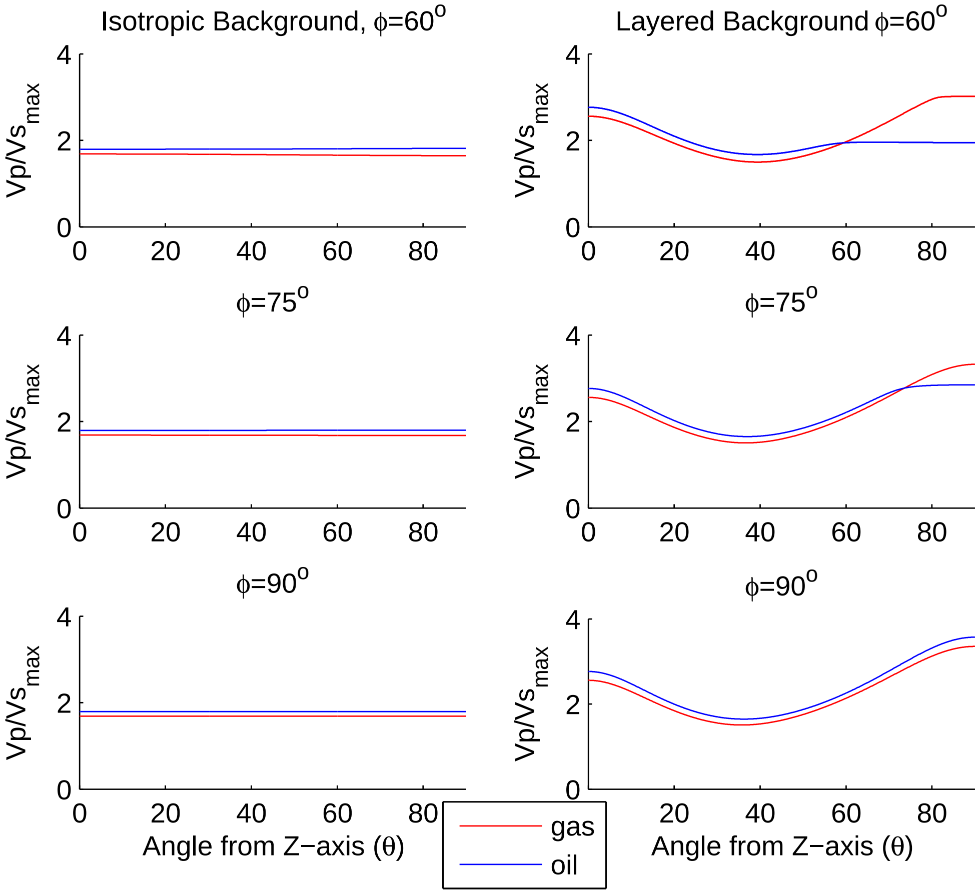


Figure 5.6: Comparison of cracks in isotropic vs. layered media $60^o$-$90^o$ azimuth

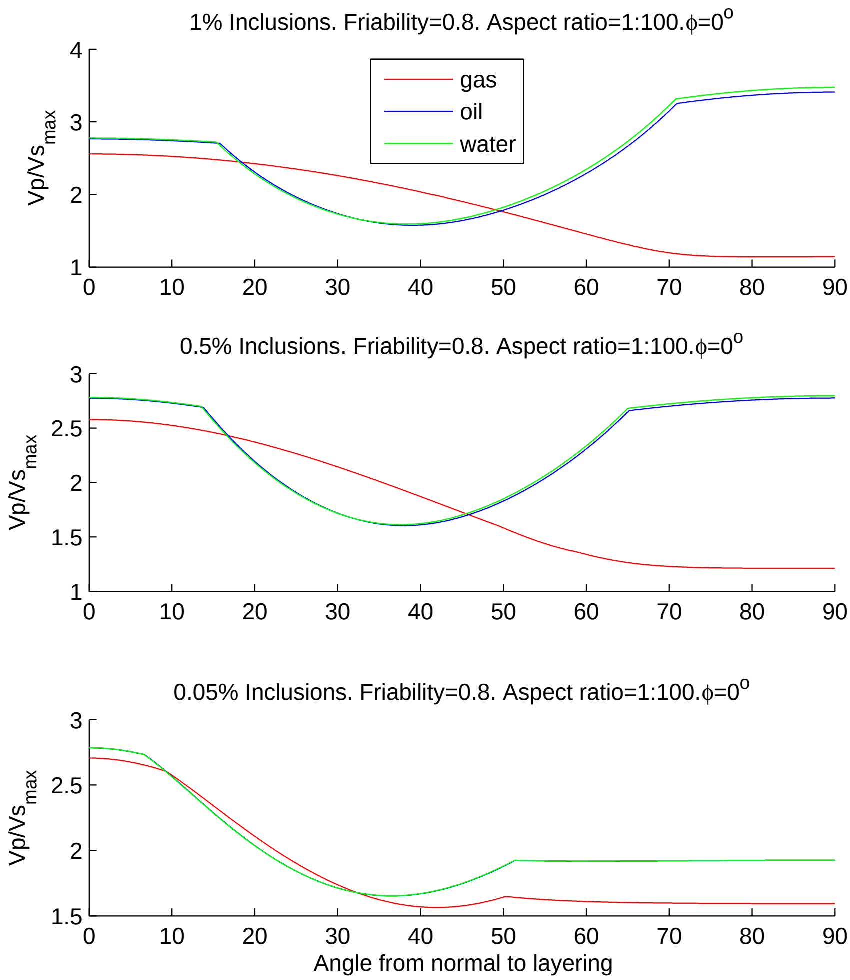


Figure 5.7: Various porosities and the effect on $V_p/V_s^{max}$

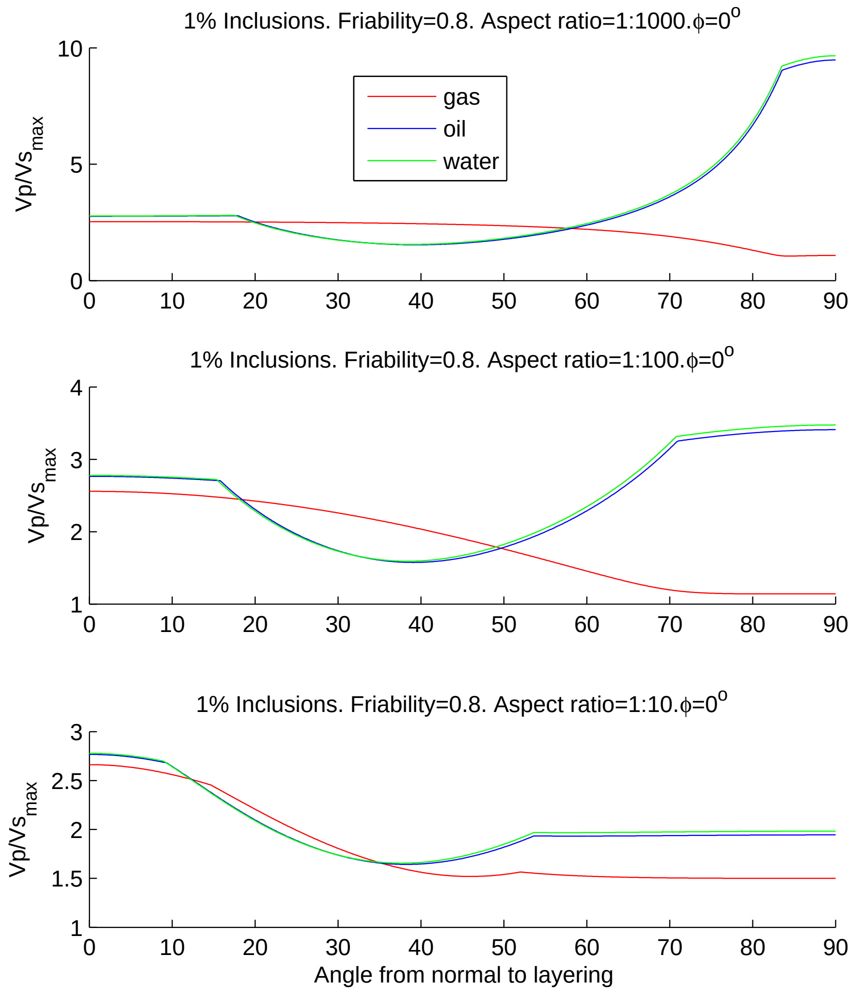


Figure 5.8: Various aspect ratios and the effect on $V_p/V_s^{max}$

# Chapter 6

# Conclusions

The purpose of this dissertation was to provide a comprehensive look at how material contrasts control wave propagation in a periodically layered media. Two different approaches, depending on scale, were used. Backus averaging was used to consider the case when the period of the media is much less than the wavelength of the insonifying field. Floquet's theory was used to consider the case when the wavelength was of the same order as the period of the media. Both of these approaches are well documented in the existing literature, and alone offer no new knowledge for the field; however, their use in modeling behavior of wave propagation with differing contrasts has offered new insight into the problem.

In the long-wave case, material contrasts were examined independently. This illustrated the importance of shear modulus contrast in long-wave anisotropy, which although previously known, is often ignored or under appreciated. The modeling of real rocks also demonstrates that $P$-wave, layer induced anisotropy is negligible at angles less then $30^\circ$ to the layering.

The inclusion of anisotropic layers demonstrated the more complex effective anisotropies that can result from a layered media. Most interesting is the demonstration that the presence of an HTI layer will cause effective anisotropy that has orthorhombic symmetry. This was demonstrated both with intrinsic layer anisotropy and anisotropy due to vertical fractures.

A comparison of electromagnetic and elastic waves demonstrates that the only differences in behavior with respect to contrast is the material property leading to the contrast, and the complication in the $S_v$ anisotropy which arises due to $P$-wave coupling in the elastic case, but is not present in electromagnetic wave propagation.

Much more interesting questions were explored that relate to the case when the wavelength is not much longer then the period of the media. An approach to determining the long-wave limit has been proposed which emphasizes the dependence of this limit on the contrast between the layers. This contrast was previously ignored in determining this limit; however, this modeling demonstrates that for normal materials this contrast can vary by a factor of two depending on the material properties.

An intensive computational approach for determining the dispersion relations has allowed consideration of dispersion to be extended beyond the first Brillouin zone. The dependence of the first and higher order stop-band widths on the material contrasts is fascinating and very important to the understanding of effective wave propagation in periodic materials. The only previous considerations come from recent papers published in the area of solid state physics which often disregard the higher order stop-bands due to their interest in discrete, not continuous structures. The demonstration of a critical angle at which there is no dispersion for the $S_h$-wave is an important observation. A fundamental behavior of higher-order stop-bands dependence on material contrasts was also demonstrated, along with the presence of critical contrasts that lead to the closing of one or more stop-bands.

One immediate application of the understanding provided by this dissertation is the seismic characterization of reservoirs based on the material contrasts manifested through anisotropic and dispersive behavior. This should prove to be particularly useful in strongly layered environments such as shale plays, where the layering contrast of clay and kerogen can be directly connected with the vertical anisotropy. Future avenues of research should address the lack of experimental data for real periodic rocks. An extension of the theory to quasi-periodic and random layering is also necessary to fully understand the anisotropic and dispersive behavior in a broader range of real materials.

# Bibliography


Arfken, G., 1970: *Mathematical Methods for Physicists*. Academic Press, New York, 2nd edition.

Assad, J. M., 2005: The effect of orthorhombic anisotropy and its implication for oil recovery and resevoir exploitation. *Geophysical Prospecting*, **53**, 121–129.

Backus, G., 1962: Long-wave elastic anisotropy reduced by horizontal layering. *J. Geophys. Res.*, **67**, 4427–4440.

Bakulin, A., V. Grechka, and I. Tsvankin, 2000: Estimation of fracture parameters from reflection seismic data-part ii fractured models with orthorhombic symmetry. *Geophysics*, **65**, 1803–1817.

Bayuk, I. O. and E. M. Chesnokov, 1997: Is it possible to discriminate between gas and liquid inclusions? *SEG Expanded Abstracts*, **16**, 968–971.

Berryman, J., 1979: Long-wave elastic anisotropy in transversely isotropic media. *Geophysics*, **44**, 896–917.

Berryman, J. G., 2005: Fluid effects on shear waves in finely layered porous media. *Geophysics*, **70**, N1–N15.

Born, M. and E. Wolf, 1999: *Principles of Optics*. Cambridge University Press, New York, 954 pp.

Braga, A. M., 1992: Floquet waves in anisotropic periodically layered composites. *J. Acoust. Soc. Am.*, **91**, 1211–1227.

Brillouin, L., 1946: *Wave Propagation in Periodic Structures*. McGraw-Hill Inc., New York.

Carcione, J., 2001: *Wave fields in real media:Wave Propagation in anisotropic, anelastic, and porous media*. Pergamon.

Carcione, J., D. Kosloff, and A. Behle, 1991: Long-wave anisotropy in stratified media: A numerical test. *Geophysics*, **56**, 245–254.

Carmichael, R. S., 1989: *Practical handbook of physical properties of rocks and minerals*. CRC Press, Boca Raton, Florida.

Castagna, J., M. Batzle, and T. Kan, 1993: Rock physics-the link between rock properties and avo response. *Offset-dependent reflectivity: Theory and practice of AVO analysis*, J. Castagna and M. Backus, eds., SEG.

Coe, A. L., D. W. Bosence, K. D. Church, S. S. Flint, J. A. Howell, and R. C. L. Wilson, 2003: *The Sedimentary Record of Sea-Level Change*. Cambridge University Press.

Daley, P. and F. Hron, 1977: Reflection and transmission coefficients for transversely isotropic media. *Bulletin of the Seismological Society of America*, **67**, 661–675.

Delph, T., G. Herrmann, and R. Kaul, 1978: Harmonic wave propagation in a periodically layered, infinite elastic body: antiplane strain. *Journal of Applied Mechanics*, **45**, 343–349.

Dukin, A., N. Feoktistov, A. Medvedev, A. Pevtsov, V. Golubev, and A. Sel'kin, 2006: Polarization inhibition of the stop-band in distributed bragg reflectors. *J. Opt. A: Pure Appl. Opt.*, **8**, 625–629.

Floquet, G., 1883: Sur les équations differentielles linéaires à coefficients périodiques. *Ann. École. Norm. Sup.*, **12**, 47–88.

Gardner, G., L. Gardner, and A. Gregory, 1974: Formation velocity and density-the diagnostic basis for stratigraphic traps. *Geophysics*, **39**, 770–780.

Gelinsky, S. and S. A. Shapiro, 1997: Poroelastic backus averaging for anisotropic layered fluid- and gas-saturated sediments. *Geophysics*, **62**, 1867–1878.

Grechka, V., 2003: Effective media: A forward modeling view. *Geophysics*, **68**, 2055–2062.

Griffiths, D. J., 1999: *Introduction to Electrodynamics*. Prentice Hall, 3rd edition.

Gu, C. and P. Yeh, 1996: Form birefringence dispersion in periodic layered media. *Optics Letters*, **21**, 504–506.

Helbig, K., 1984: Anisotropy and dispersion in periodically layered media. *Geophysics*, **49**, 364–373.

—, 1994: *Foundations of Anisotropy for Exploration Seismics*. Pergamon.

Hood, J. A. and R. B. Mignogna, 1994: Experimantal separation of constituent anisotropies using contact measurements. *Seismic Physical Modeling*, D. A. Ebrom and J. A. McDonald, eds., SEG, number 15 in Geophysics reprint series, 333–345.

Hovem, J. M., 1995: Acoustic waves in finely layered media. *Geophysics*, **60**, 1217–1221.

Jackson, J. D., 1998: *Classical Electrodynamics*. John Wiley and Sons Inc., 3rd edition.

Kittel, C., 1976: *Introduction to Solid State Physics*. John Wiley and Sons, Inc., New York, New York.

Landau, L. and E. Lifshitz, 2003: *Fluid Mechanics*. Butterworth-Heinemann, 2nd edition.

Lee, E., 1975: Wave propagation in composites with periodic structures. *Proceedings of the Fifth Congress of Applied Mechanics*, G49–G59.

Lee, E. and W. H. Yang, 1973: On waves in composite materials with periodic structure. *Siam J. Appl. Math.*, **25**, 492–499.

Lekner, J., 1994: Light in periodically stratified media. *J. Opt. Soc. Am. A*, **11**, 2892–2899.

Mah, M. and D. Schmitt, 2001: Experimental determination of the elastic coefficients of an orthorhombic material. *Geophysics*, **66**, 1217–1225.

Manzanares-Martinez, B. and F. Ramos-Mendieta, 2000: Transverse elastic waves in superlattices: The brewster acoustic angle. *Physical Review B*, **61**, 12877–12881.

Marion, D. and R. Coudin, 1992: From ray to effective media theories in stratified media: An experimental study. *62nd Ann. Internat. Mtg. SEG Expanded Abstracts*, 1341–1343.

Marion, D., T. Mukerji, and G. Mavko, 1994: Scale effects on velocity dispersion: from ray to effective medium theories in stratified media. *Geophysics*, **59**, 1613–1619.

Mavko, G., T. Mukerji, and J. Dvorkin, 1998: *The Rock Physics Handbook: Tools for Seismic Analysis in Porous Media*. Cambridge University Press.

Melia, P. and R. Carlson, 1984: An experimental test of p-wave anisotropy in stratified media. *Geophysics*, **49**, 374–378.

Mukerji, T., G. Mavko, D. Mujica, and N. Lucet, 1995: Scale-dependent seismic velocity in heterogeneous media. *Geophysics*, **60**, 1222–1233.

Nayfeh, A. H., 1991: The general problem of elastic wave propagation in multilayered anisotropic media. *J. Acoust. Soc. Am.*, **89**, 1521–1528.

Olhoeft, G., 1989: Electrical properties of rocks. *Physical properties of rocks and minerals*, Y. Touloukian, W. Judd, and R. Roy, eds., Hemisphere Publishing Corp., New York, New York, 257–329.

Postma, G., 1955: Wave propagation in a stratified medium. *Geophysics*, **20**, 780–806.

Potel, C., J.-F. de Belleval, and Y. Gargouri, 1995: Floquet waves and classical plane waves in an anisotropic periodically multilayered medium: Application to the validity domain of homogenization. *J. Acoust. Soc. Am.*, **97**, 2815–2825.

Rumpker, G., R. J. Brown, and C. J. Thomson, 1996: Shear wave propagation in orthorhombic phenolic: A comparison of numerical and physical modeling. *Journal of Geophysical Research*, **101**, 27765–27777.

Rytov, S., 1956a: Acoustical properties of a thinly laminated media. *Soviet Physics: Acoustics*, **2**, 68–80.

—, 1956b: Electromagnetic properties of a finely stratified media. *Soviet Physics JETP*, **2**, 466–475.

Schoenberg, M., 1980: Elastic behavior across linear slip interfaces. *J. Acoust. Soc. Am.*, **68**, 1516–1521.

—, 1983: Reflection of elastic waves from periodically stratified media with interfacial slip. *Geophysical Prospecting*, **31**, 265–292.

Schoenberg, M. and K. Helbig, 1997: Orthorhombic media: Modeling elastic wave behavior in a vertically fractured earth. *Geophysics*, **62**, 1954–1974.

Schoenberg, M. and F. Muir, 1989: A calculus for finely layered media. *Geophysics*, **54**, 581–589.

Shul'ga, N., 1982: Propagation of volumetric shear waves of arbitrary direction in layered composites. *Prikladnaya Mekhanika*, **18**, 11–16.

Sve, C., 1971: Time-harmonic waves traveling obliquely in a periodically laminated medium. *Journal of Applied Mechanics*.

Thomsen, L., 1986: Weak elastic anisotropy. *Geophysics*, **51**, 1954–1966.

Ting, T. C., 1996: *Anisotropic Elasticity: Theory and Applications*. Number 45 in Oxford Engineering Science series, Oxford Science Publications.

Van Wagoner, J., R. Mitchum, K. Campion, and V. Rahmanian, 1990: *Siliciclastic Sequence Stratigraphy in Well Logs, Cores, and Outcrops: Concepts for High-Resolution Correlation of Time and Facies*. AAPG, Tulsa, Ok.

Vernik, L. and A. Nur, 1992: Ultrasonic velocity and anisotropy of hydrocarbon source rocks. *Geophysics*, **57**, 727–735.

Wang, L. and S. Rokhlin, 2002: Floquet wave homogenization of periodic anisotropic media. *J. Acoust. Soc. Am.*, **112**, 38–45.

Wyllie, M., A. Gregory, and L. Gardner, 1956: Elastic wave velocities in heterogeous and porous media. *Geophysics*, **21**, 41–70.

Ziman, J., 1972: *Principles of the Theory of Solids*. Cambridge Press, 2nd edition.

# Appendix A

# Overview of Anisotropy and the Anisotropic Wave Equation

In an isotropic medium there are two possible solutions to the wave equation, $P$- and $S$-waves, and their corresponding velocities are independent of the direction of propagation. When considering anisotropic media two complications arise which affect the velocities. The first is the direction the wave is propagating in, and the second is the polarization of the $S$-wave. An understanding of these effects can be achieved by examining the anisotropic wave equation, and where it comes from.

If linear elasticity is assumed, such that deformations of a medium are small Hooke's law can be written as:

$$\sigma_{ij} = C_{ijkl}\epsilon_{kl}$$

where $\sigma_{ij}$ is the stress, $\epsilon_{kl}$ is the strain and $C_{ijkl}$ is a forth rank tensor composed of the so called elastic constants which relates the stress to the strain. The elastic tensor $C_{ijkl}$ possesses full symmetry such that,

$$C_{ijkl} = C_{jilk} = C_{ijlk} = C_{jikl}$$

As a result of this symmetry any given system can contain at most 21 unique elastic constants. This symmetry is commonly used to represent the elastic constants in a more tractable notation. Using the mapping,

$$11 \rightarrow 1; 22 \rightarrow 2; 33 \rightarrow 3; 23, 32 \rightarrow 4; 13, 31 \rightarrow 5; 12, 21 \rightarrow 6$$

the elastic constants can be represented in the form of a $6 \times 6$ matrix which is symmetric about its diagonal.

According to Newton's second law the force exerted an a unit volume in the $i_{th}$ direction is:

$$f_i = \rho a_i = \rho \frac{\partial^2 u_i}{\partial t^2}$$

where $u_i$ is the displacement. From continuum mechanics it is known that:

$$f_i = \frac{\partial \sigma_{ij}}{\partial x_j}$$

giving,

$$\frac{\partial \sigma_{ij}}{\partial x_j} = \rho \frac{\partial^2 u_i}{\partial t^2}$$

Now using Hooke's law for linear elasticity and the relation between linear strain and displacement,

$$\epsilon_{kl} = \frac{1}{2} \left( \frac{\partial u_k}{\partial x_l} \frac{\partial u_l}{\partial x_k} \right)$$

This can be rewritten as:

$$\frac{\partial}{\partial x_j} C_{ijkl} \frac{\partial u_k}{\partial x_l} = \rho \frac{\partial^2 u_i}{\partial t^2}$$

or in the case of homogeneous media:

$$C_{ijkl}\frac{\partial^2 u_k}{\partial x_j \partial x_l} = \rho\frac{\partial^2 u_i}{\partial t^2} \tag{1.1}$$

This is clearly a wave equation, and it completely characterizes wave behavior in any general anisotropic, homogeneous media. Substitution of the elastic constants for an isotropic media, will reduce the preceding to two independent isotropic wave equations for $P$- and $S$-waves. This is demonstrated in Chapter 3 as part of the derivation of the Floquet solution, so it will not be repeated here. The elasticity matrix for the specific types of anisotropy discussed in this dissertation are:

Isotropic (2 unique elastic constants):

$$\begin{bmatrix} C_{11} & C_{11}-2C_{44} & C_{11}-2C_{44} & 0 & 0 & 0 \\ C_{11}-2C_{44} & C_{11} & C_{11}-2C_{44} & 0 & 0 & 0 \\ C_{11}-2C_{44} & C_{11}-2C_{44} & C_{11} & 0 & 0 & 0 \\ 0 & 0 & 0 & C_{44} & 0 & 0 \\ 0 & 0 & 0 & 0 & C_{44} & 0 \\ 0 & 0 & 0 & 0 & 0 & C_{44} \end{bmatrix}$$

Transverse Isotropy (5 unique elastic constants):

$$\begin{bmatrix} C_{11} & C_{11}-2C_{66} & C_{13} & 0 & 0 & 0 \\ C_{11}-2C_{66} & C_{11} & C_{13} & 0 & 0 & 0 \\ C_{13} & C_{13} & C_{33} & 0 & 0 & 0 \\ 0 & 0 & 0 & C_{44} & 0 & 0 \\ 0 & 0 & 0 & 0 & C_{44} & 0 \\ 0 & 0 & 0 & 0 & 0 & C_{66} \end{bmatrix}$$

Orthorhombic (9 unique elastic constants):

$$\begin{bmatrix} C_{11} & C_{12} & C_{13} & 0 & 0 & 0 \\ C_{12} & C_{22} & C_{23} & 0 & 0 & 0 \\ C_{13} & C_{23} & C_{33} & 0 & 0 & 0 \\ 0 & 0 & 0 & C_{44} & 0 & 0 \\ 0 & 0 & 0 & 0 & C_{55} & 0 \\ 0 & 0 & 0 & 0 & 0 & C_{66} \end{bmatrix}$$

The wave equation 1.1 has plane wave solutions for the vector displacement of the form,

$$\mathbf{u}(\mathbf{r}, \mathbf{t}) = \mathbf{a}\mathbf{e}^{\imath(\mathbf{k}\cdot\mathbf{r}-\omega\mathbf{t})}$$

.

The reader is reminded that it is sufficient to limit ourselves to plane wave solutions because a point source is simply the sum of plane waves propagating in all possible directions.

In particular for any given medium three mutually orthogonal solutions may exist; i.e.

$$\mathbf{u_a}(\mathbf{r}, t) = (\mathbf{b} \times \mathbf{c}) e^{\imath(\mathbf{k}\cdot\mathbf{r} - \omega t)}$$

$$\mathbf{u_b}(\mathbf{r}, t) = (\mathbf{c} \times \mathbf{a}) e^{\imath(\mathbf{k}\cdot\mathbf{r} - \omega t)}$$

$$\mathbf{u_c}(\mathbf{r}, t) = (\mathbf{a} \times \mathbf{b}) e^{\imath(\mathbf{k}\cdot\mathbf{r} - \omega t)}$$

In the special case of an isotropic medium these three solutions will be orthonormal to the wave vector, $\mathbf{k}$ such that:

$$\hat{\mathbf{u}}_\mathbf{a} \cdot \hat{\mathbf{k}} = 1$$

$$\hat{\mathbf{u}}_\mathbf{b} \cdot \hat{\mathbf{k}} = \hat{\mathbf{u}}_\mathbf{c} \cdot \hat{\mathbf{k}} = \mathbf{0}$$

where $\mathbf{u_a}$ is referred to as a compressional or '$P$-wave', and $\mathbf{u_b}$ and $\mathbf{u_c}$ are referred to as shear or '$S$-waves'. In the case of general anisotropy however, this orthonormal condition does not hold. In this case the displacement vector which is closest in direction to the wave vector is referred to as the 'quasi $P$-wave'. The other two orthogonal displacement solutions are referred to as 'quasi $S$-waves', although for simplicity the 'quasi' qualifier is sometimes dropped.

In mathematical terms the quasi $P$-wave is the displacement which maximizes:

$$\mathbf{\hat{u}_{a,b,c}} \cdot \hat{\mathbf{k}}$$

Another important thing to recognize is that for an isotropic system there always exists a coordinate system such that equation 1.1 reduces to three separate (two unique) scalar wave equations for $u_1, u_2$ and $u_3$ such that:

$$\mathbf{u_a} = u_1\hat{\imath} + 0\hat{\jmath} + 0\hat{k}$$

$$\mathbf{u_b} = 0\hat{\imath} + u_2\hat{\jmath} + 0\hat{k}$$

$$\mathbf{u_c} = 0\hat{\imath} + 0\hat{\jmath} + u_3\hat{k}$$

These relationships also hold for a few special cases of anisotropic systems such as propagation parallel or normal to the axis of symmetry for a VTI system and normal to each of the three symmetry axes for an orthogonal system. This can be demonstrated by substituting the elastic constants into wave equation 1.1 and considering the special cases mentioned. In other cases for general anisotropy the wave equation does not separate and solutions are referred to as 'coupled' solutions.

It is clear that a wave is characterized by the wave vector and frequency. The phase velocity is defined by considering a wave at some point $(\mathbf{r}, t)$ and then some later point in space and time $(\mathbf{r} + d\mathbf{r}, t + dt)$. We require that the phase is the same such that

$$\omega dt - \mathbf{k} \cdot d\mathbf{r} = 0$$

or

$$\frac{dt}{d\mathbf{r}} = \frac{dt}{\hat{\mathbf{r}} \cdot dr} = \frac{\hat{\mathbf{r}} \cdot \mathbf{k}}{\omega} = \mathbf{S}$$

**S** is defined as the phase slowness. The phase velocity is the reciprocal of slowness, which is clearly just a function of 'how fast' a mono-frequency wave changes in space over a given time. It is also clear that in general $\frac{\omega}{|\mathbf{k}|} \neq C$ where $C$ is a constant. This means that velocity of a mono-frequency wave is the function of both frequency, $\omega$ and the direction of travel characterized by the wave vector $\mathbf{k}$. The first case is referred to as dispersion while the latter is commonly known as anisotropy. The standard approach is to write $\mathbf{k}(\omega)$ so it becomes apparent that both anisotropy and dispersion are general effects arising from variations of the wave vector.

In the real world we never deal with these ideal mono-frequency waves, instead we produce and/or measure waves which contain 'groups' of mono-frequency waves. In the general case $\frac{\omega}{|\mathbf{k}|} \neq C$ from above it is apparent this will cause more complex behavior of the 'group' than is described by the individual phase velocities. In this case the group of waves about some center frequency will travel with a velocity that is defined as

$$V_{group} = \left( \frac{\partial \omega}{|\partial \mathbf{k}|} \right)_{\omega_0}$$

For a more detailed explanation of phase, group and energy velocities for general waves Born and Wolf (1999) is an excellent reference.